4-2020

Fatigue Damage Characterization by Surface Roughness and Instrumented Micro – Hardness Measurements

Suraj Sanjay Nikam
Western Michigan University, suraJnikam200@gmali.com

FATIGUE DAMAGE CHARACTERIZATION BY SURFACE ROUGHNESS AND INSTRUMENTED MICRO – HARDNESS MEASUREMENTS

by

Suraj Sanjay Nikam

A thesis submitted to the Graduate College
in partial fulfillment of the requirements
for the degree of Master of Science in Engineering
Mechanical Engineering
Western Michigan University
April 2020

Thesis Committee:

Dr. Daniel Kujawski, Ph.D., Chair
Dr. Muralidhar Ghantasala, Ph.D.
Dr. Jinseok Kim, Ph.D.

FATIGUE DAMAGE CHARACTERIZATION BY SURFACE ROUGHNESS AND INSTRUMENTED MICRO – HARDNESS MEASUREMENTS

Suraj Sanjay Nikam, M.S.E.

Western Michigan University, 2020

Fatigue is an essential consideration in the design of high performance, safety-critical structures, and components, as fatigue failure constitutes more than 70% of failures in dynamically loaded components. This research aims to shed light on the effect of surface roughness on the micro-hardness in metals through experimental techniques (Part 1), the correlation between the traditional fatigue testing and instrumented cyclic micro-hardness testing to determine the material properties modeled by Ramberg - Osgood relationship(Part 2), and the effect of the fatigue damage on micro-hardness and surface roughness (Part 3).

For this research, Al 7075 - T651 and Al 6061 - T651 chosen as the materials due to their vast range of applications in the aerospace industry for the fuselage, wings of airplanes, and in the automotive industry for engine radiators, wheels, body parts of the automobiles. Depending on the data acquired from all the experiments, the fatigue damage characterization can be evaluated using the surface roughness and the instrumented micro-hardness indentation measurements, which are aimed to predict the remaining life of components while at service.

ACKNOWLEDGMENTS

I want to take this opportunity to express my sincerest gratitude to Dr. Daniel Kujawski, who has supported me through my thesis with his patience and knowledge. It would not have been possible to make this thesis a reality without his vision.

Secondly, I would also like to thank the members of my committee Dr. Jinseok Kim and Dr. Muralidhar Ghantasala, for spending the time to review my work. I would like to thank Peter Thannhauser, Mike Konkel, and Allin Kahrl for their assistance in fatigue & fracture laboratory and fabrication workshops.

Finally, I would like to express my appreciation to my colleagues Zahra Salemi, Pranav Bhale, Vikram Srinivasan, and Vedang Naik for extending their assistance in this thesis project. Special thanks to my colleague and a dear friend Vivek Iddum for supporting me and reviewing my work beforehand.

I wish to acknowledge the support and great love of my family, my mother, Hemlata; my father, Sanjay; and my sister, Preeti. They kept me going on, and this work would not have been possible without their input.

Suraj Sanjay Nikam

TABLE OF CONTENTS

Table of Contents– Continued

Table of Contents – Continued

LIST OF TABLES

LIST OF FIGURES

NOMENCLATURE

Al 6061 – T651 will be called as Al 6061

Al 7075 – T651 will be called as Al 7075

Sample numbering

Al 6061 – sample # will be called as Al 6061 – 2

Al 7075 – sample # will be called as Al 7075 – 4

1 INTRODUCTION

In modern technical applications like aircraft, cars, and trains, the durability of the engineering components and structures is a significant concern for engineers. These engineering structures must be designed and ensured in such a way that they should not fail from varied or repeated loads in service. The design life should be larger than the service life.

In service, many engineering components and structures are subject to varying loads and, although the average stresses are often low, the local concentration of stress, which does not much reduce the static strength, may often lead to failure by fatigue. Indeed, by far, the more significant number of failures in service is by fatigue and relatively few by static failure [1].

The deterioration of a material initiated by repeated loading across a period termed as fatigue. The fatigue life highly depends on the surface quality of structures. According to Suraratchai et al. [2], the surface qualities which influence fatigue life typically characterized in three parameters: (i) a geometrical parameter: surface roughness, (ii) a mechanical parameter: residual stress and (iii) a metallurgical parameter: microstructure. These parameters can differ independently and in a considerable amount based on the machining, polishing conditions.

The effects of surface parameters could be observed and validated using various fatigue tests. These fatigue tests are expensive and time-consuming test methods. This research investigates the impact of surface parameters such as surface roughness on micro-hardness and the effect of fatigue damage on surface roughness and micro-hardness.

1.1 Background

The expression fatigue has been in use for a very long time; Fatigue is the structural damage that occurs in a material when subjected to cyclic stresses that are below the ultimate tensile strength or even yield strength of the material [3–5]. As found by other researchers, surface finish plays a substantial influence. Surface roughness could be described as near-surface stress or strain concentration caused by surface asperities [6].

1.2 Standard Tensile Testing

Tension tests are often utilized to assess the strength and ductility of materials due to their simplicity and the ability to determine the most fundamental mechanical properties used in engineering design. Tensile test specimens usually have a cylindrical or rectangular cross-section, which is uniform over a gage length. Figure 1.1 shows the schematics of a cylindrical sample where 'G' is gauge length, 'D' is a diameter, and 'R' is the radius of the fillet; the standard test specimen's dimensions and test procedure can be found in ASTM E8 – 16a standard [7].

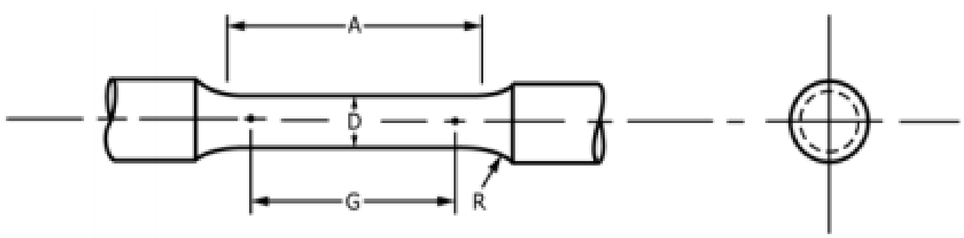

Figure 1.1 Schematics of a cylindrical specimen geometry [7].

Tensile tests are carried out by gradually stretching a specimen in tension until it breaks. During tension tests, a load cell records resultant load built up in the material as the test machine elongates the specimen. An extensometer is a device used to measure elongation across the gauge length of the sample. Load determined from load cell can be translated into engineering stress (σ) acting on a specimen, whereas an extensometer reading can be translated into engineering strain (ε). Engineering stress is computed as the ratio of the load over the initial cross-sectional area of the specimen, Equation 1.1, and strain is determined as the ratio of change in gauge length over the initial gauge length, Equation 1.2. The calculated stresses, when plotted as a function of strains, yield the well-known tensile stress-strain curve [3], as demonstrated in figure 1.2.

$$\boldsymbol{\sigma} = \frac{\boldsymbol{P}}{\boldsymbol{A_i}} \tag{1.1}$$

Where σ is the engineering stress, *P* is load, and A_i is the initial cross-sectional area.

$$\boldsymbol{\varepsilon} = \frac{\boldsymbol{\Delta L}}{\boldsymbol{L_i}} \tag{1.2}$$

Where ε is the engineering strain, ΔL is a change in gauge length, and L_i is the initial gauge length.

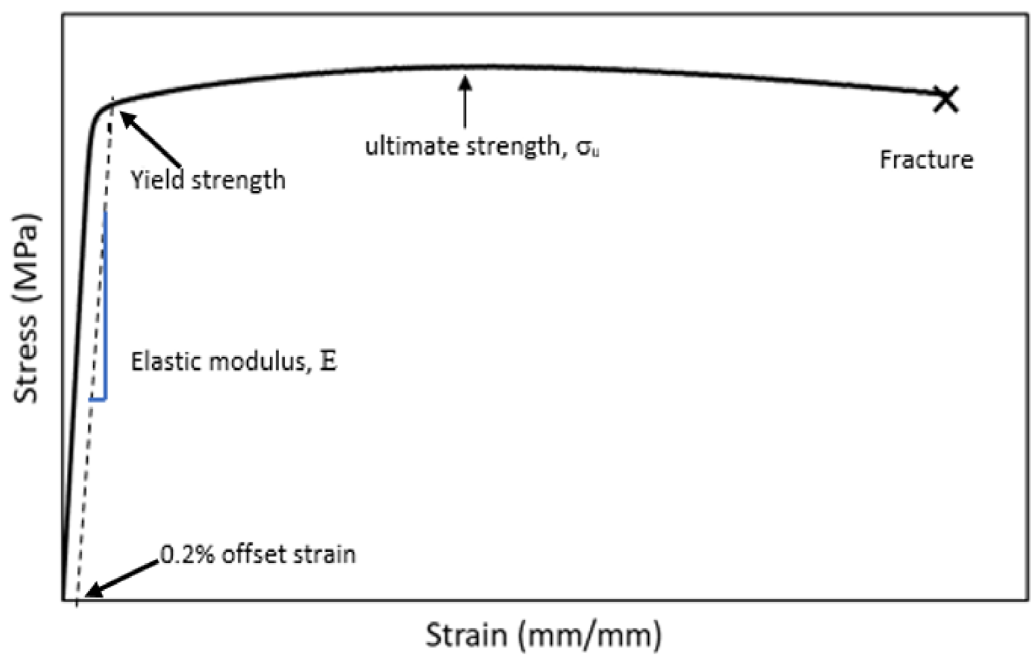

Figure 1.2 Schematics of the engineering stress-strain plot [3].

The stress-strain curve is used to evaluate the fundamental properties of a material. Material properties such as Young's modulus, *E*, is defined as a slope of the stress-strain curve within the linear range indicating the fact that the stresses in this elastic region follow the same path back during unloading. Yield stress occurs when the curve diverges from the linear path at a specific stress level. After the stress level crosses yield strength, the material is said to undergo elastic-plastic deformation. Yield strength is calculated by drawing a parallel line with the elastic slope *E*, using an offset of 0.2% strain, as shown in figure 1.2. Ultimate tensile strength, σ_u is defined as the maximum load a material can withhold before failure occurs. Strain at fracture is termed as a fracture strain (ε_f). Equation 1.3 shows the relation between stress, strain, and Young's modulus of elasticity.

$$\boldsymbol{\sigma = E\varepsilon} \tag{1.3}$$

It is generally assumed that when the applied stress is below yield stress or in the elastic region that no damage would occur. This assumption, however, would not hold true if the material is subjected to repeated stresses over a long period of time, although below yield stress. These repeated stresses are term as cyclic stress and would trigger damage at microscopic levels, which cumulates with time and causes materials fatigue.

1.3 Total fatigue life prediction

Total fatigue life is portrayed as a function of variables such as the applied stress amplitude, strain amplitude, mean stress, and environment. These stress- or strain-based methodologies embody the damage evolution, crack nucleation, and crack growth stages of fatigue into a single, experimentally characterizable continuum formulation. In these approaches, the fatigue life of a component is defined as a total number of cycles or time to induce the fatigue damage and to initiate the dominant fatigue flaw, which is propagated to a final failure [4].

1.3.1 Stress-life approach

Groundbreaking work followed from August Wöhler [3,4,8] during 1860-1870 when he examined the failure mechanism of locomotive axles by applying controlled load cycles. He presented the concept of rotating-bending fatigue test that successively lead to the development of the stress-life (S-N) plot for assessing the fatigue life and endurance limit of the material. Wöhler established that fatigue life decreased with higher stress amplitude, σ_a given by Eq. 1.4.

$$\sigma_a = \frac{\sigma_{max} - \sigma_{min}}{2} \tag{1.4}$$

The test method for stress-life response is explained in the ASTM standard E466-15 [9] (American Society for Testing and Materials, Philadelphia). The results obtained from such experiments are drawn as stress amplitude (σ_a) versus cycles to failure (N_f). Figure 1.3 displays the schematics of an S-N curve for 1045 steel and 2014-T6 aluminum. Stress amplitude for 1045 steel decreases and then becomes steady with an applied number of cycles, whereas for 2014-T6 aluminum stress amplitude continues to decrease until failure occurs.

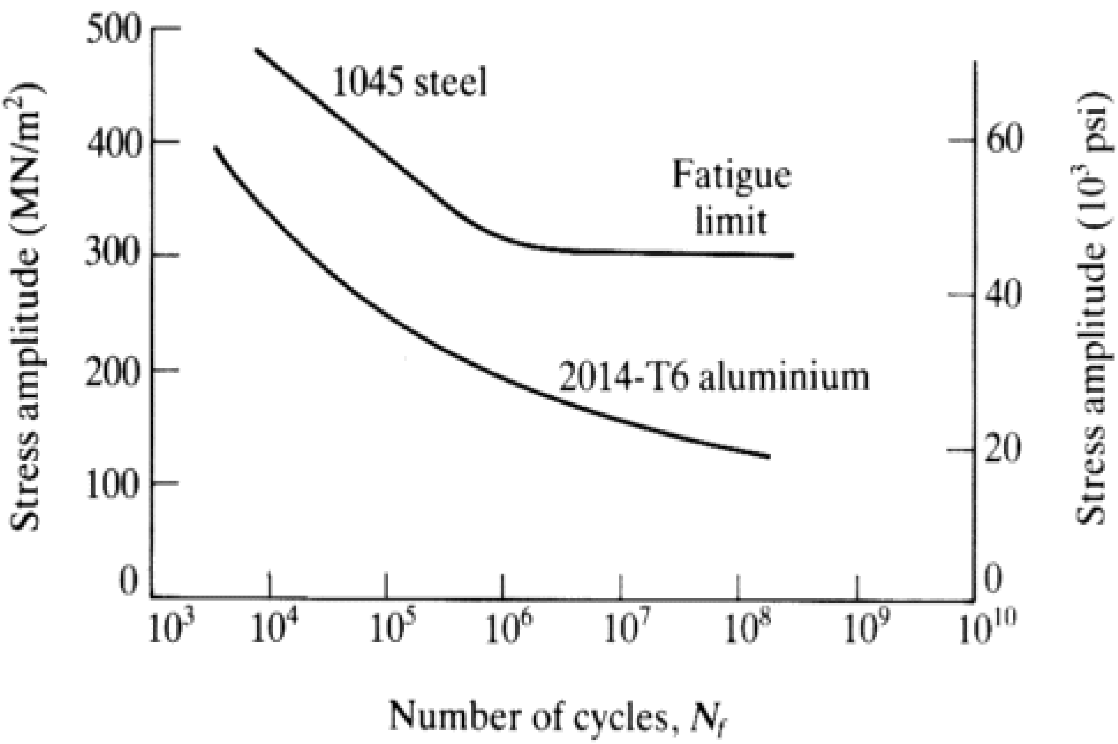

Figure 1.3 Stress-life curves of 1045 steel and 2014-T6 aluminum [3].

1.3.2 Strain-life approach

Strain-based approach to fatigue considers the plastic deformation that may occur in localized regions where fatigue crack begins, as at edges of beams and stress raisers [3]. The test procedure for strain-life response is described in ASTM standard E606/E606M – 12 [10]. Standard also mentions that strain-controlled fatigue can be an essential consideration in the design of industrial products. It is crucial for situations in which components or portions of components undergo either mechanically or thermally induced cyclic plastic strains that cause failure within relatively low life (that is, approximately $<10^5$) cycles. The information gained from strain-controlled fatigue testing may be a critical element in the establishment of design criteria to safeguard against component failure by fatigue.

Dowling [3] mentions that a strain versus life curve is a plot of strain amplitude versus cycles to failure. Tests are continued until the specimen fails by fatigue, and results for various distinct strain amplitudes (ε_a) deliver the desired curve. For strain-life curves, a log-log plot is usually used. The strain amplitude can be decomposed into elastic and plastic components, as shown in Eq. 1.5.

$$\boldsymbol{\varepsilon_a = \varepsilon_{ea} + \varepsilon_{pa}} \tag{1.5}$$

where the elastic strain amplitude is related to the stress amplitude by $\boldsymbol{\varepsilon_{ea} = \sigma_a / E}$. The plastic strain amplitude (ε_{pa}) is a measure of the width of the stress-strain hysteresis loop. A schematic graph and a curve fitted to actual data are given in the curves labeled total strain in figure 1.4. Equation 1.6 forms the foundation for the strain-life approach to fatigue design and has found an extensive application in industrial practice.

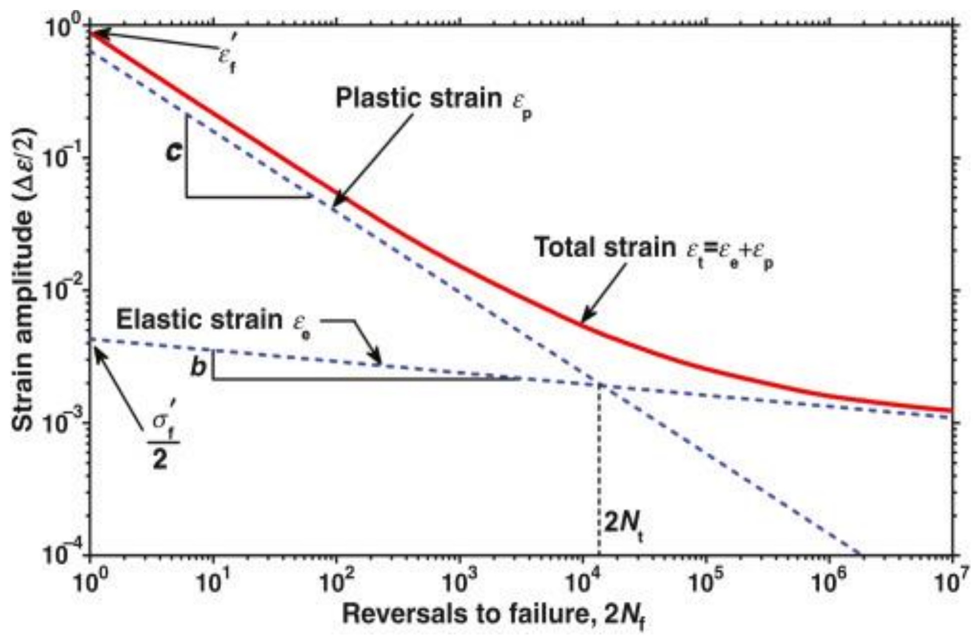

Figure 1.4 Schematics of elastic, plastic, and total strain-life curves [11].

$$\varepsilon_a = \frac{\sigma'_f}{E}\left(2N_f\right)^b + \varepsilon'_f\left(2N_f\right)^c \tag{1.6}$$

where σ'_f is the fatigue strength coefficient, *E* is elastic modulus, N_f is number of cycles to failure, *b* is fatigue strength exponent, *c* is the fatigue ductility exponent and ε'_f is a fatigue ductility coefficient.

1.4 Surface roughness

Surface roughness, often shortened to roughness, is a measure of the texture of a surface. Vertical deviations of a real surface from its ideal form quantifies surface roughness. If these deviations are large, the surface is rough; if they are small, the surface is smooth. Roughness is typically considered to be the high frequency, short wavelength component of a measured surface [11]. Surface roughness, which is an unavoidable phenomenon at machining, has a pronounced effect on the materials' mechanical properties such as fatigue strength, hardness, and fatigue limit. Rough surfaces usually wear more quickly and have higher friction coefficients than smooth surfaces do. Often surface roughness is a good predictor of the performance of a mechanical component since irregularities in the surface may cause stress concentrations and form nucleation sites for cracks or corrosion [12].

This research uses surface roughness parameters, average arithmetic height (Ra), and Root means square roughness (Rq) for the characterization of surface topography. Gadelmawla [13], describes the Ra and Rq surface parameter as follows.

1.4.1 Arithmetic average height (Ra)

Arithmetic average height parameter, also known as the centerline average (CLA), is the most universally used roughness parameter for general quality control. It is defined as the average absolute deviation of the roughness irregularities from the mean line over one sampling length, as demonstrated in figure 3.1. This parameter is easy to define, easy to measure, and gives an excellent general description of height variations. It does not provide any information about the wavelength, and it is not sensitive to small changes in profile. The mathematical definition and the digital implementation of the arithmetic average height parameter are, respectively, as follows:

$$R_a = \frac{1}{l}\int_0^l |y(x)|\, dx \tag{1.7}$$

$$R_a = \frac{1}{n}\sum_{i=1}^{n} |y_i| \tag{1.8}$$

where "l" is the relative length of the profile, and "n" is the number of intersections of the profile at the mean line.

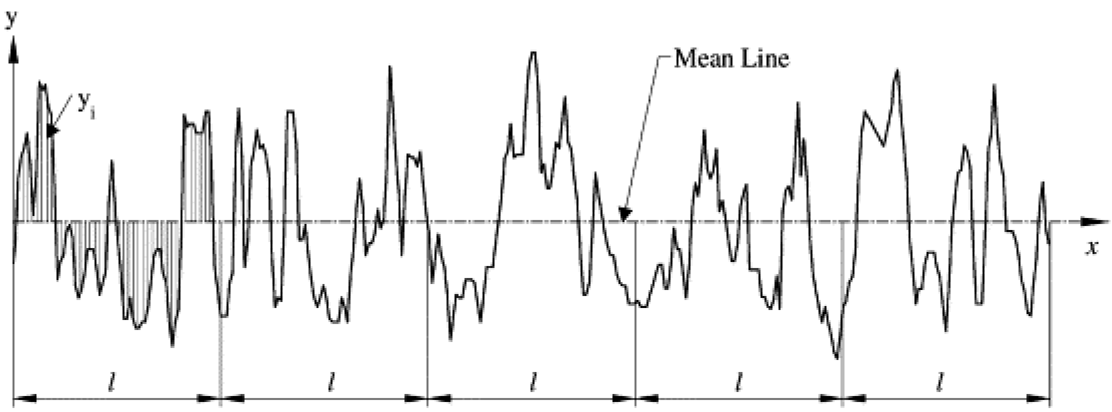

Figure 1.5 Definition of the average arithmetic height (Ra) [14].

1.4.2 Root mean square roughness (Rq)

This parameter is also known as RMS. It represents the standard deviation of the distribution of surface heights, so it is an important parameter to describe the surface roughness by statistical methods. This parameter is more sensitive than the average arithmetic height (R_a) in no small deviation from the mean line. The RMS mean line is the line that divides the profile so that the sum of the squares of the deviations of the profile height from it is equal to zero. The mathematical definition and the digital implementation of this parameter are as follows:

$$R_q = \sqrt{\frac{1}{l}\int_0^l \{y(x)\}^2\, dx} \tag{1.9}$$

$$R_q = \sqrt{\frac{1}{n}\sum_{i=1}^{n} y_i^2} \tag{1.10}$$

1.5 Instrumented micro-hardness

The hardness of the material is nothing but the resistance of a material to deformation, indentation, or penetration. Vickers microhardness tests are an essential method for the classification of material properties at small scales. It has been extensively employed as a quantitative technique to study the mechanical behavior of materials since the 1990s [6].

ASTM E384 standard [14] mentions that hardness tests are useful for materials evaluation, quality control of manufacturing processes, and research and development efforts. Hardness, although empirical, can be correlated to tensile strength for many metals and alloys, and is also an indicator of machinability, wear resistance, toughness, and ductility. Figure 1.6 displays the schematics plot of the cross-section of an indentation.

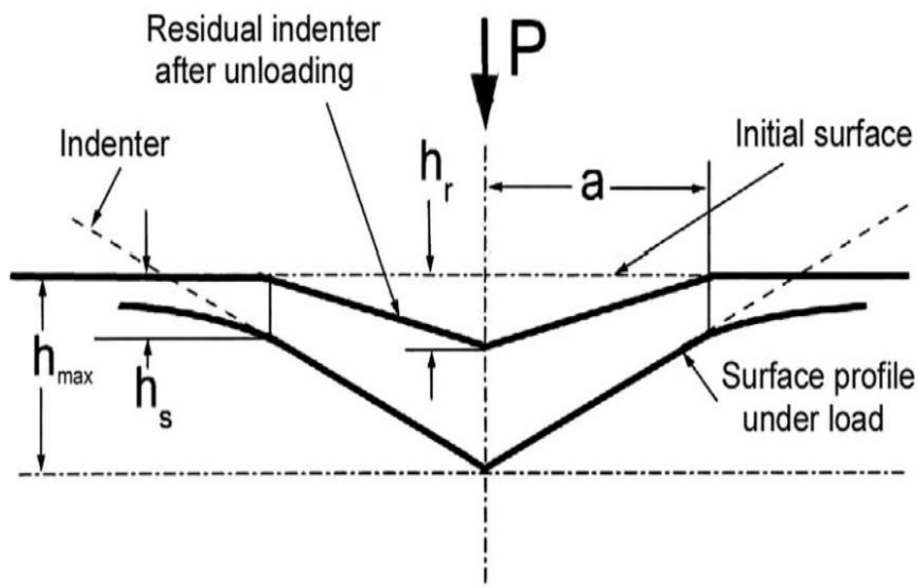

Figure 1.6 Definition of the average arithmetic height (Ra) [14].

The Vickers microhardness test method employs a hard indenter (Vickers diamond pyramid) that penetrates the specimen with a given load. After the unloading, the dimensions of the indentation in the specimen evaluated and the hardness, defined as the ratio of the load applied to the projected area of the indentation and is stated by the following relation [6],

$$H_v = 1 \cdot 854 \left({}^{F}/_{d^2} \right) \quad (1.11)$$

where “*HV*“ is the Vickers’s microhardness, “*F”* is applied load, and “*d*” is the diagonal length of the impression. This method of instrumented micro-indentation continuously records load and penetration and can determine, besides hardness, a complex of mechanical characteristics: Young’s modulus, yield strength, strain hardening exponent, residual stress, fracture toughness, and many more [15–18].

1.6 Literature review

Many researchers [2,19–22] have said that the surface quality of the mechanical structures has a significant impact on fatigue life. A variety of material removal processes is generally employed for the manufacturing of engineering structures. Research works concerning the influence of machined surface roughness on the fatigue life have studied in past decades. Suraratchal et al. [2] and Sigmund and Bjorn [19] modeled the stress state of the microsurface profile and established a numerical method for fatigue life prediction of components with rough surfaces using the finite element method. Smaga and Eifler [20] studied the outcomes of the residual stress induced from surface roughness.

Xiao et al. [21] carried out low cycle fatigue (LCF) tests on the alloy steel samples with discrete surface roughness to investigate the effect of roughness on fatigue life. Figure 1.7 displays the test results obtained from the testing, and it validates that the higher the roughness, the lower the fatigue life. A power function curve was used to fit the data points; as a result, the curve is expressed by the following equation (1.8),

$$N_f = 2559 * R_a^{-0.1166} \quad (1.12)$$

where “N_f“ is the fatigue life in cycles, and “*Ra”* is the surface roughness.

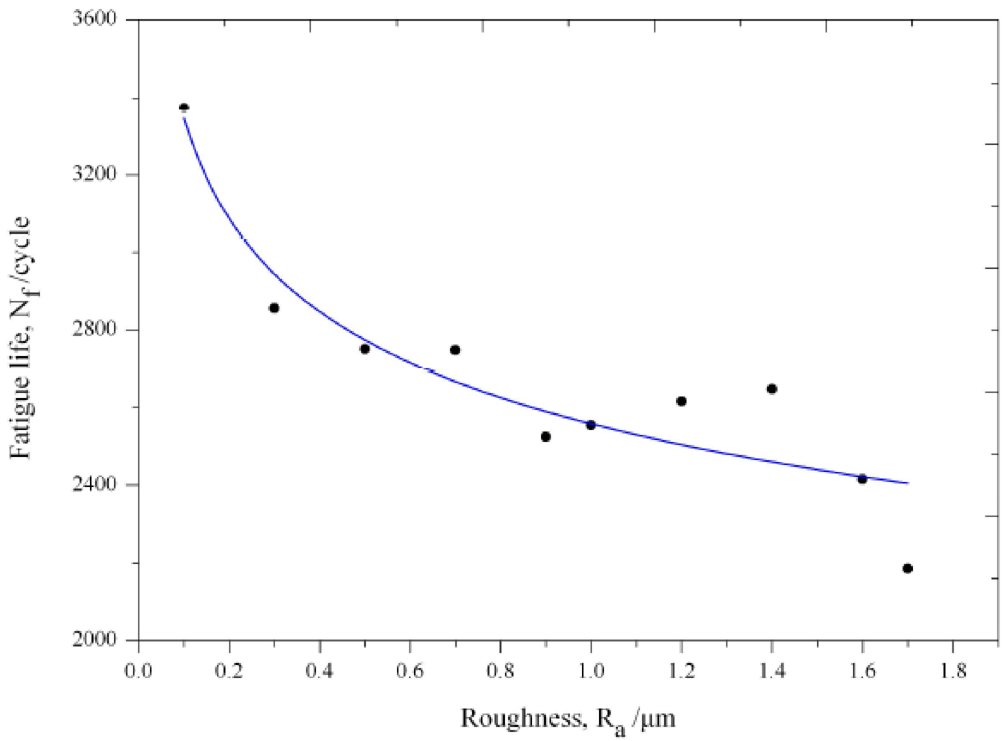

Figure 1.7 Relationship between the roughness "Ra" and fatigue life [23].

In the early 1980s, Fine [22] performed a study that reveals, in a notch and scratch-free metals which contain only small precipitates, fatigue cracks are noticed to initiate near slip bands or along the grain boundaries. He also explained that during cyclic deformation, slip steps form on the surface of the metal and accumulate with cycles. Eventually, regions of severe roughness lead to the initiation of the fatigue cracks. This surface roughening from cyclic loading has also been modeled to determine the crack initiation life [23].

Numerous studies [24–26] presenting a microhardness technique based on the optical measurements residual indentations were used to study the surface mechanical properties. The traditional microhardness technique, nonetheless, can only offer the deformation resistance at material surfaces. As fatigue damage may also result in the reduction of stiffness, the exhaustion of toughness, and more [24]. Investigation of surface mechanical properties such as strength, plasticity, and toughness using instrumented micro-indentations will be useful for meticulously understanding the fatigue damage-induced deterioration in the surface mechanical properties.

2 SPECIMEN AND MATERIAL PROPERTIES

2.1 Materials and Specimens

2.1.1 Materials

This research was conducted to examine the effects of surface roughness on instrumented micro-hardness and effects of fatigue damage on surface roughness and micro-hardness. The materials selected for this research were an aerospace-grade type aluminum alloys, Al 6061 and Al 7075 due to their wide range of applications in the aerospace industry for the fuselage, wings of airplanes and in the automotive industry for engine radiators, wheels, body parts for automobiles.

The chemical composition and mechanical properties of aluminum alloys Al 6061 and Al 7075 are provided in Tables 2.1 and 2.2, respectively; the following table data were obtained from the certified test reports provided by Kaiser aluminum and Hydro extrusion USA.

Table 2.1 Chemical composition of materials

Materials	**Chemical composition**
Aluminum 6061-T651	Si 0.4%, Fe 0.7%, Cu 0.15%, Mn 0.15%, Mg 0.8%, Cr 0.04%, Zn 0.25%, Ti 0.15%, Others 0.15%, Al balance
Aluminum 7075-T651	Si 0.08%, Fe 0.24%, Cu 1.4%, Mn 0.02%, Mg 2.8%, Cr 0.19%, Zn 5.8%, Ti 0.03%, Zr 0.02%, Others 0.15%, Al balance

Table 2.2 Mechanical properties of materials

Materials	0.2% Proof stress (MPa)	Tensile strength (MPa)	Elongation (%)
Aluminum 6061-T651	290	317	15.5
Aluminum 7075-T651	524	570	17.5

2.1.2 Specimens

A ¾" of aluminum alloy round bar of 12' length was cut into 8" long pieces using a horizontal band saw. The cut pieces of material were subsequently machined into a rectangular cross-section of dog-bone fatigue test specimens having 0.75" gage length and 3.14" gripping length. Figure 2.1 depicts the dimensions of machined specimens.

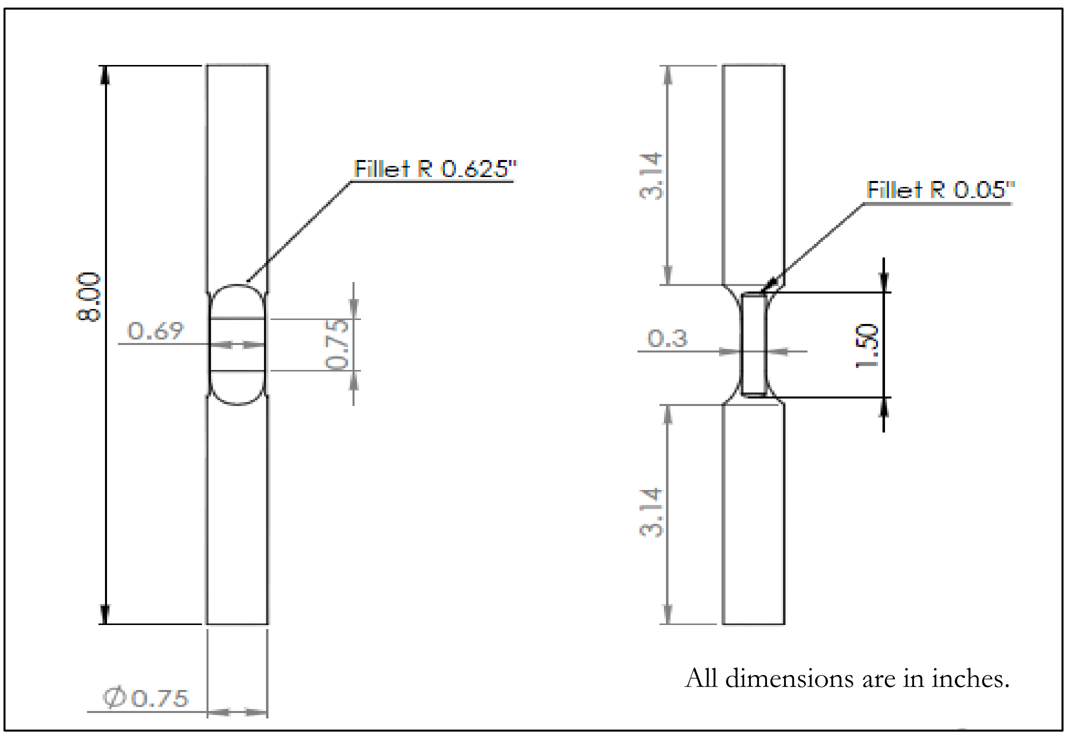

Figure 2.1 Schematic of machined specimen for fatigue testing.

Furthermore, using both aluminum alloys metallographic samples of ¾" diameter and 1" length were prepared following the ASTM E3-11 standard [27]. Specimens were polished with different grit papers to obtain the surface finish with different roughness. The primary objective of these sample preparation was to perform instrumented micro-indentations and to measure the impact of surface roughness.

2.2 Monotonic testing

After preparing all the samples, the two specimens from each aluminum alloys were chosen to perform a monotonic tension and compression test to determine the mechanical properties such as ultimate tensile strength, elastic modulus, yield stress, and other. Both tension and compression tests were designed by following the ASTM E8/E8M – 16a and ASTM E9 – 19 standards [7,28].

2.2.1 Tension test

Monotonic tension tests under displacement control mode performed at the rate of 0.13mm/sec. up to failure. The tests were carried out on a uniaxial servo-hydraulic MTS 810 machine having a maximum load capacity of 100 kN and maximum actuator displacement of 100 mm. Test results for monotonic tension tests of two aluminum alloys shown in the below figures.

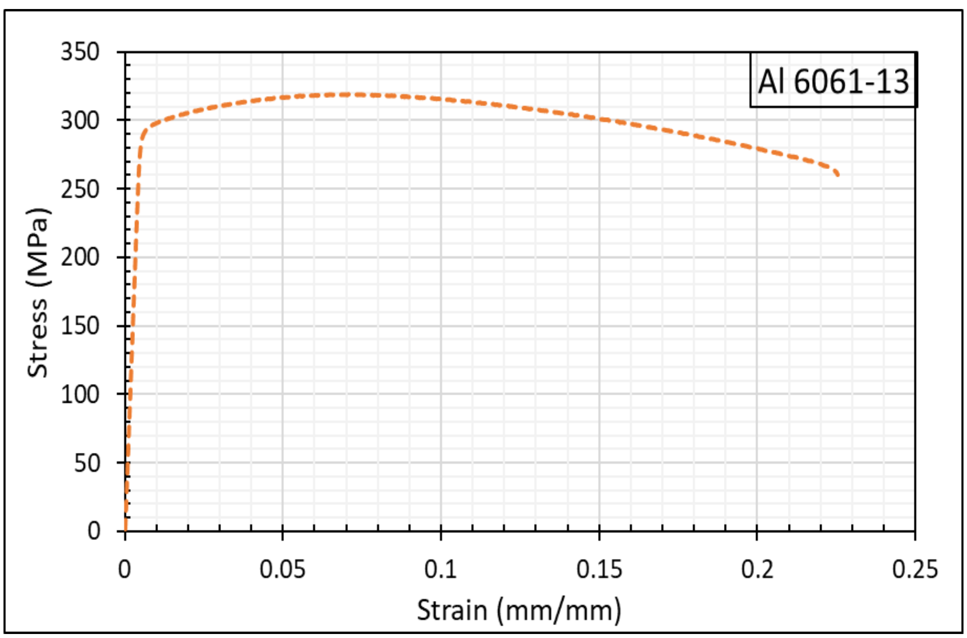

Figure 2.2 Monotonic tensile test result for Al 6061 – 13.

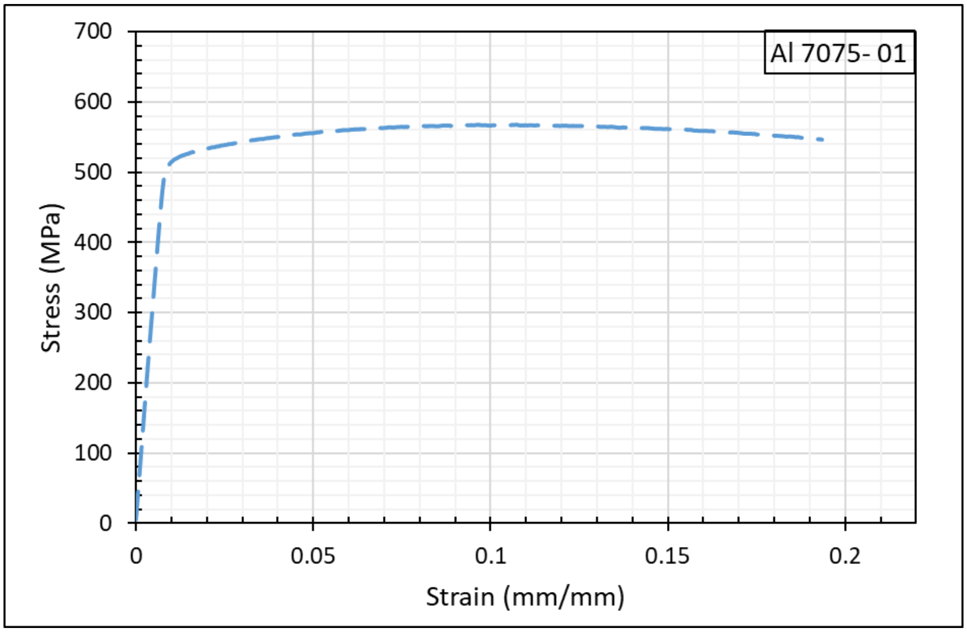

Figure 2.3 Monotonic tensile test result for Al 7075 – 01.

The acquired test data and the above figures were analyzed to determine the material properties like Young's elastic modulus (*E*), yield stress (σ_Y), and ultimate tensile strength (σ_u). These properties are listed in Table 2.3.

Table 2.3 Tensile properties of aluminum 6061 and 7075 alloys.

Material	E (GPa)	σ_Y (MPa)	σ_u (MPa)
Aluminum 6061 - 13	63.4	293	319
Aluminum 7075 - 01	67.5	513	568

2.2.2 Compression test

Monotonic compression tests also were executed to compare the monotonic behavior of aluminum alloys under tension and compression. The tests carried out in displacement control mode at the rate of 0.13mm/sec. All tests were conducted until the specimen buckles, or the maximum compressive strain reaches 10% (0.1 mm/mm). The stress-strain plots obtained from monotonic compression tests shown in Figs. 2.4 and 2.5.

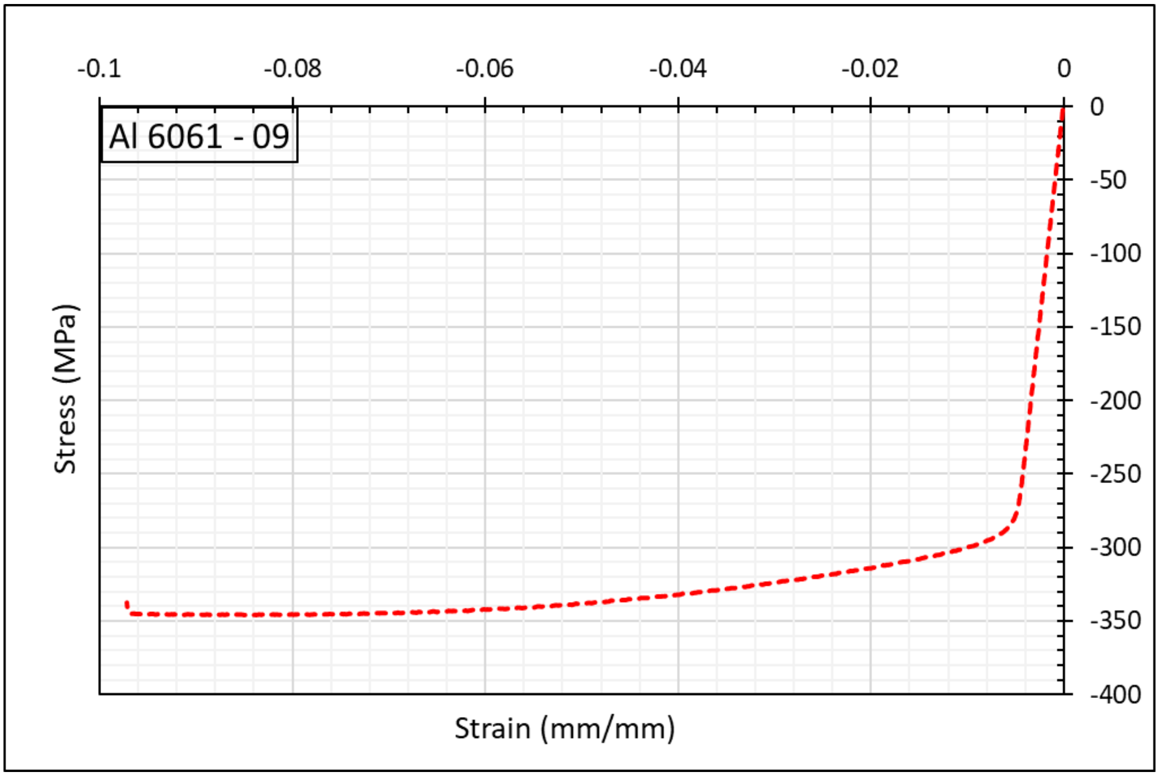

Figure 2.4 Monotonic compression test result for Al 6061 – 09.

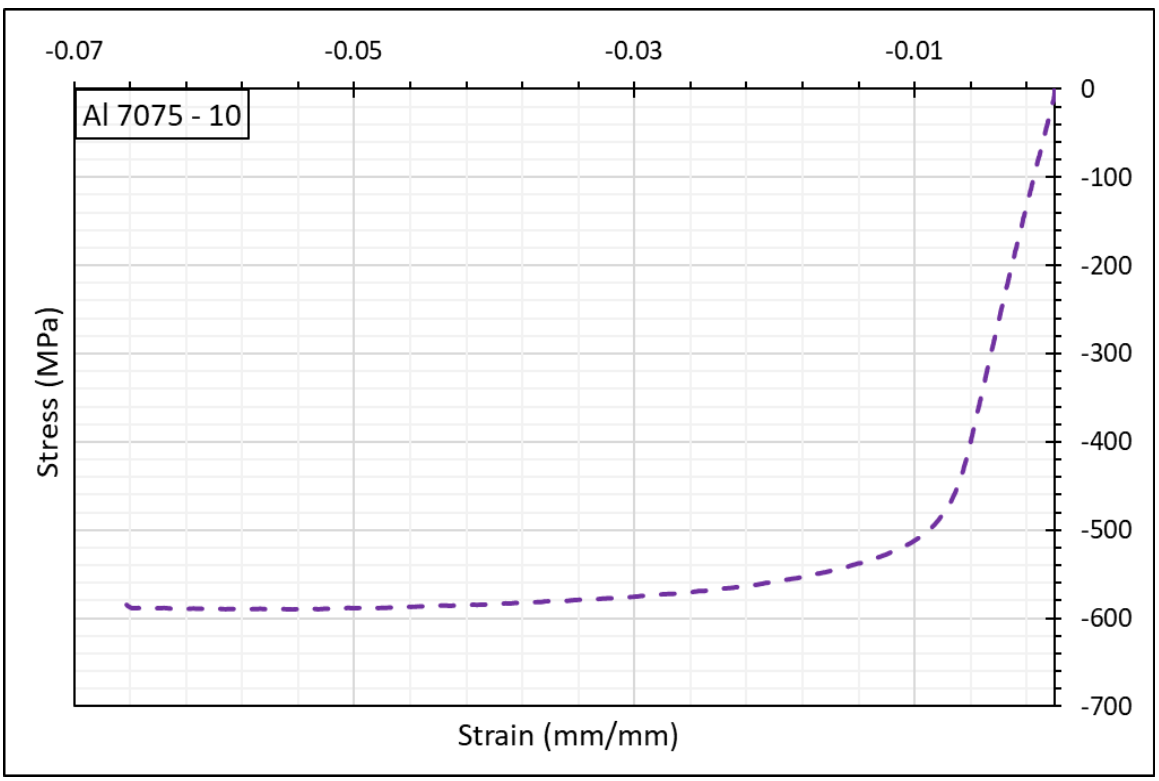

Figure 2.5 Monotonic compression test result for Al 7075 – 10.

Young's modulus under monotonic compression and tension seems to be the same. When calculated, it was determined that the yield stress obtained from the compressive test is nearly identical to the tensile test; the data is shown in Table 2.4.

Table 2.4 Compressive properties of aluminum 6061 and 7075 alloys.

Material	0.2 % yield stress (MPa)
Aluminum 6061 - 09	291
Aluminum 7075 - 10	509

2.3 Discussion

In the mechanical behavior of materials book, Dowling [3] mentions that the initial portions of the compressive stress-strain curve have the same general nature as those in tension. Thus, the material properties may be defined from the initial portion in the same manner as for tension, such as elastic modulus *E*, and the yield strength [3].

Figures 2.6 and 2.7 show the comparison between the engineering stress-strain curve for tensile and compressive tests in the same plot. The compression values are converted to absolute values to show the similarities between tension and compression. When compared, it can be noted that the tension and compressive curves follow the same trend in the elastic region. However, once the material passes the yield limit, the compression stress increases more than the tensile one. This behavior was seen in both aluminum alloys Al 6061 and Al 7075, respectively.

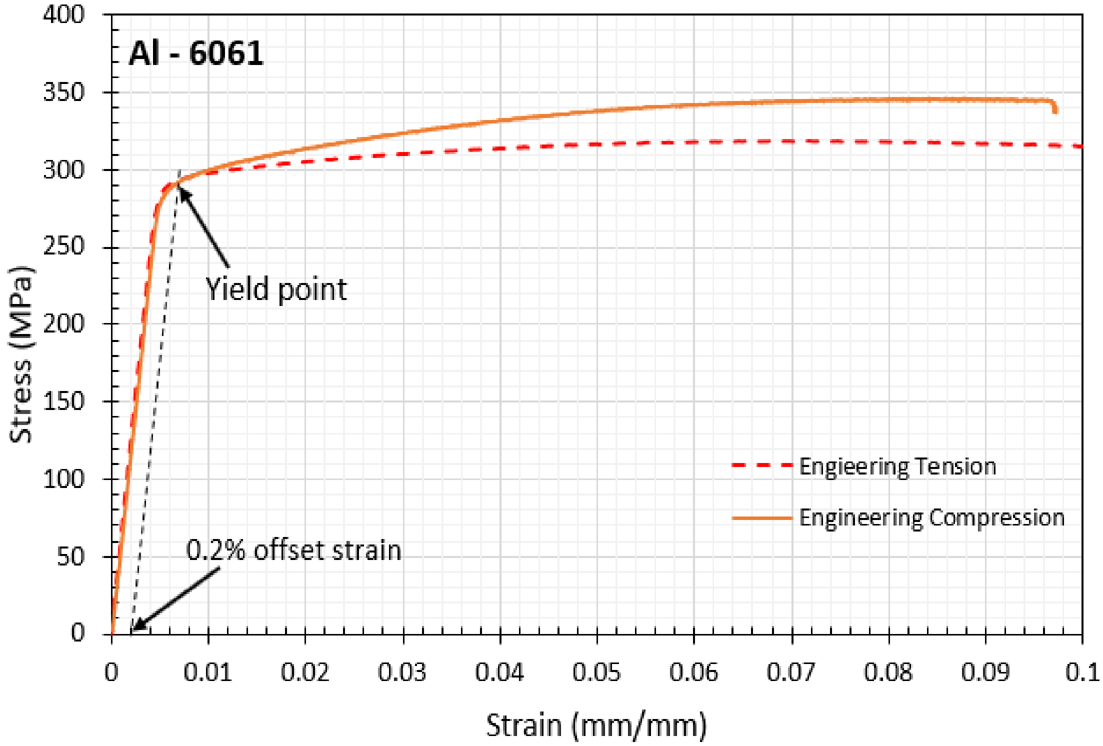

Figure 2.6 Tensile and compression test result for Al 6061.

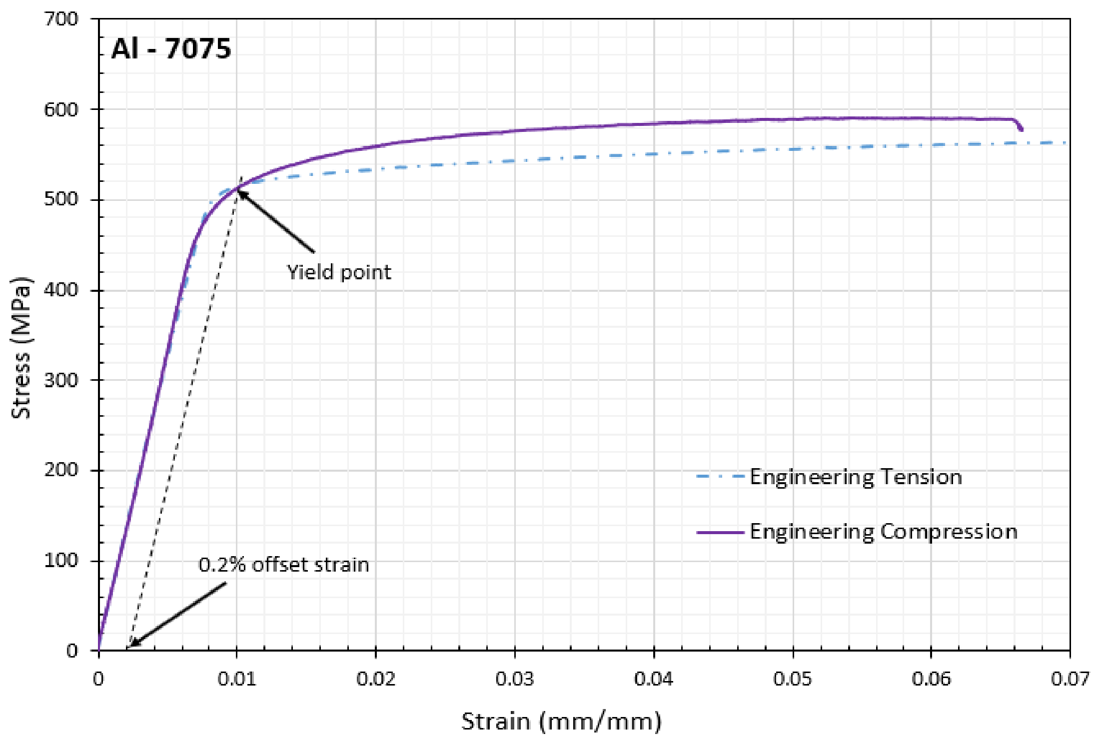

Figure 2.7 Tensile and compression test result for Al 7075.

The ultimate tensile strength behavior in compression differs qualitatively from that in tension [3]. Generally, the tensile test is associated with necking and may be sensitive to the defects, unlike the compression test, and every defect in the material will act as a stress raiser that will reach the test into the plasticity region at lower stress levels when compared to the compression test. From the above figures, it was monitored that the buckling does not occur until 9.5% for Al 6061 and 6.5% for Al 7075 alloy. Table 2.5 shows the comparison of yield stress at 0.2% strain offset for both aluminum alloys under monotonic tensile and compressive loading.

Table 2.5 Comparing mechanical properties of Al 6061 and Al 7075 alloys.

Material	Tensile yield stress (MPa)	Compressive yield stress (MPa)
Aluminum 6061	293	291
Aluminum 7075	513	509

3 EXPERIMENTAL DETAILS & TEST PROCEDURES

3.1 Introduction

As discussed in the previous chapter, monotonic tensile and compressive tests were carried out to compare their behavior under tension and compression. This chapter focuses on the different test procedures employed to characterize the fatigue damage based on the microhardness in Al 6061 and Al 7075. The carefully chosen test methods are categorized into three areas: i) strain-controlled fatigue tests, ii) micro-indentation tests, and iii) surface roughness measurements.

Furthermore, for the characterization of the fatigue damage versus micro-hardness and surface roughness, the study is grouped into three key sections; 1) influence of surface roughness on instrumented micro-hardness, 2) relationship in the cyclic elastoplastic behavior of materials during the work hardening achieved from cyclic instrumented micro-indentations and the strain-controlled fatigue tests, and 3) variation in the surface quality parameters such as roughness and micro-hardness of the material with the increasing percentage of fatigue damage.

3.2 Test procedures applied to Al 6061

The preceding chapter details of monotonic tensile and compression experiments were described. In addition to that, as explained above, three different test methods are addressed in the following sections.

3.2.1 Micro-hardness as a function of surface roughness

Instrumented micro-indentation testing emphasis the continuous observation of penetration depth, and the load as indenter is driven into a material and then withdrawn from it. Figure 3.1 illustrates the typical indentation response curve where the y-axis shows load (F), and the x-axis shows penetration depth (h). The indentation curve comprises loading and unloading sections.

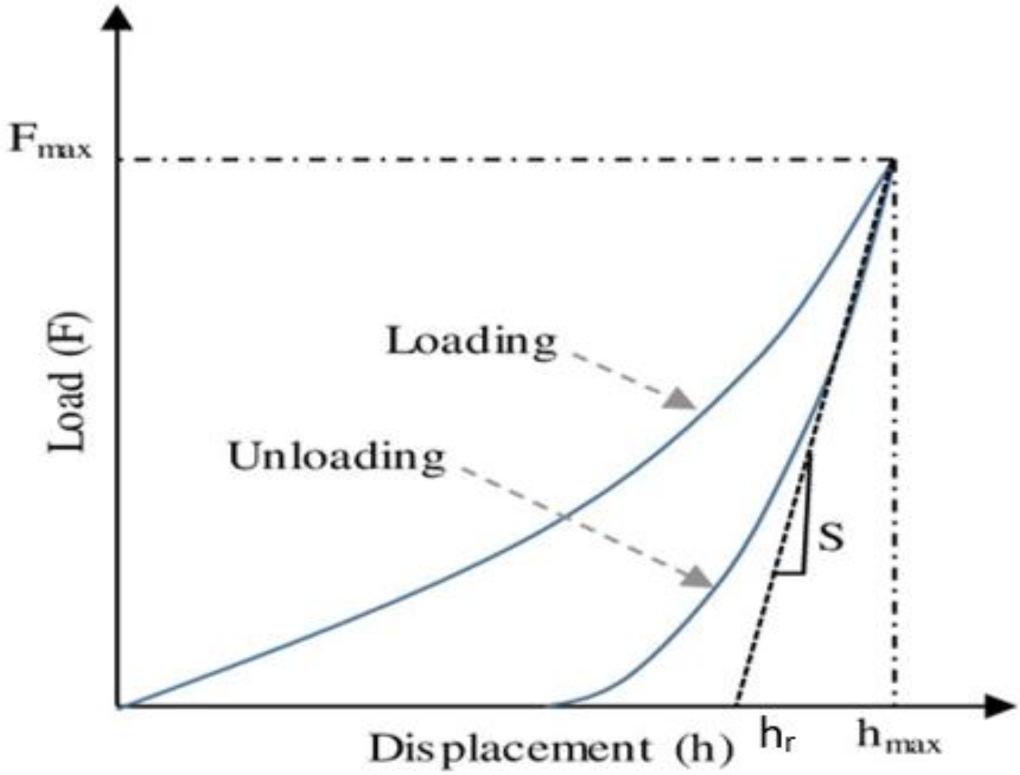

Figure 3.1 Comparing mechanical properties of Al 6061 and Al 7075 alloys.

3.2.1.1 Instrumented micro-indentation test at different max. loads

The Instrumented micro-indentation measurements were carried out on the metallographically prepared samples [28] of aluminum alloy 6061 using FISCHERSCOPE HM 2000 S micro-hardness tester equipped with a Vickers pyramidal indenter. In order to determine the effect of indentation load, multiple indentation measurements under several loads varying from 500 mN to 1750 mN were applied to the aluminum samples. Indentation load rate 50 mN/sec. was used to perform all measurements.

The obtained data from each indentation load test were analyzed, and the mean indentation curves recorded. Figure 3.2 demonstrates a series of load- penetration depth plots recorded at different maximum loads of Al 6061 alloy. The mean indentation curves are shown in figure 3.2 reveals the elastoplastic deformation during Vickers indentation for Al 6061.

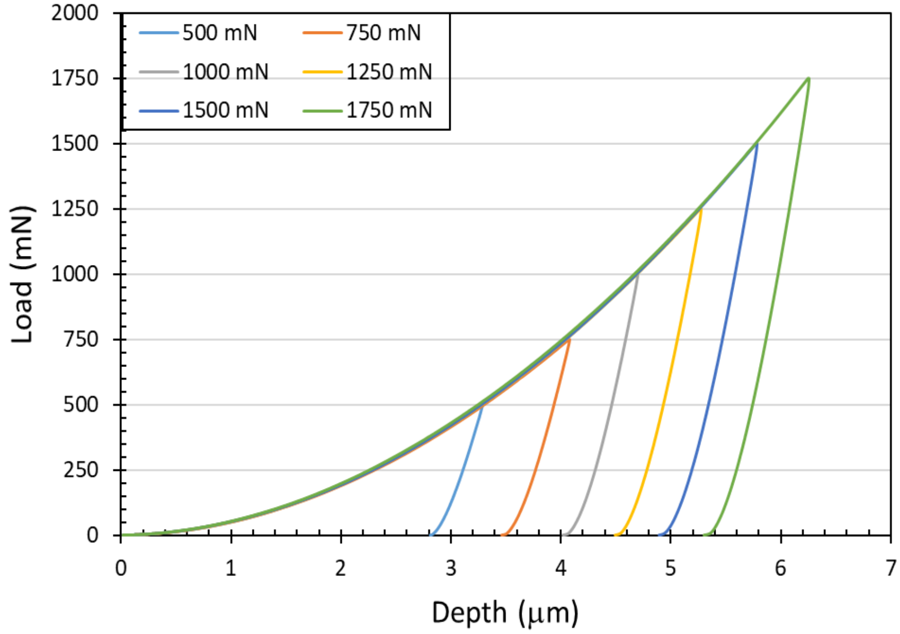

Figure 3.2 Load – depth curves of Al 6061 under different indentation loads.

The above figure also demonstrates that with the increase in the indentation load, both the maximum depth (h_{max}) and the residual depth (h_r) increase. The Vickers hardness (HV) is plotted as a function of the indentation load for the Al 6061 alloy, as shown in figure 3.3.

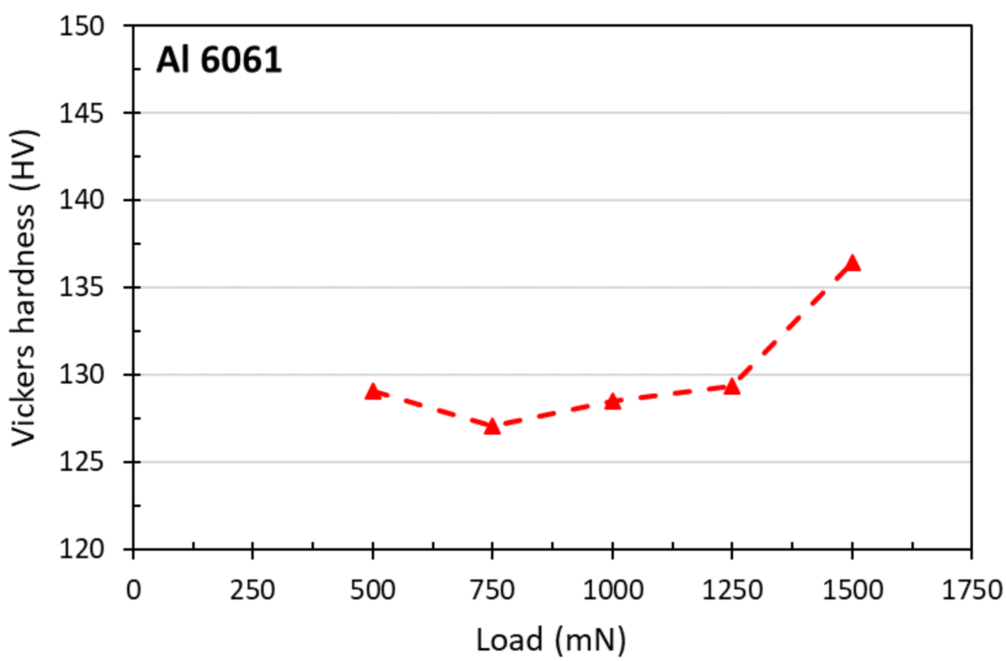

Figure 3.3 Relationship between the Vickers hardness (HV) and indentation load for Al 6061 alloy.

It is clear that the indentation loads ranging from 500mN to 1250 mN have no substantial effect on the Vickers' hardness. However, when the indentation load exceeds 1250 mN, a significant effect on the indentation responses observed since Vickers hardness (HV) alters substantially.

Taking into the account the Vickers hardness (HV) response to the varying indentation load, it was concluded that the indentation load of 1250 mN would be a maximum indentation load. This indentation load can be used without having any significant effect on surface damage, with the size of the indentation. In conclusion, the indentation load of 1250 mN at the load rate of 50 mN/sec was chosen for further instrumented micro-indentation measurements.

3.2.1.2 Micro-hardness and surface roughness test procedures

For the current experimental procedures, six metallographic specimens of Al 6061 alloy were prepared using the ASTM E3 standard [27]. According to the standard, every prepared sample was ground and polished with silicon carbide papers at different grit sizes by using LECO VP-160 variable speed polisher. Each metallographic sample was ground or/and polished to a certain level to accomplish differing surface roughness, and the details appear in table 3.1.

Table 3.1 Polishing details of aluminum 6061 alloy samples.

Al 6061 Samples	**Ground / polished up to**
02	220 Grit
03	320 Grit
01	400 Grit
06	600 Grit
05	Polishing paste 5 μm
04	Polishing paste 1 μm

All the samples prepared have measured for surface roughness by using a non-contact optical interferometer ZeGageTM Pro. As displayed in figure 3.4 and reviewed in section 1.4, two roughness parameters, average arithmetic height (Ra) and Root mean square roughness (Rq), have been evaluated. Six to seven measurements have been taken to calculate the average surface roughness. Following figure 3.4 illustrates the surface roughness profile, Ra, and Rq values for Al 6061 - 02 sample.

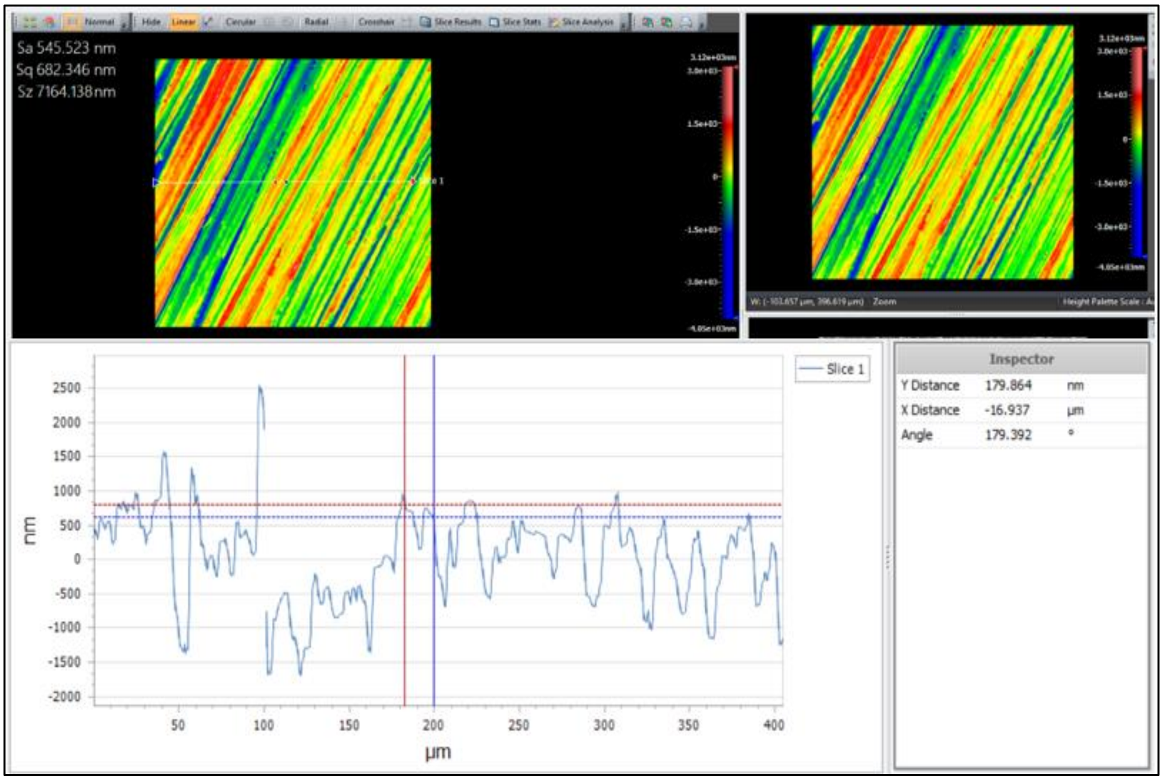

Figure 3.4 Surface roughness measurement of Al 6061 – 2 ground with 220 grit silicon carbide paper resulting in the surface roughness "Ra" of 545.5 nm.

Subsequent to the surface roughness measurements, instrumented micro-indentations were carried out to assess the Vickers micro-hardness for given surface roughness. As conferred and determined in section 3.2.1.1, the indentation load of 1250 mN at a load rate of 50 mN/sec under no creep used for micro-indentation measurements. As exhibited in figure 3.5, for every single specimen, seven to eight micro-indentations were carried out, and the average value noted for additional analysis.

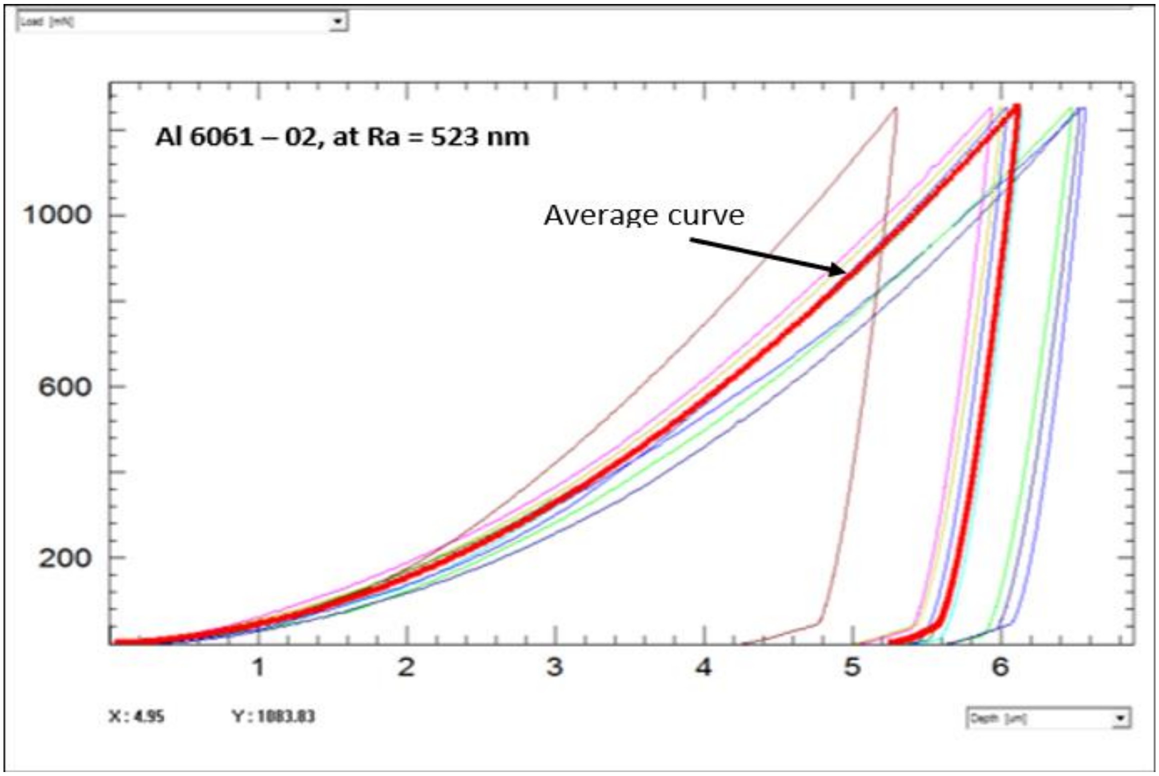

Figure 3.5 Indentation responses and a mean indentation curve as a function of the Indentation load for Al 6061 - 02 at 1250mN/sec for average surface roughness "Ra" of 523 nm.

Figure 3.5 shows the scatter of multiple indentation responses and a mean indentation curve for Al 6061 - 02 alloy, at surface roughness "Ra" 523 nm and "Rq" 674 nm under an indentation load of 1250 mN/sec. Similar experiments performed on other samples of Al 6061 alloy and the data is recorded for future analysis. The detailed results for micro-hardness versus roughness obtained from the above testing are illustrated in chapter 4.

3.2.2 Destructive (fatigue tests) and non-destructive test methods

Cyclic loading is one of the most prevalent service loadings for the majority of the stress-bearing components. In numerical simulations and analysis of their behavior, cyclic properties are required. In general, cyclic properties are often modeled using the Ramberg-Osgood relationship, which is determined from cyclic strain-controlled fatigue testing. However, cyclic strain-controlled testing is time-consuming and expensive. In the present work, non-destructive cyclic micro-hardness indentation has been utilized to examine the practicality to determine the cyclic strain hardening of a given material.

3.2.2.1 *Cyclic micro-hardness indentations (Non-destructive test method)*

For the non-destructive test method, five samples were selected. According to the standard [28], the surface of each as-milled sample was ground using 240 – 600 grit silicon carbide paper followed by final polishing with the 3 μm and 1 μm aluminum oxide compound to achieve mirror surface finish as shown in below Figs. 3.6 (1) and (2).

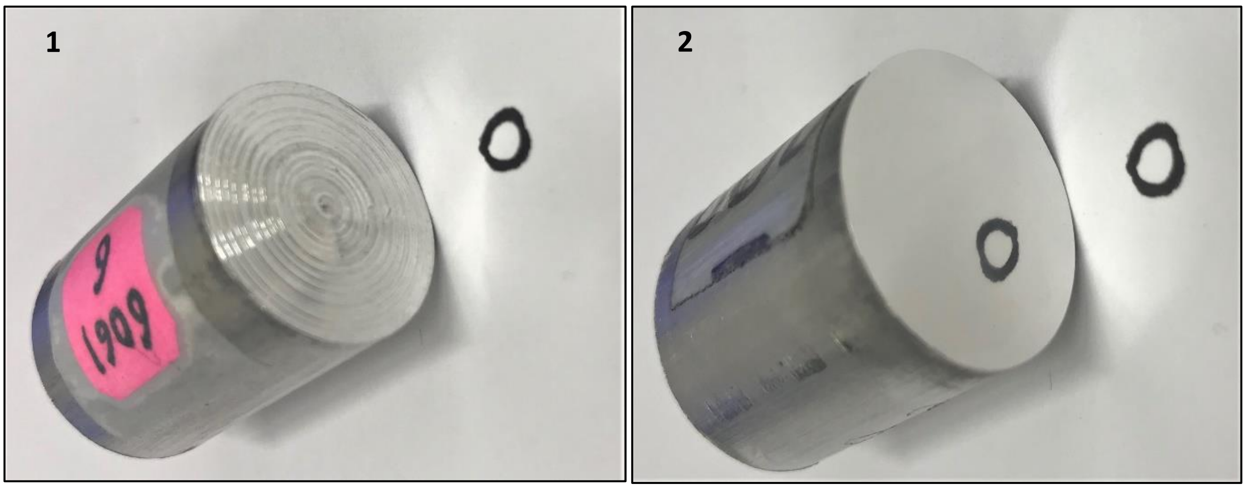

Figure 3.6 Metallographic aluminum 6061 – 06 sample (1) as-milled and (2) after polishing.

Load controlled cyclic indentations have been conducted using Fischer HM200s instrumented micro-indenter at six different maximum indentation load levels of 500, 750, 1000, 1250, 1500, and 1750 mN with a constant loading rate of 50 mN/sec. As shown in figure 3.7 at each indentation load level, 25 cycles have applied during which loading and unloading of the hysteresis loop were recorded. Figure 3.8 displays the second and 25th cycle from the above test. It is clear that with the applied number of cycles, the width of the indentation loop decreases. The obtained loops will be further used to calculate the material response under cyclic micro-indentations.

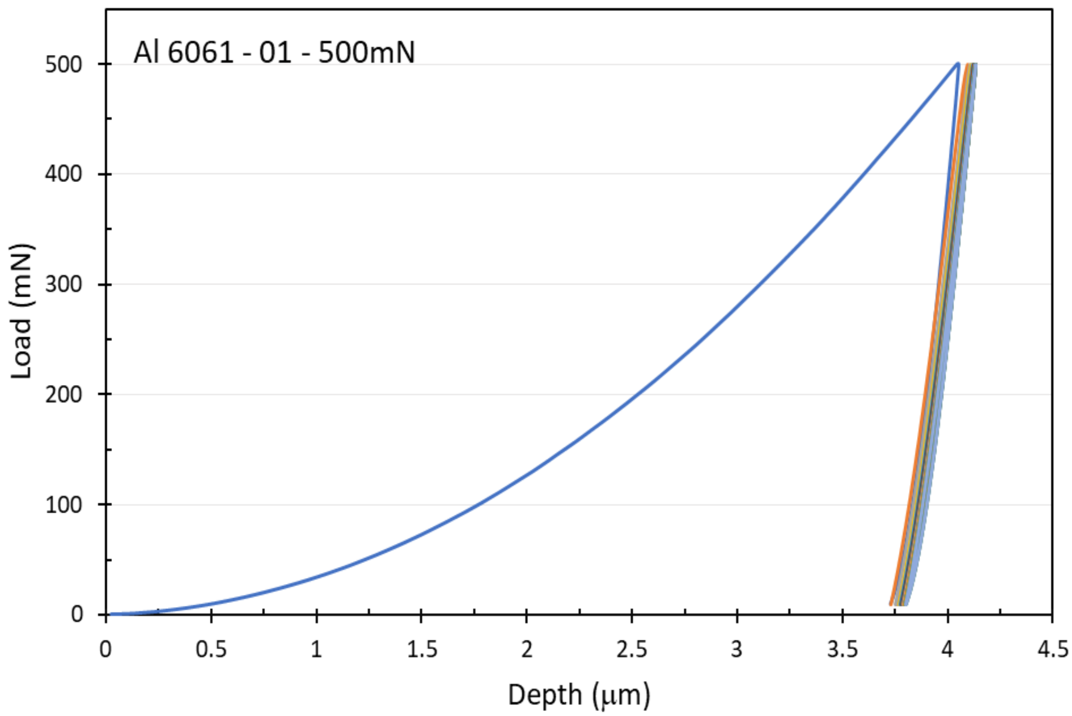

Figure 3.7 Indentation response curve for Al 6061 - 01 displaying 25 cycles applied using load level of 500 mN at 50 mN/sec.

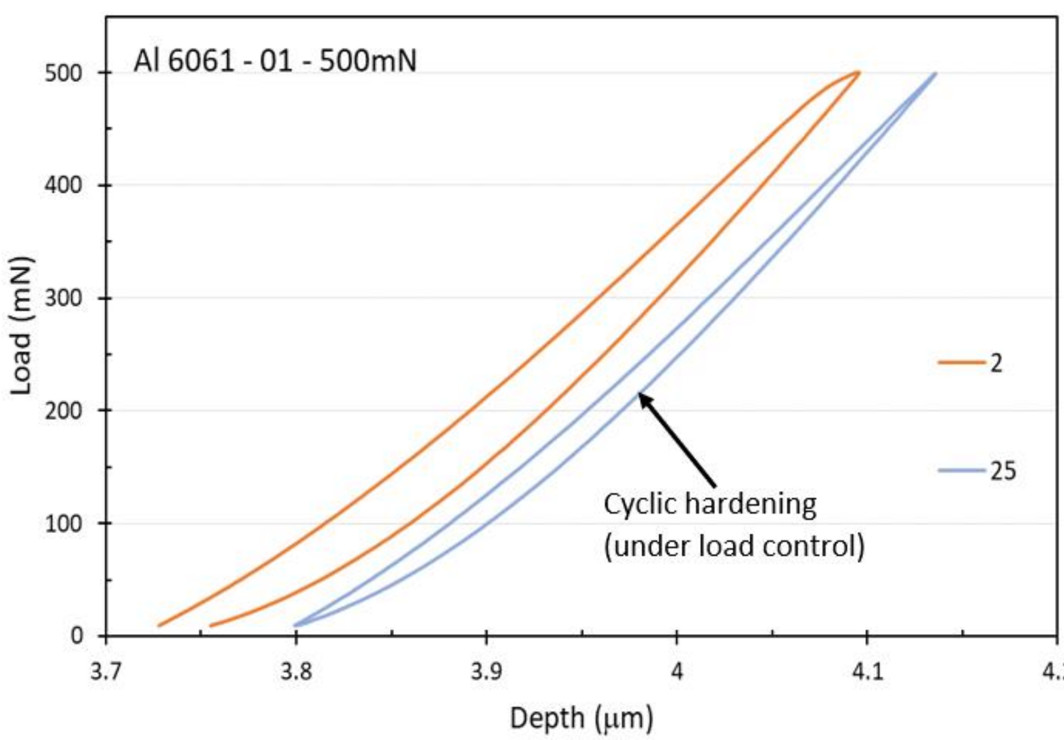

Figure 3.8 Load-depth curve of Al 6061 – 01 at the load level of 500 mN showing the 2nd and 25th cycle.

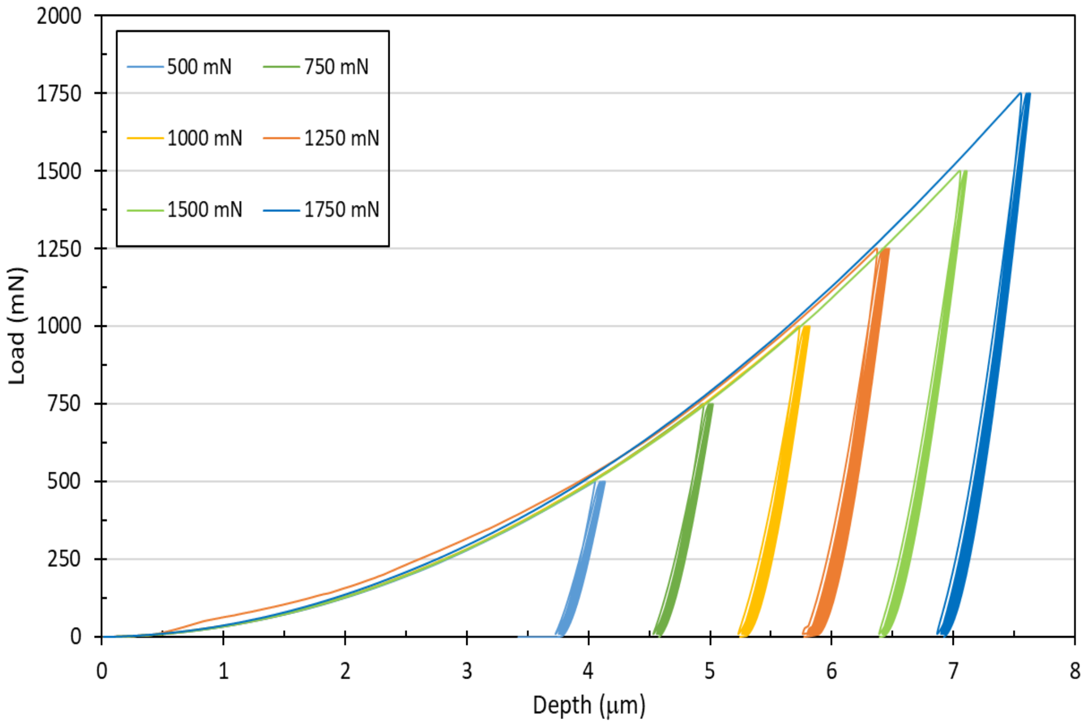

Figure 3.9 Combined indentation response curves of Al 6061 exhibiting 25 cycles for each max load levels ranging from 500 to 1750 mN applied at 50 mN/sec.

The above figure 3.9 illustrates the 25 indentation response curves at all maximum load levels. As the indentation load increases from 500 mN to 1750 mN, penetration depth also increases. For every load level, the width of each indentation loading-unloading curve was measured for further analysis. Simultaneously, the obtained loading-unloading curves were used to determine the material properties and to develop a correlation between the destructive and non-destructive test methods. The resulted findings are explained in chapter 4.

3.2.2.2 Cyclic strain-controlled tests (Destructive test method)

According to ASTM standard E606/E606M-12 [10], cyclic strain-controlled tests were designed for Al 6061 alloy. All experiments were carried out at room temperature using an axial extensometer under strain control at 0.5 Hz under fully reversed (R=-1) loading until failure. Strain amplitudes tested were 0.005 mm/mm, 0.01mm/mm and 0.02mm/mm were selected. Failure of the cyclic strain-controlled test was defined as a 50% drop in the peak stress amplitude achieved.

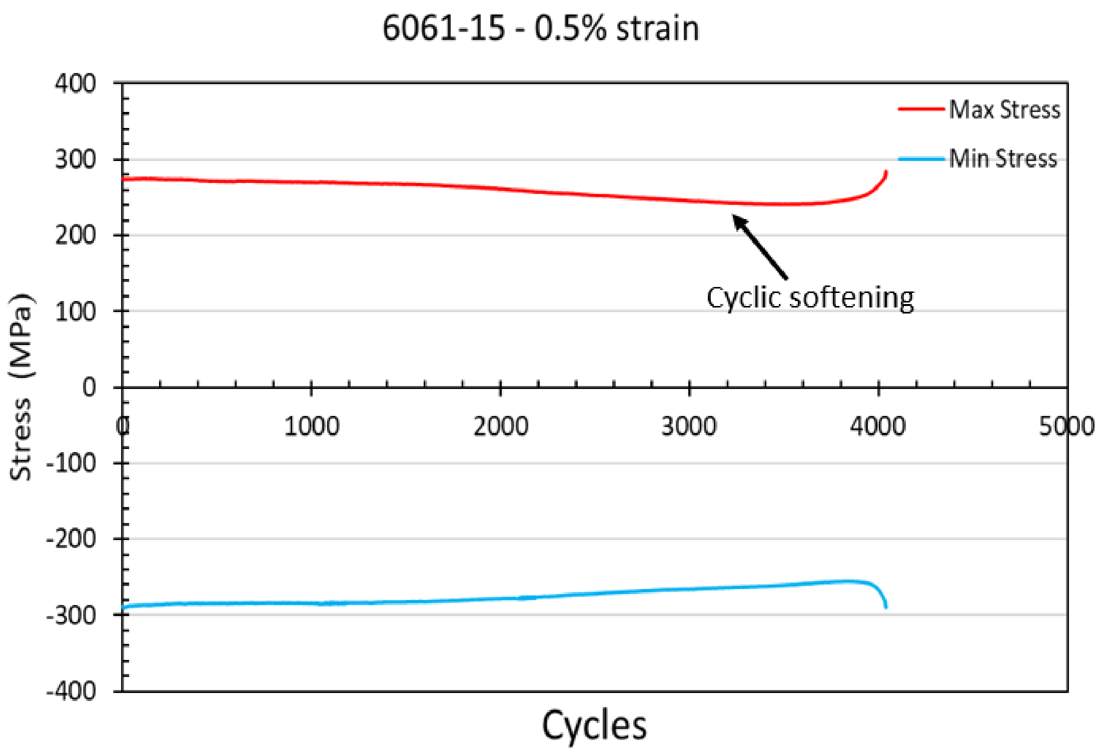

Figure 3.10 Stress-cycle plot for Al 6061 – 15 at 0.005 mm/mm strain amplitude.

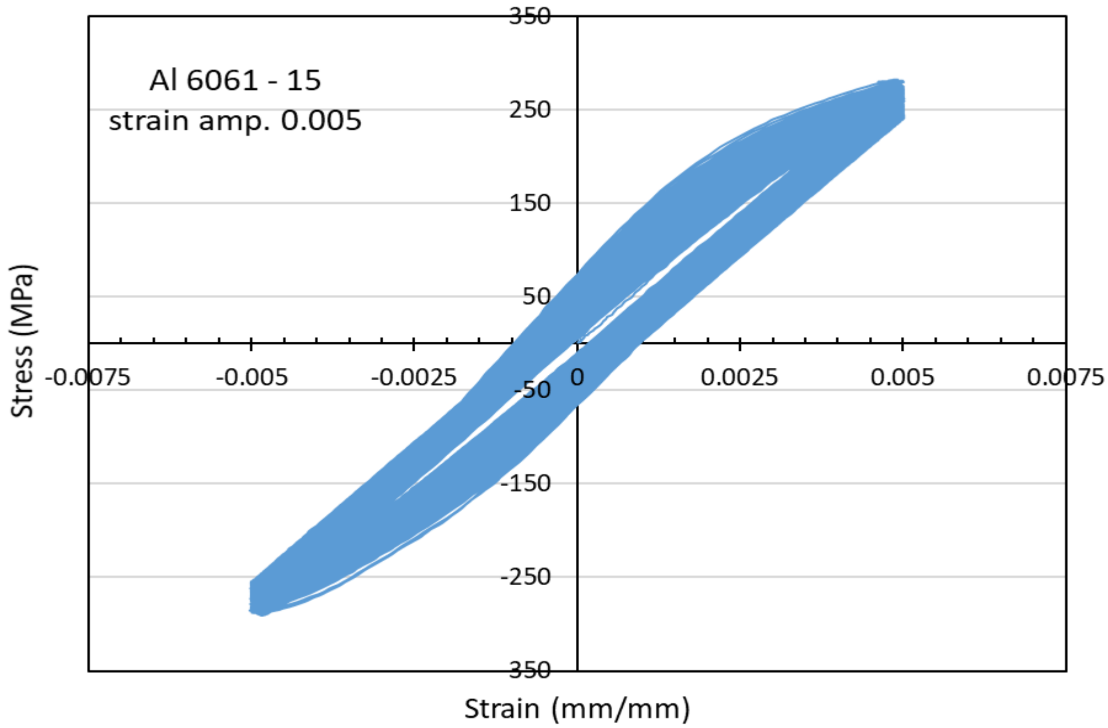

Figure 3.11 Hysteresis loop for Al 6061 – 15 at 0.005 mm/mm strain amplitude.

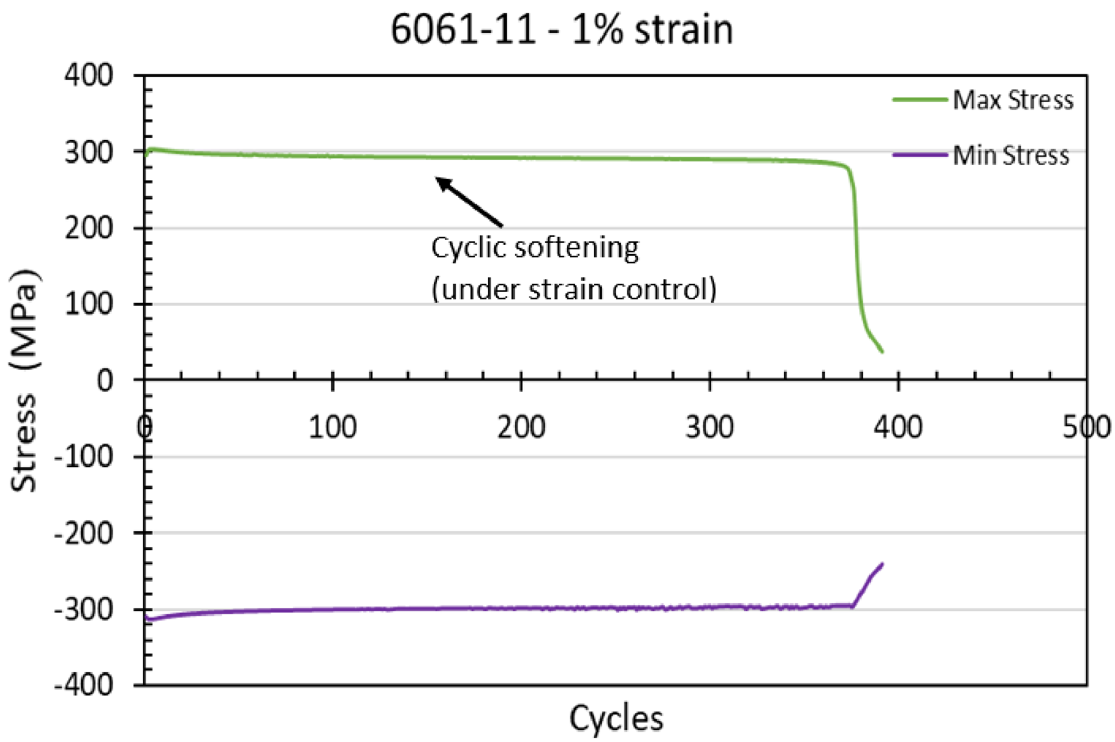

Figure 3.12 Stress-cycle plot for Al 6061 – 11 at 0.01 mm/mm strain amplitude.

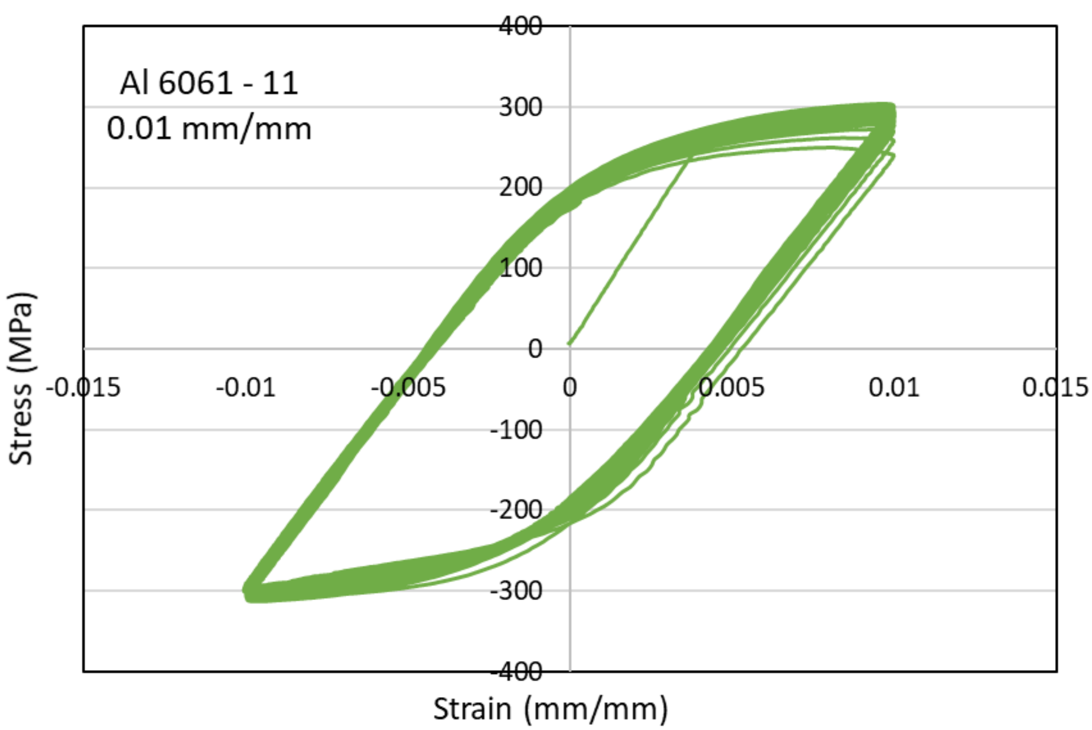

Figure 3.13 Hysteresis loop for Al 6061 – 11 at 0.01 mm/mm strain amplitude.

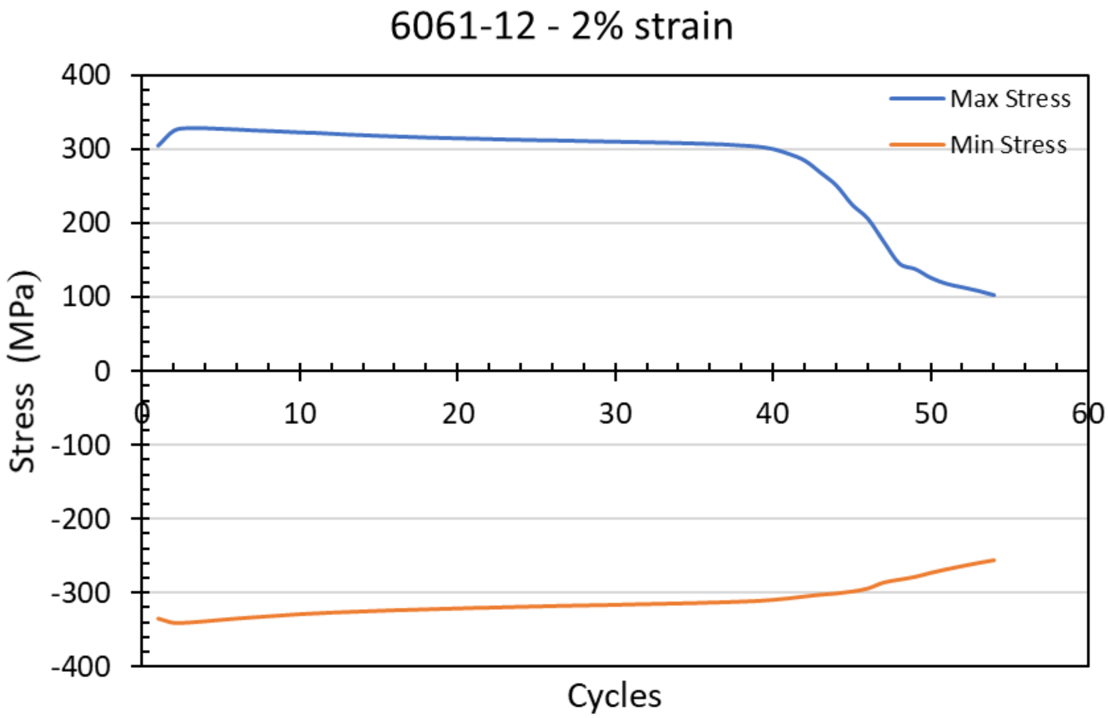

Figure 3.14 Stress-cycle plot for Al 6061 – 12 at 0.02 mm/mm strain amplitude.

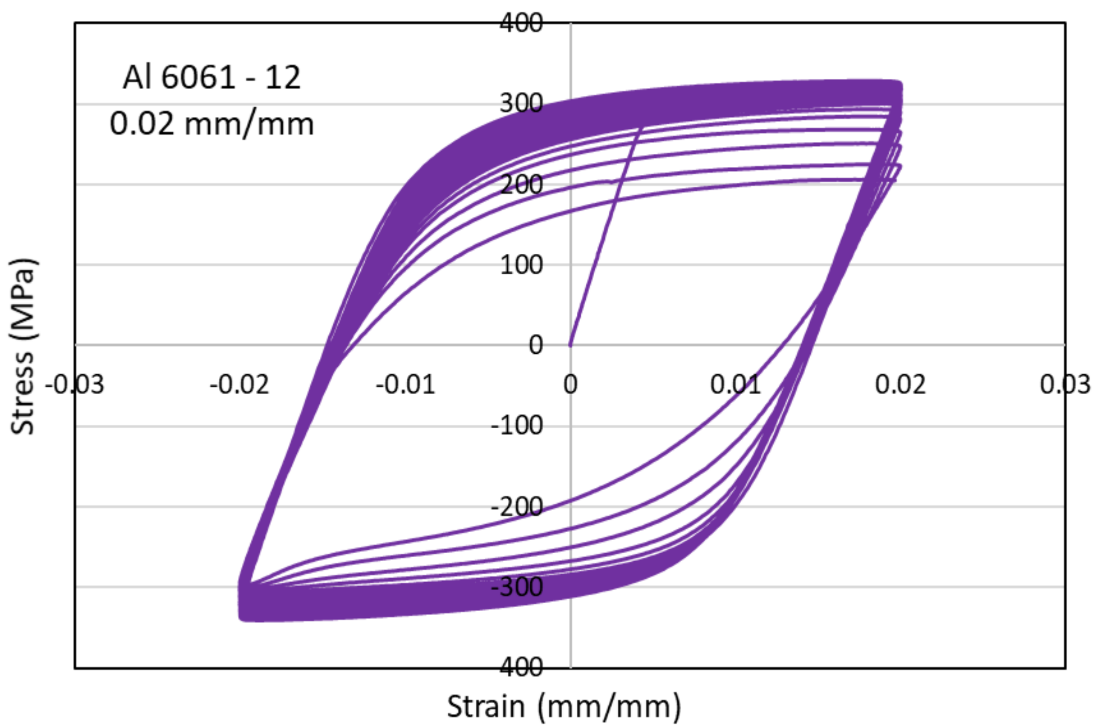

Figure 3.15 Hysteresis loop for Al 6061 – 12 at 0.02 mm/mm strain amplitude.

The obtained test data utilized to plot the maximum and minimum stress vs. the number of cycles. Also, the hysteresis loops were plotted for Al 6061 alloy at different strain amplitudes. The cyclic peak stress-cycle number and hysteresis loops plots are depicted in Figs. 3.10 – 3.15. The above-plotted hysteresis loops were used to calculate plastic strain amplitude (ε_{pa}) as the total width of the loop at mean stress divided by two. The obtained data of peak stress and hysteresis loop were utilized to correlate the cyclic strain behavior with micro-hardness indentation.

3.2.2.3 Cyclic compression tests (Destructive test method)

In a cyclic compression test method, the asymmetric stress-controlled test approach has been chosen. The test was developed to have most of the hysteresis loop in the compression side and rest in the tension, as shown in figure 3.16, to achieve the plasticity in the material. All experiments were conducted at room temperature using an axial extensometer under load control at 0.5 Hz frequency. For every test 3 – 4 stress levels were chosen, the maximum compression stress for all stress levels kept constant, and only tension peak stress was increased.

For each stress level, 150 cycles applied, and the stress values have been laid down from the monotonic curve. The compression stress value was chosen to be the yield stress of the monotonic curve, and the tension stress values were selected so that all the values for it could be below the yield stress. The stress conditions used for the asymmetric stress-controlled test are listed in Table 3.2 and figure 3.16 illustrates the schematics of the designed cyclic compression test method.

Table 3.2 Stress conditions used for the cyclic compression test for Al 6061 alloy.

Compression Stress (MPa)	**Tension Stress (MPa)**	**Applied cycles**
-285	200	150
-285	220	150
-285	240	150
-285	260	150

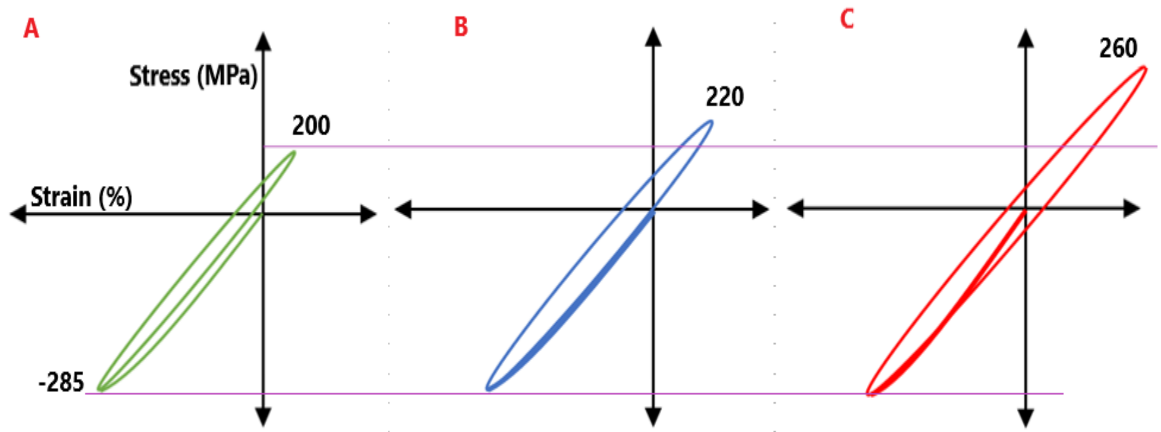

Figure 3.16 Schematics of a designed cyclic compression test showing stress levels (A) -285 to 200 MPa, (B) -285 to 220 MPa, and (C) -285 to 260 MPa.

After performing the tests, the achieved results are plotted as follows on subsequent figures. From the obtained test findings, the width of the hysteresis loop at mean stress was measured; if we recollect, an analogous methodology that was employed in the cyclic micro-hardness indentation test method. Half of the resulted value of the width of the hysteresis loop is merely the plastic strain amplitude (ε_{pa}).

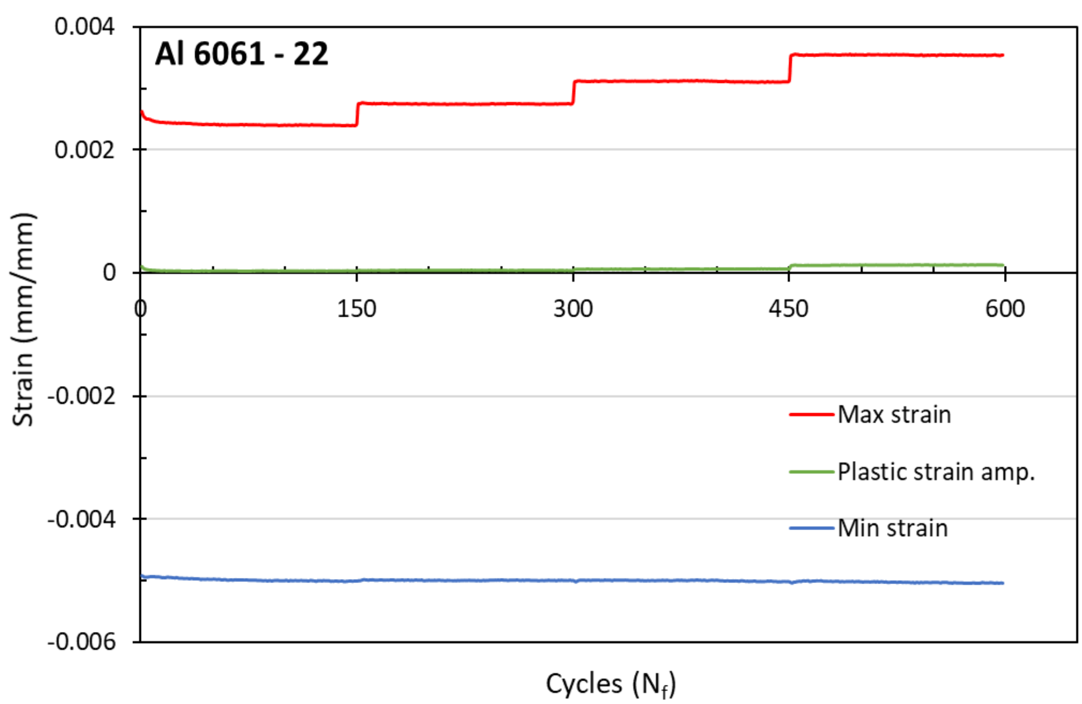

Figure 3.17 Strain – cycle plot showing the maximum, minimum, and plastic strain amplitude as a function of a cycle (N_f) for the Al 6061 – 22.

Figure 3.17 displays the calculated plastic strain amplitude (ε_{pa}), maximum, and minimum strain plotted vs. the number of cycles (N_f). The plastic strain amplitude when plotted versus the number of cycles for the Al 6061 – 22, it is noticed that during the first stress level, the material goes under plastic deformation, and then it stabilizes after a certain number of cycles, as illustrated in figure 3.18.

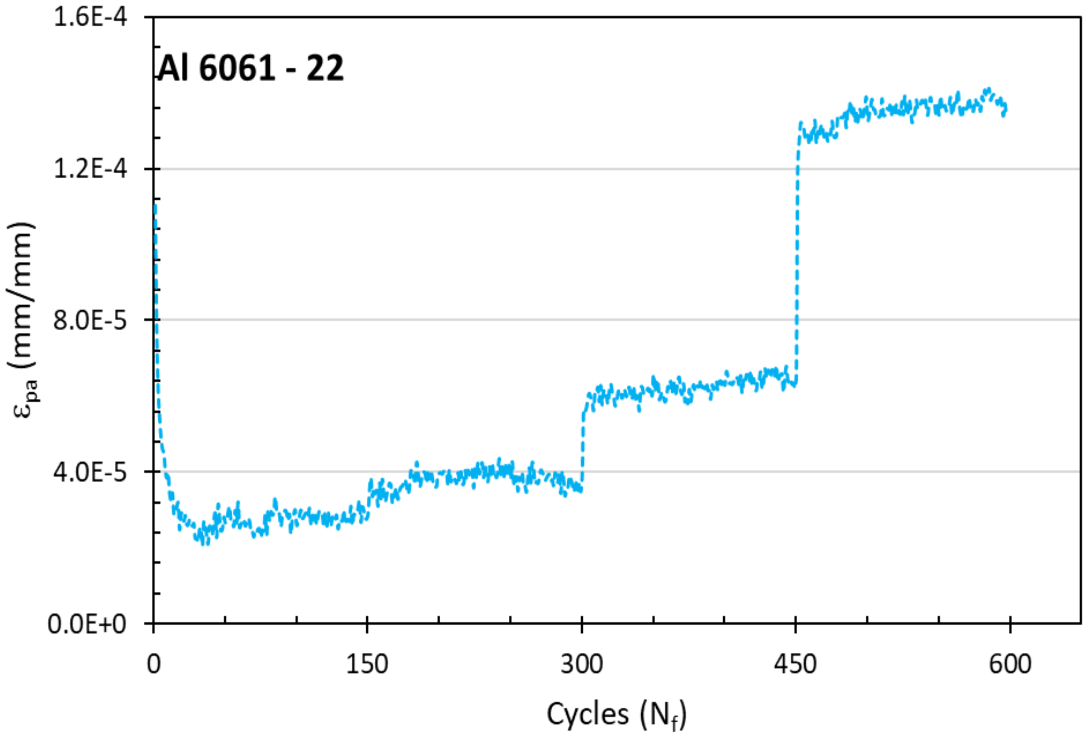

Figure 3.18 Plastic strain amplitude (ε_{pa}) vs. the number of cycles (N_f) for Al 6061 – 22.

3.2.3 Fatigue damage characterization based upon the surface parameters (roughness and micro-hardness)

The two samples of aluminum 6061 alloys were selected to characterize the effect of fatigue damage versus surface parameters. All as-milled samples were polished initially by 800 Grit, followed by 1200 and 1500 Grit using cushioned sanding belts. Samples were polished until the surface defects, and scratches in the transverse direction are eliminated to avoid its impact on the fatigue strength of the material. After polishing, samples were then marked with "R" (surface roughness) on one side and "HV" (Vickers micro-hardness) symbol on the other side of the sample, as shown in figure 3.19. The surfaces were marked to avert the influence of micro-indentations on the surface roughness. Figure 3.19 illustrates the two sides of a fatigue test sample marked.

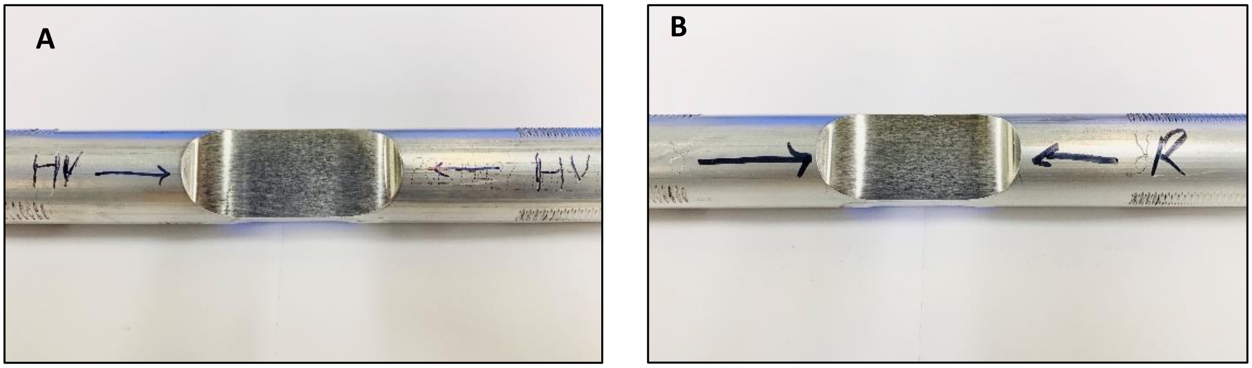

Figure 3.19 Al 6061 specimen prepared for fatigue damage test shows sides (A) for performing micro-indentations (B) for measuring surface roughness.

The strain-controlled fatigue tests using an axial extensometer at 0.5 Hz frequency under fully reversed (R= -1) loading was performed to demonstrate the effect of fatigue damage on the surface parameters. The strain amplitudes of 0.005 mm/mm & 0.01 mm/mm have been chosen. Each test was stopped at certain pre-defined intervals to perform the instrumented micro-hardness indentations, and to measure the surface roughness. All tests were continued until failure or a 50% drop in the peak stress amplitude achieved.

3.2.3.1 Damage test with fully reversed 0.005 mm/mm strain amplitude

Al 6061 – 26 chosen for the experiment. Before running the fatigue test, the benchmark measurements for surface roughness (Ra) and the instrumented micro-indentations have been taken. For surface roughness (Ra), measurements at 5 - 6 different locations were taken, and the average value utilized in the study. Similarly, such as the surface roughness, instrumented micro-indentations were also performed at 6 – 7 various locations, and the mean value was employed.

Following the above measurements, the fatigue test was performed and stopped at certain pre-defined intervals. The computation for the pre-defined life interval was based upon the cyclic strain-controlled test results, as discussed in section 3.2.2.2, and the details are presented in Table 3.3.

Table 3.3 Pre-defined life intervals for Al 6061 – 26 at 0.005 mm/mm strain amplitude showing the number of reversals/cycles to apply.

Al 6061 - 26		
Life Interval (%)	Life in cycles (N_f)	Life in reversals ($2N_f$)
10	380	760
25	950	1900
50	1900	3800
80	3040	6080
90	3420	6840
95	3610	7220
100	3800	7600
until failure	-	-

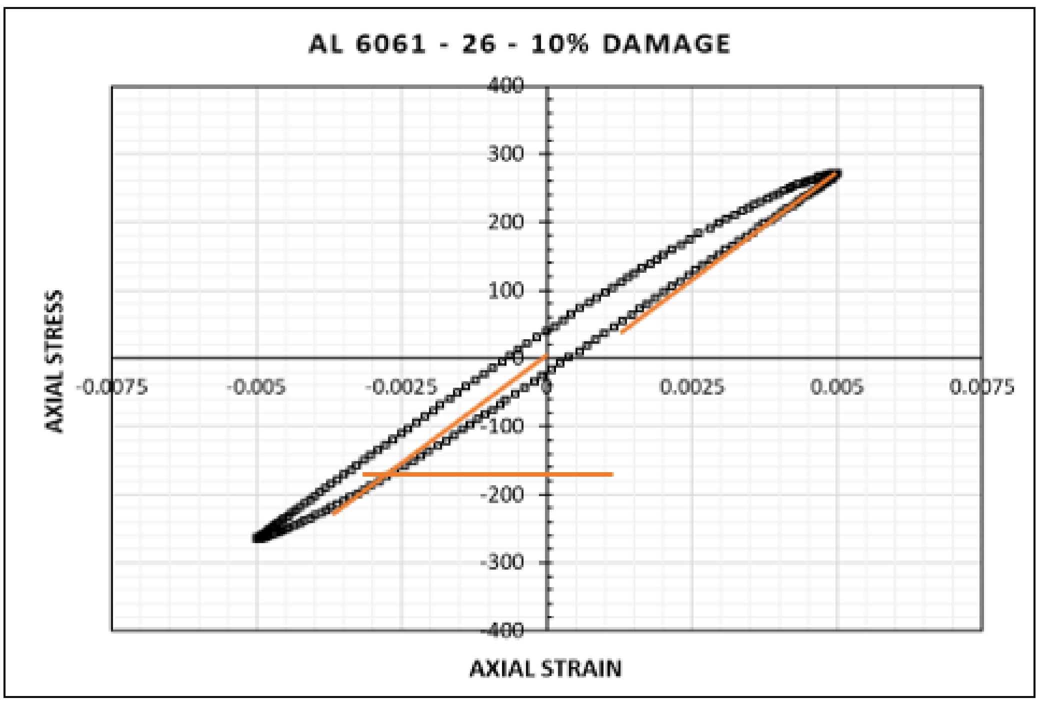

Figure 3.20 Unloading of a sample from determined stress to zero stress and strain for Al 6061 – 26.

Following every cyclic loading interval, a specimen has been manually unloaded to approximate zero stress-strain value under the load control. To do so, the hysteresis loop for the last cycle of each damage interval plotted to find out the slope of the unloading curve. The resulting slope line was drawn from zero stress-strain to locate the compression stress point, as appeared in figure 3.20. Afterward, the sample was unloaded from the maximum stress point to an obtained compression value and then loaded to zero stress-strain points.

The above procedure was conducted to eliminate the residual stresses and plastic strain from the specimens generated during the previous fatigue step. Once completed, the surface roughness measurements and instrumented micro-indentations were carried out, and specimens were again applied to a next cyclic interval. The above-said process ensued until the specimen failure.

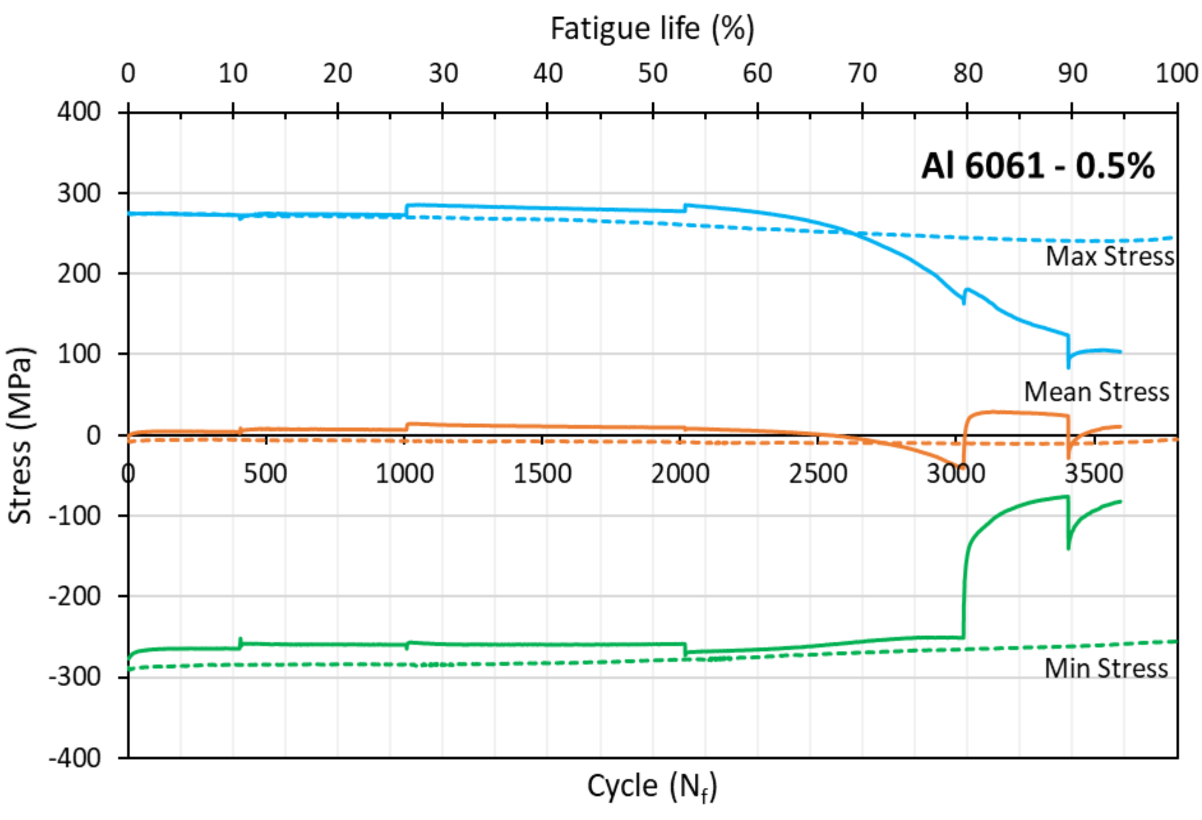

Figure 3.21 Stress (MPa) versus fatigue life (%) for Al 6061 – 26 at 0.005 mm/mm strain amplitude.

The experimental data gained from a cyclic strain-controlled test in section 3.2.2.2, mapped with stress data from the above fatigue damage test as a function of fatigue life in percentile for Al 6061, as demonstrated in figure 3.21. The above plot explains that the fatigue damage test curve follows a similar pattern with the cyclic strain-controlled test curve until 70% of the total fatigue life. Following 70% of total fatigue life, a significant drop observed at peak tension and compression stress. The likely clarification for this substantial peak stress fall could be the crack initiation.

As described earlier, the surface roughness measurements and instrumented micro-indentations were carried out. The mean indentation curves for every fatigue life level plotted in figure 3.22. It was noticed that before applying any number of cycles, maximum penetration depth (h_{max}) found to be 6.444 μm. After applying initial fatigue life, change was spotted in penetration depth. However, the sizable change in depth was seen up to 25% of fatigue life.

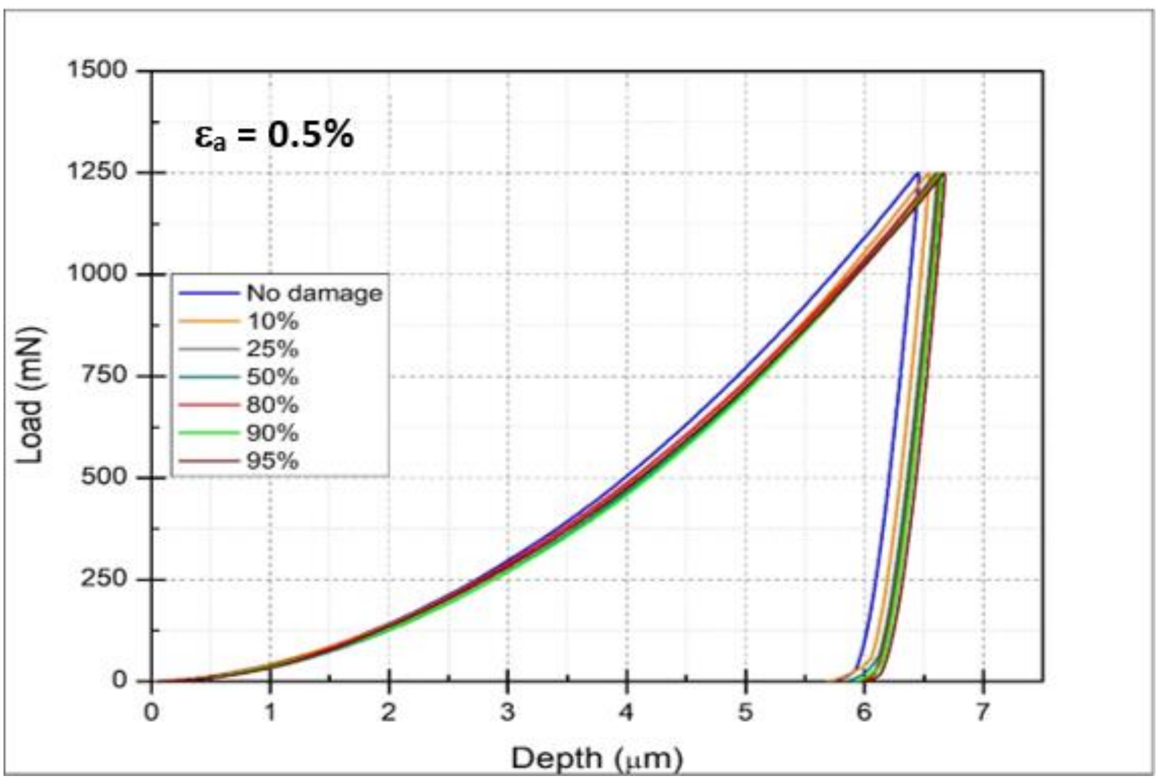

Figure 3.22 Indentation load (mN) versus the mean indentation depth (μm) curves at different fatigue life (%) levels for Al 6061 – 26 at peak load of 1250 mN.

3.2.3.2 Damage test with fully reversed 0.01 mm/mm strain amplitude

Fatigue test under a fully reversed 0.01 mm/mm strain amplitude at 0.5Hz frequency applied on Al 6061 – 31 sample. The test procedure employed was very similar, as described in section 3.2.3.1, except the strain amplitude is changed from 0.005 to 0.01 mm/mm. The life intervals were calculated through the data resulting in a cyclic strain-controlled test for Al 6061 – 11 in section 3.2.2.2, and the details are contained in table 3.4.

Table 3.4 Pre-defined life intervals for Al 6061 – 31 at 0.01 mm/mm strain amplitude showing the number of reversals/cycles to apply.

Al 6061 - 31		
Life Interval (%)	Life in cycles (N_f)	Life in reversals ($2N_f$)
10	38	76
25	94	188
50	188	376
80	301	602
90	338	678
95	357	714
100	376	752
until failure	-	-

Following every life interval sample was unloaded in the identical approach, as described in section 3.2.3.1. Furthermore, the surface roughness measurements and the instrumented micro-indentations performed, and the next life interval was applied. A similar procedure has been repeated until sample failure. The resulted stress – life data from the fatigue test illustrated in figure 3.23, also includes the outcomes from the cyclic strain-controlled test for Al 6061 – 11.

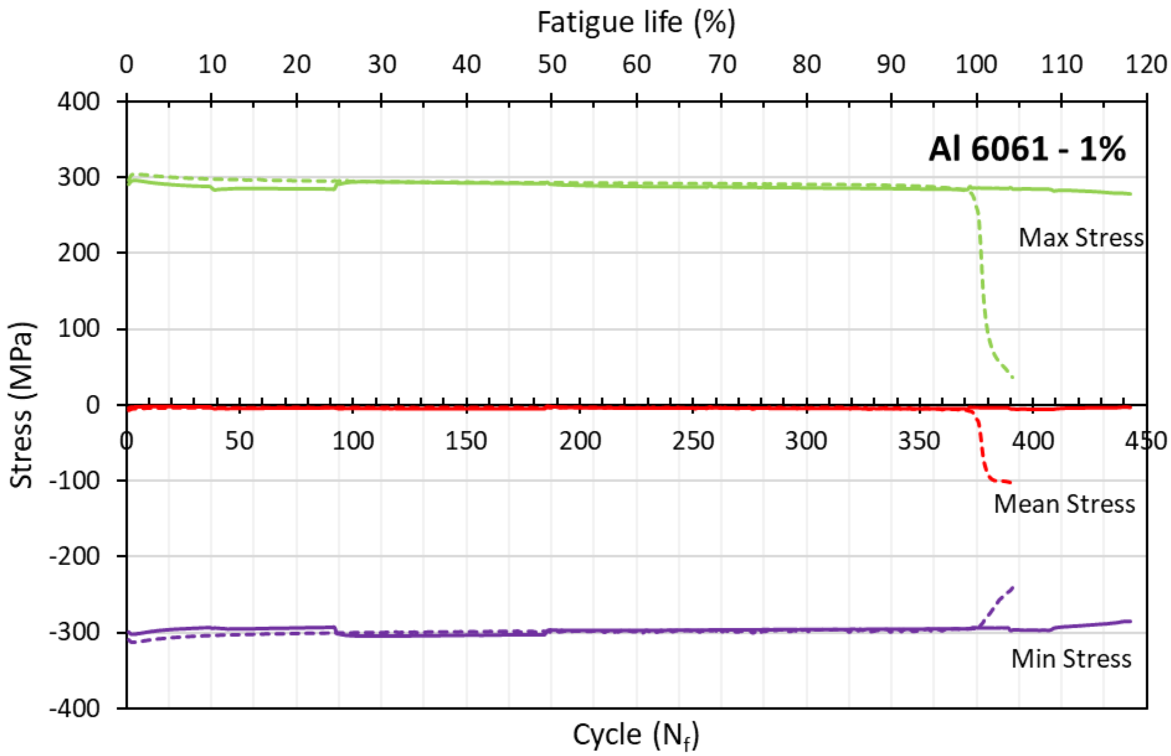

Figure 3.23 Stress (MPa) versus fatigue life (%) for Al 6061 – 31 at 0.01 mm/mm strain amplitude.

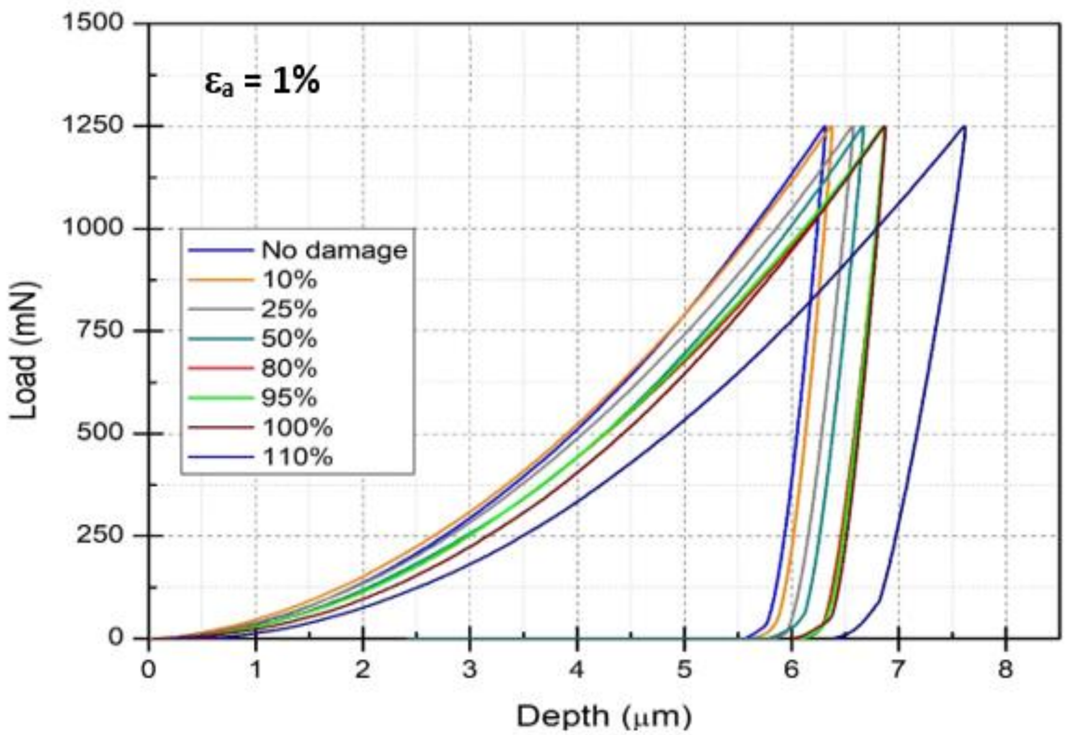

Figure 3.24 Indentation load (mN) versus the mean indentation depth (μm) curves at different fatigue life (%) levels for Al 6061 – 31 at peak load of 1250 mN.

Likewise, the roughness and instrumented micro-indentations completed. Figure 3.24 illustrates the obtained results for Al 6061 – 31 sample. As seen above, the maximum penetration depth (h_{max}) progressively increases as the fatigue life was applied. Nevertheless, after 50% of life was applied, the abrupt change in "h_{max} " observed, and after that, no considerable difference was seen until 100% of life. However, following the sample was loaded to failure and measured, the "h_{max}" altered drastically, as shown in figure 3.24. The effects of the percentage of fatigue damage on micro-hardness and surface roughness obtained from the above experiments are discussed in chapter 4.

3.3 Test procedures applied to Al 7075

As described in previous sections for Al 6061, similar test procedures applied to Al 7075 alloy.

3.3.1 Micro-hardness as a function of surface roughness for Al 7075

As described in section 3.2.1.1, an analogous test method has been used for determining the maximum indentation load for Al 7075. The achieved results plotted in figure 3.25 shows a minimal reduction in hardness was observed at first soon after hardness is becoming stabilized until it reaches 1250 mN, and again, a slight increase has seen.

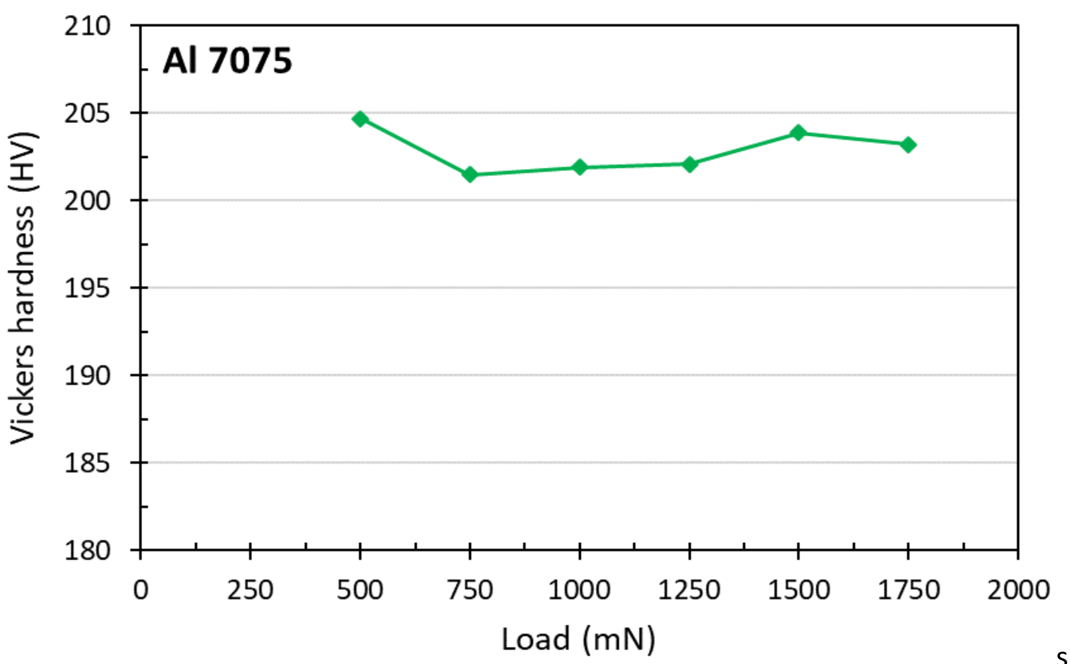

Figure 3.25 Relationship between the Vickers hardness (HV) and indentation load for Al 7075 alloy.

Considering the Vickers hardness (*HV*) response to the varying indentation load, it can be concluded that the indentation load of 1250 mN is a maximum indentation load. This peak load can be applied without having any significant effect on surface roughness. In conclusion, the indentation load of 1250 mN at the load rate of 50 mN/sec carefully chosen to perform further instrumented micro-indentation measurements.

3.3.1.1 Micro-hardness and surface roughness test procedures for Al 7075

Six metallographic specimens prepared for Al 7075 alloy using the ASTM E3 standard [27] and, as explained in section 3.2.1.2. Specimens were ground or/and polished to a particular level for which the details are listed in table 3.5.

Table 3.5 Polishing details of aluminum 7075 alloy specimens.

Al 7075 Samples	**Ground / polished to**
01	220 Grit
06	320 Grit
02	400 Grit
04	600 Grit
05	Polishing paste 5 μm
03	Polishing paste 1 μm

As shown in figure 3.26, two surface roughness parameters arithmetic average height (Ra) and Root mean square roughness (Rq) have been evaluated. For every average roughness measurement, six to seven data points were taken. Figure 3.26 illustrates the roughness profile of the scan and the generated values for Ra and Rq. It also shows the high and low roughness spots with red and blue colors. Similar measurements have been taken for all other specimens, and roughness values noted down for further analysis.

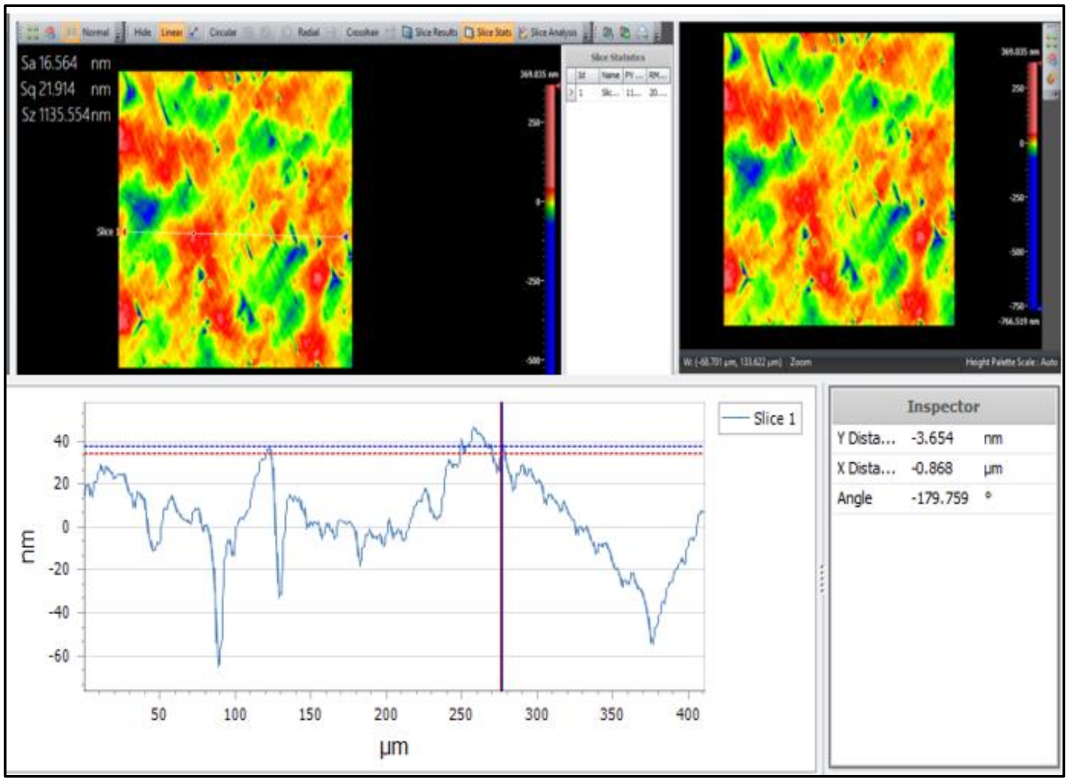

Figure 3.26 Surface roughness measurement of Al 7075 – 03 polished to 1μm with alumina slurry resulting in the surface roughness "Ra" of 16.6 nm.

As discussed earlier, instrumented micro-indentations performed to evaluate the Vickers hardness of the specimen. Indentation load of 1250 mN at a load rate of 50 mN/sec with no creep used for micro-indentation measurements. As shown in Figs. 3.27 and 3.28, seven to eight micro-indentations conducted, and average value noted for additional analysis.

Scatter of multiple indentation responses for Al 7075 – 03 and Al 7075 – 01 alloy displayed in figures 3.27 and 3.28 below. A noticeable difference discovered in scatter, a sample ground with 220 grit, had more scatter than a sample polished with 1mm alumina slurry. The potential cause for scatter could be the surface irregularities formed during grinding and polishing process. The surface irregularities may be lowered by carrying out polishing techniques that help to decrease scatter in the micro-indentation measurements. The results obtained from the above experiments are described in chapter 4.

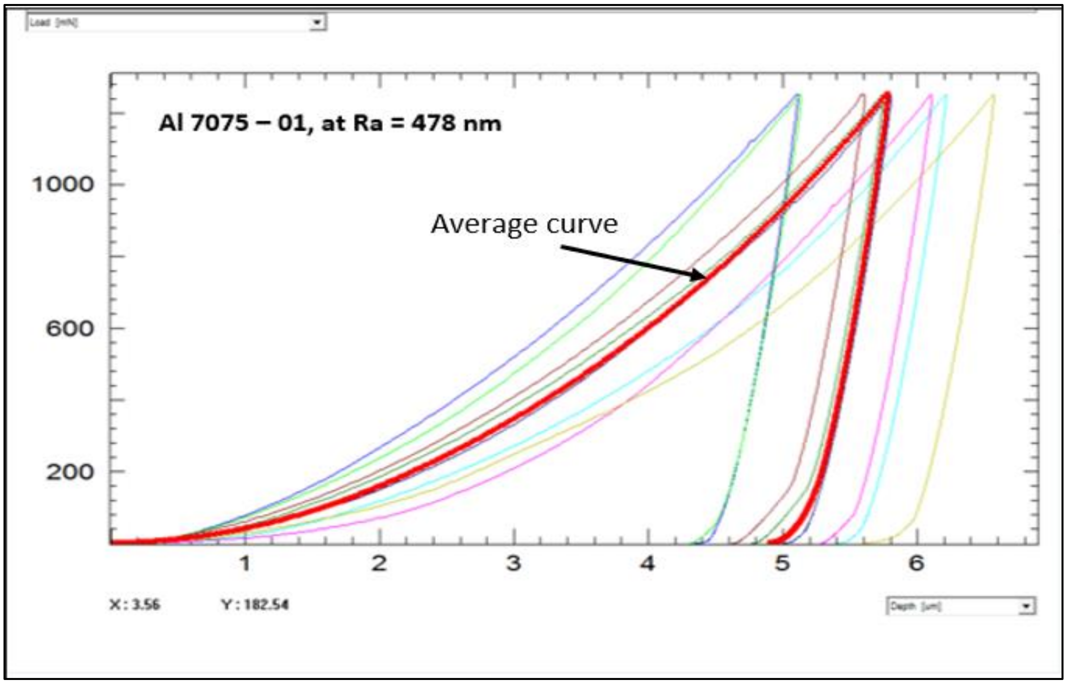

Figure 3.27 Indentation responses and a mean indentation curve as a function of the Indentation load for Al 7075 – 01 at 1250 mN/sec for average surface roughness "Ra" of 478 nm.

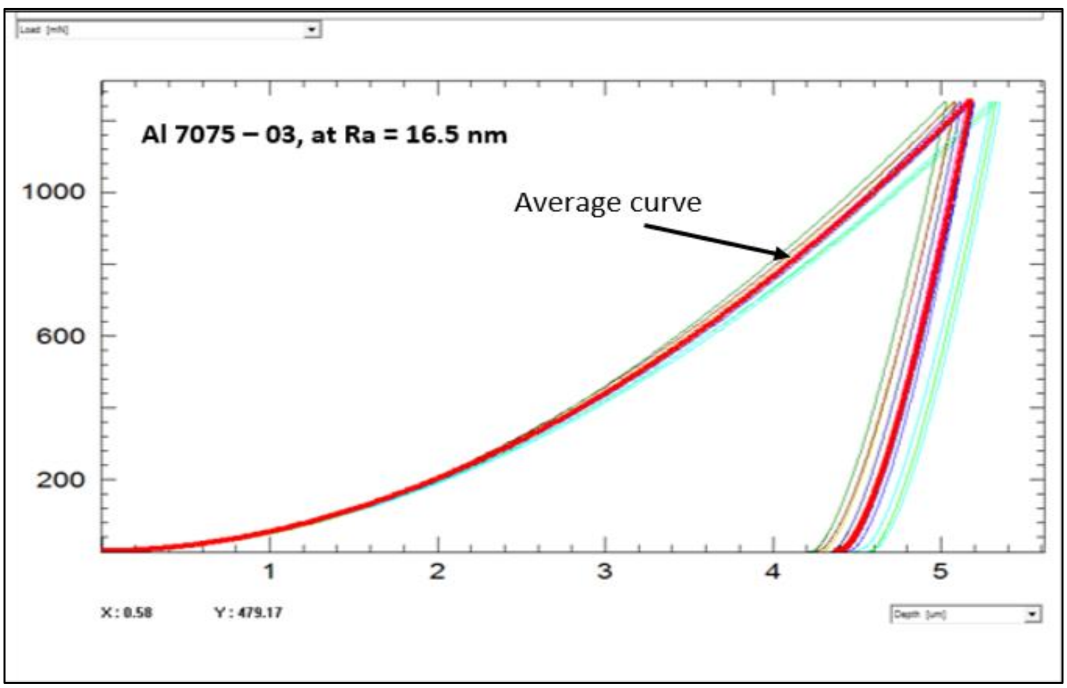

Figure 3.28 Indentation responses and a mean indentation curve as a function of the Indentation load for Al 7075 – 03 at 1250 mN/sec for average surface roughness "Ra" of 16.5 nm.

3.3.2 Destructive (fatigue tests) and non-destructive test methods for Al 7075

3.3.2.1 Cyclic micro-hardness indentations (Non-destructive test method) for Al 7075

Five different specimens of Al 7075 alloy selected for cyclic micro-hardness indentations. A similar test procedure, as described in section 3.2.2.1, is employed. The resulted cyclic indentation responses were recorded and displayed below.

Figure 3.29 illustrates the 25 cyclic indentations performed at a peak load of 1000 mN at the rate of 50 mN/sec on Al 7075 – 01 specimens. The maximum penetration depth (h_{max}) of 4.73 μm has been observed after applying 25 cycles. The hysteresis loops for each cycle were extracted, and the width of loop calculated for additional assessment.

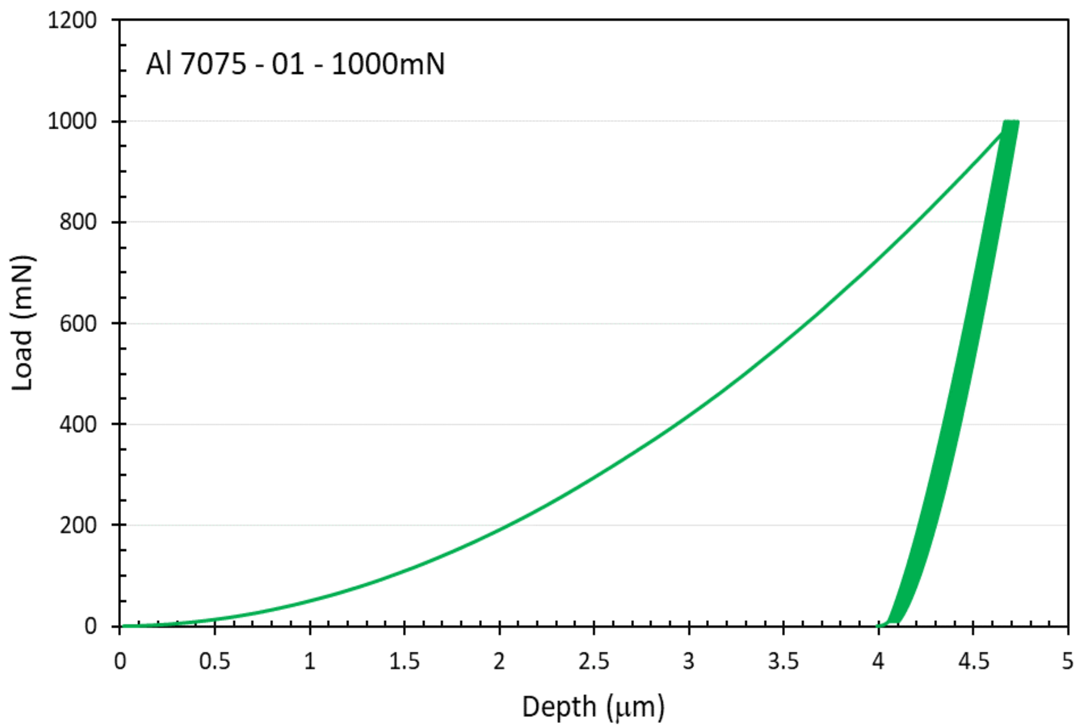

Figure 3.29 Indentation response curves for Al 7075 – 01 displaying 25 cycles applied using load level of 1000 mN at 50 mN/sec.

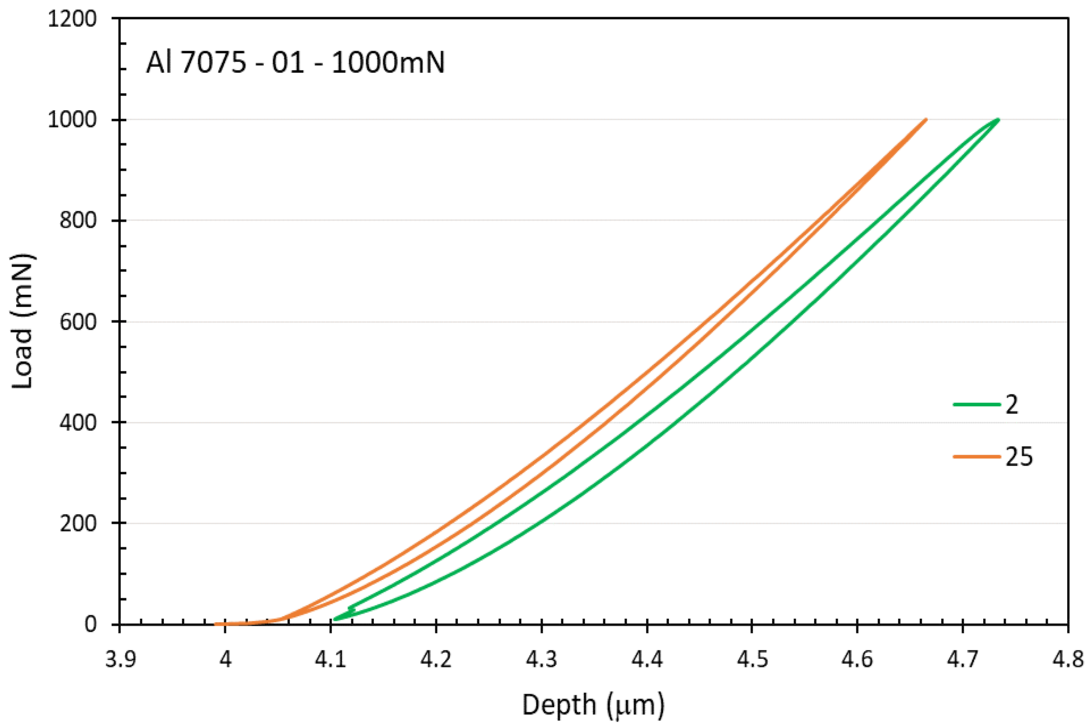

Figure 3.30 Load–depth curve of Al 7075–01 at the peak load of 1000 mN showing the 2nd and 25th cycle.

Two cycles, 2nd, and 25th were chosen from all 25 cycles for closer observation of hysteresis loops. As seen in the above figure 3.30, the second cycle has a much wider loop, whereas 25th cycle has a comparatively narrower loop. Furthermore, the penetration depth (h_{max}) at the second cycle found to be 4.73 μm while at the 25th cycle 4.66 μm. Thus, with an increasing number of cycles, penetration depth and width of the loop were noticed to be lessening.

Similar to a peak load of 1000 mN other load levels were tested, the resulted data is plotted below. Figure 3.31 shows a series of load – depth curves for 500, 750, 1000, 1250, 1500, and 1750 mN peak load levels. With an increase in peak indentation load, penetration depth (h_{max}) is also increasing. Data gathered from all cyclic indentations was utilized to determine the width of the hysteresis loops and subsequently employed for additional analysis, outlined in chapter 4.

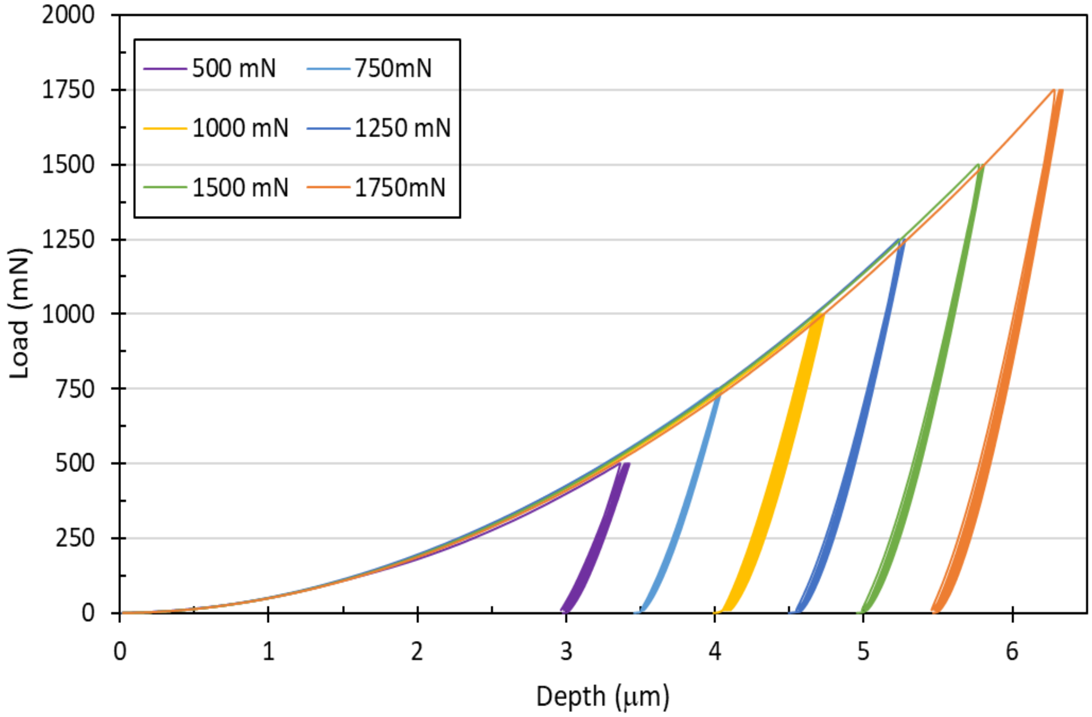

Figure 3.31 Combined indentation response curves of Al 7075 exhibiting 25 cycles for each peak load levels ranging from 500 to 1750 mN applied at 50 mN/sec.

3.3.2.2 Cyclic strain-controlled tests (Destructive test method) for Al 7075

As clarified in section 3.2.2.2, cyclic strain-controlled tests were planned and performed for Al 7075 alloy at three distinctive strain amplitudes. Resulted data is plotted in terms of Stress-life curves and the stress-strain (hysteresis loop), as displayed in Figs. 3.32 – 3.37.

On account of 0.005 mm/mm strain amplitude, tests continued to approximately 7000 cycles. However, cyclic hardening and asymmetry were witnessed in the material. Besides, the 0.01 and 0.02 mm/mm strain amplitude tests lasted to roughly around 600 and 54 cycles, individually and no cyclic asymmetry was detected. Likewise, hysteresis loops have been spotted getting broader as the strain amplitude was heightened.

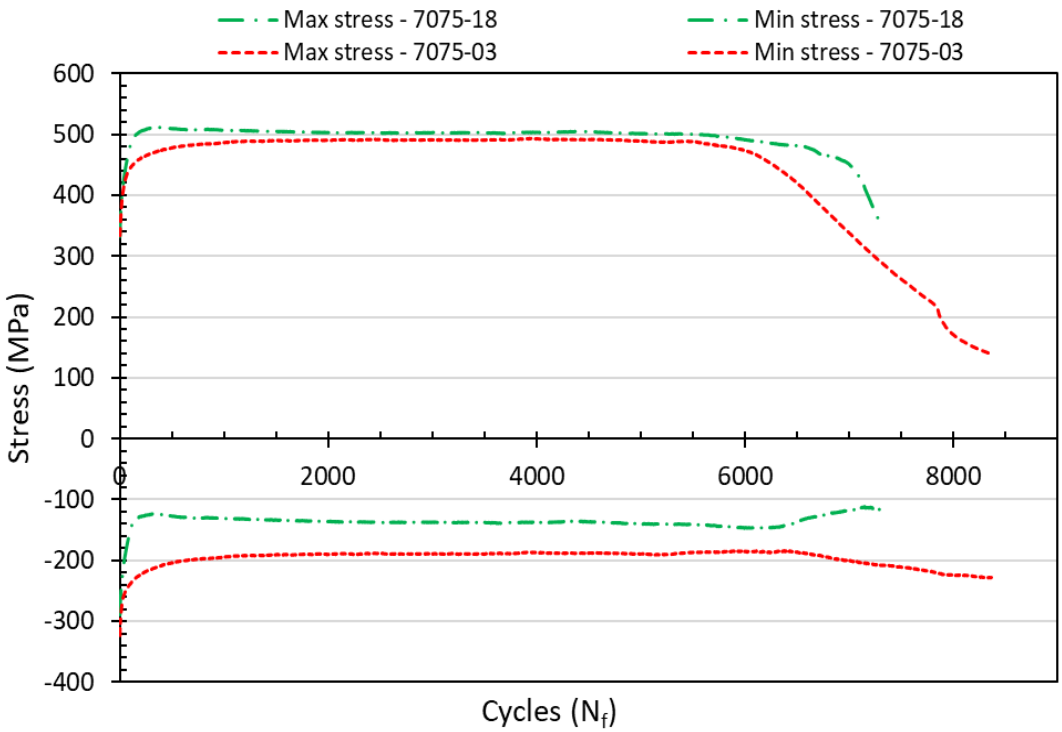

Figure 3.32 Stress-cycle plot for Al 7075 – 18 & Al 7075 – 03 at 0.005 mm/mm strain amplitude.

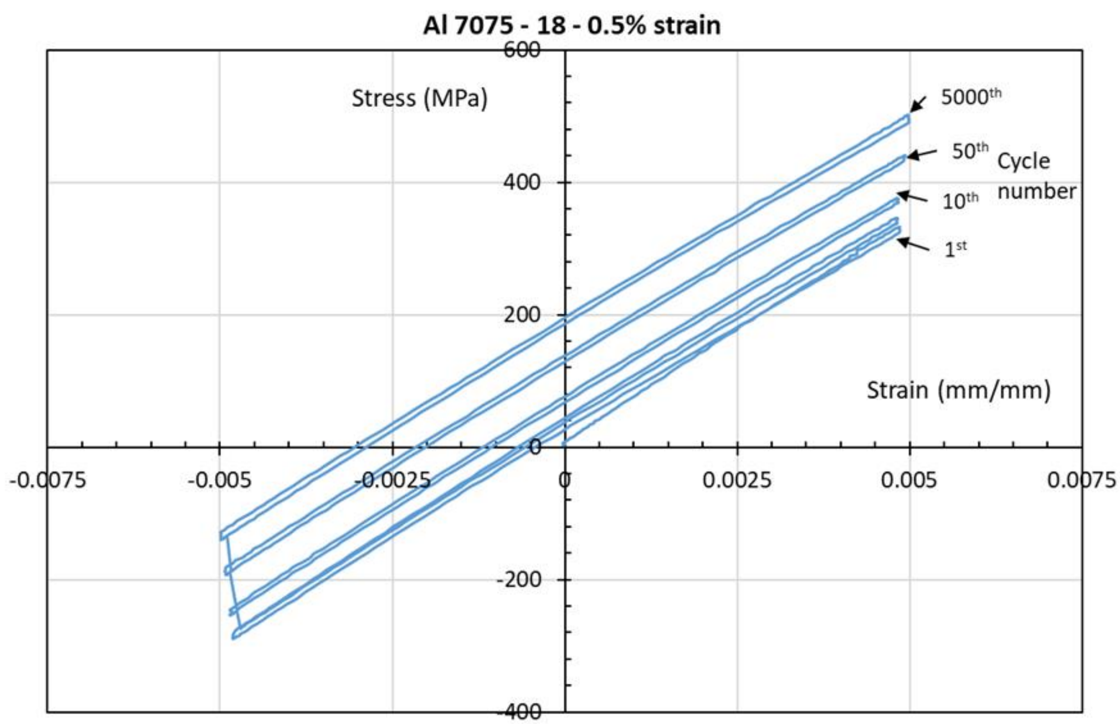

Figure 3.33 Hysteresis loop for Al 7075 – 18 at 0.005 mm/mm strain amplitude.

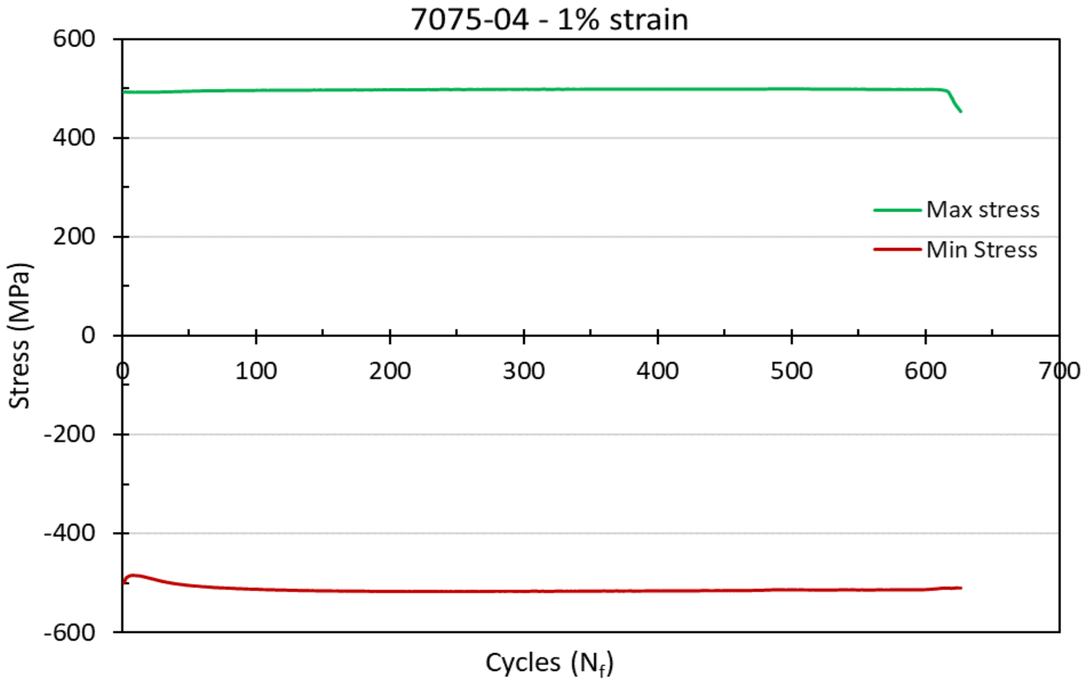

Figure 3.34 Stress-cycle plot for Al 7075 – 04 at 0.01 mm/mm strain amplitude.

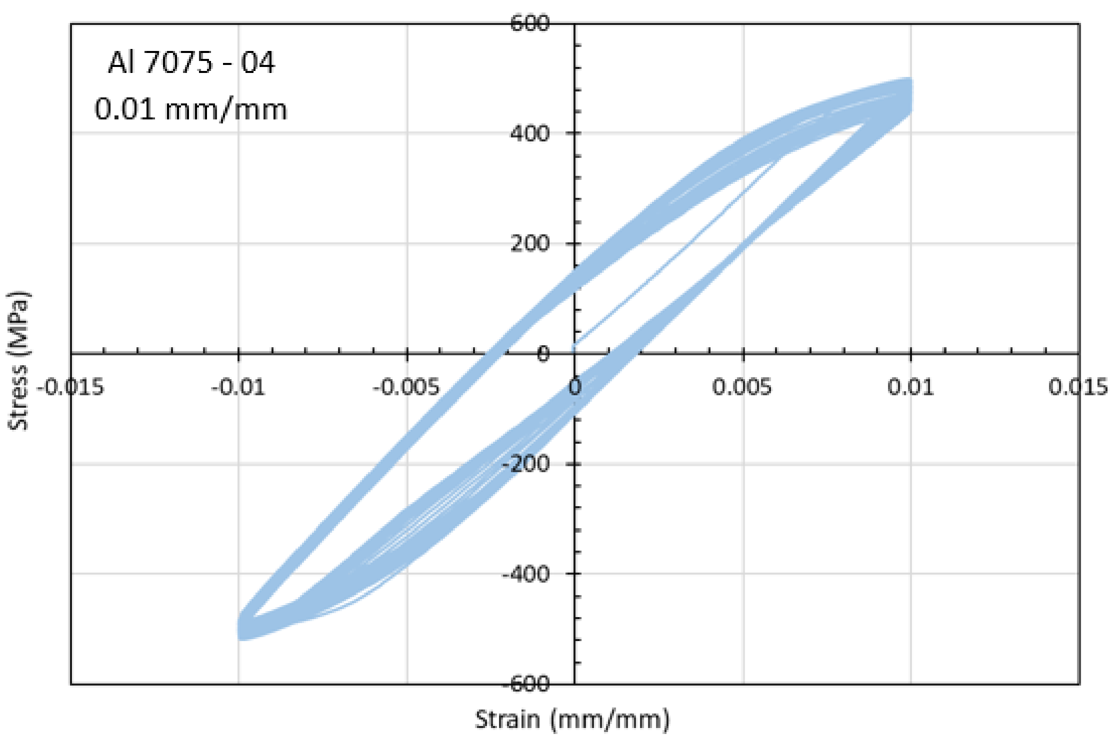

Figure 3.35 Hysteresis loop for Al 7075 – 04 at 0.01 mm/mm strain amplitude.

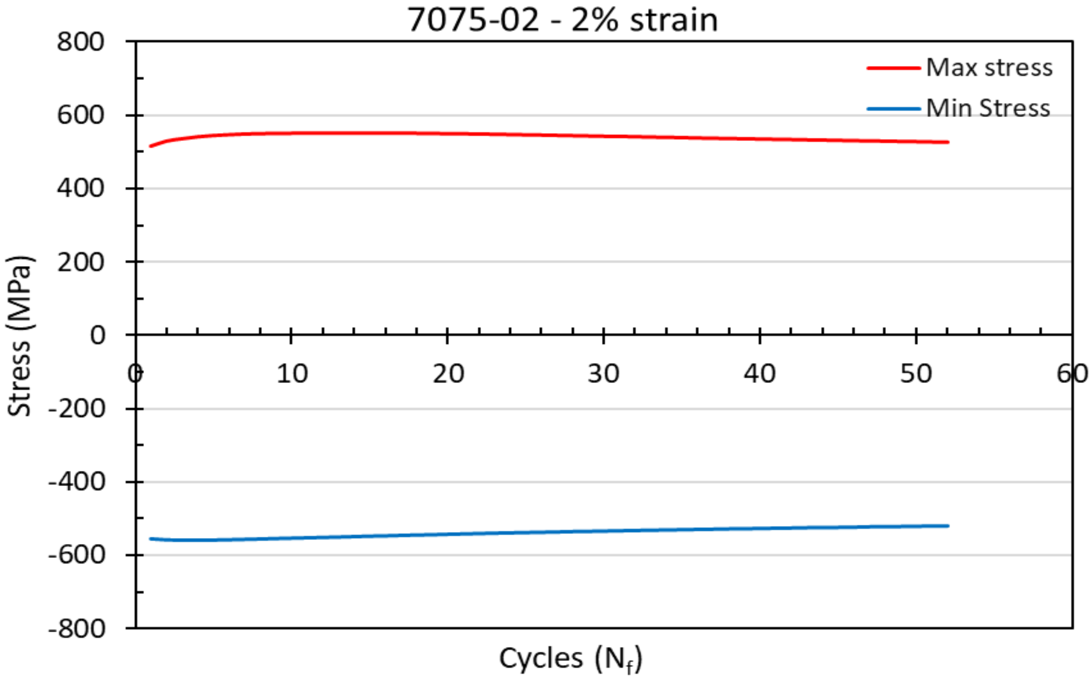

Figure 3.36 Stress-cycle plot for Al 7075 – 02 at 0.02 mm/mm strain amplitude.

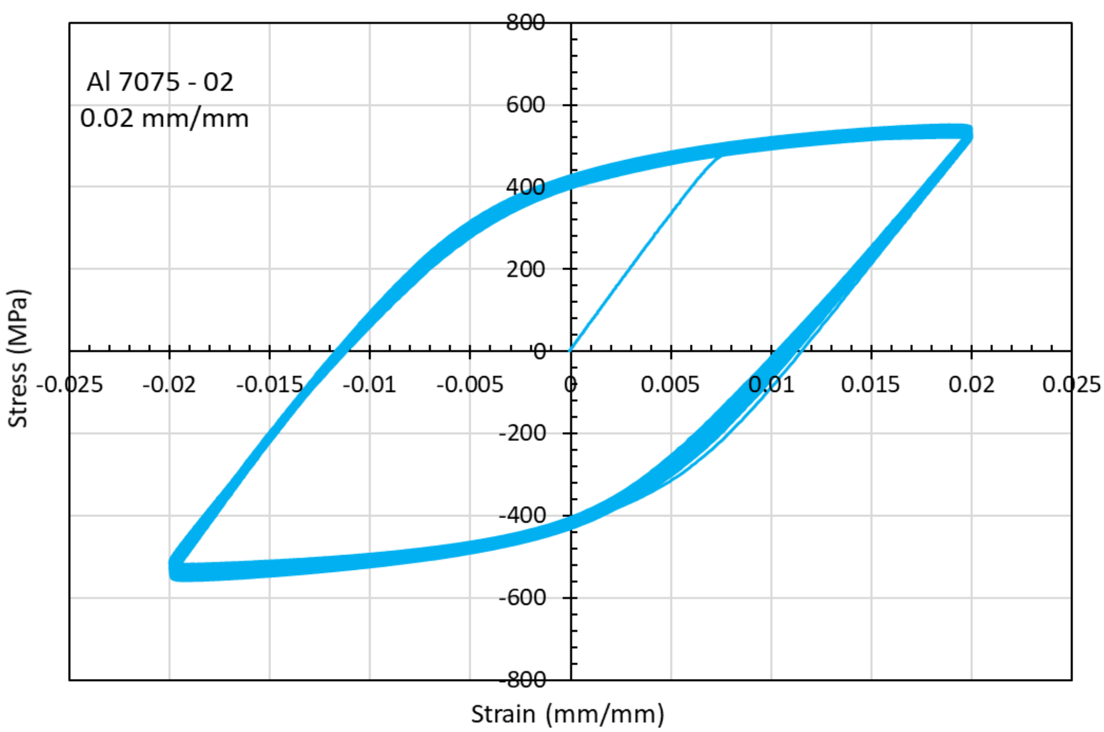

Figure 3.37 Hysteresis loop for Al 7075 – 02 at 0.02 mm/mm strain amplitude.

After studying the above plots, it was discovered that even though the material loaded to symmetric strain amplitudes, cyclic asymmetry in the stress has been noticed. Plots of 0.01 and 0.02 mm/mm strain amplitude illustrates the symmetric response; however, stress – life curves of 0.005 mm/mm strain amplitude reveal asymmetry. Moreover, a hysteresis loop for similar strain amplitude appears to be more of elastic deformation due to which no broader hysteresis loops were seen. Another test was carried and out to validate the results mentioned above, and the outcomes plotted. Gained information has been demonstrated in figure 3.32 for correlation, and as viewed earlier, identical results found.

3.3.2.3 Cyclic compression tests (Destructive test method) for Al 7075

Similar to that of Al 6061, an asymmetric stress-controlled compression fatigue test was planned for Al 7075. Test circumstances were calculated by using the tensile stress-strain curve. As discussed in section 3.2.2.3, stress conditions have been chosen, where compressive stress limit was maintained consistent, and nothing but tensile stress was increased after applying 250 cycles at every stress level.

All experiments were carried out at 0.5 Hz frequency, and data have been recorded. The stress conditions utilized are detailed in the following Table 3.6, and the test results are given in Figs. 3.38 and 3.39.

Table 3.6 Stress conditions used for the cyclic compression test for Al 7075 alloy.

Compression Stress (MPa)	Tension Stress (MPa)	Applied cycles
-520	350	250
-520	400	250
-520	425	250
-520	450	250

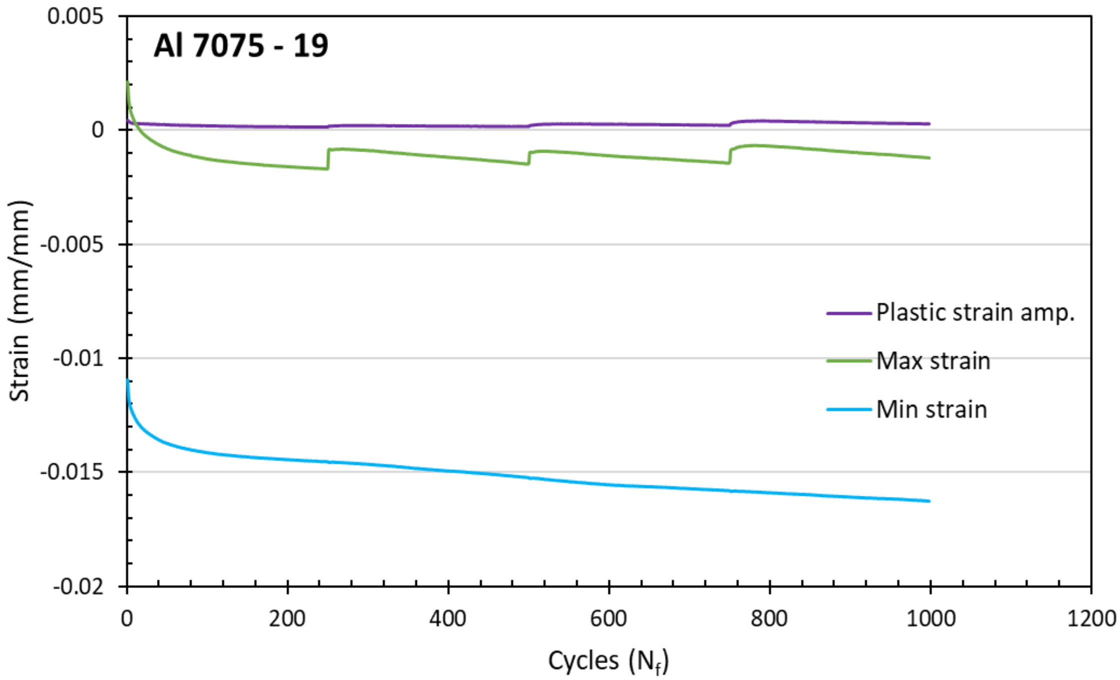

Figure 3.38 Strain – cycle plot showing the maximum, minimum, and plastic strain amplitude as a function of a cycle (N_f) for Al 7075 – 19.

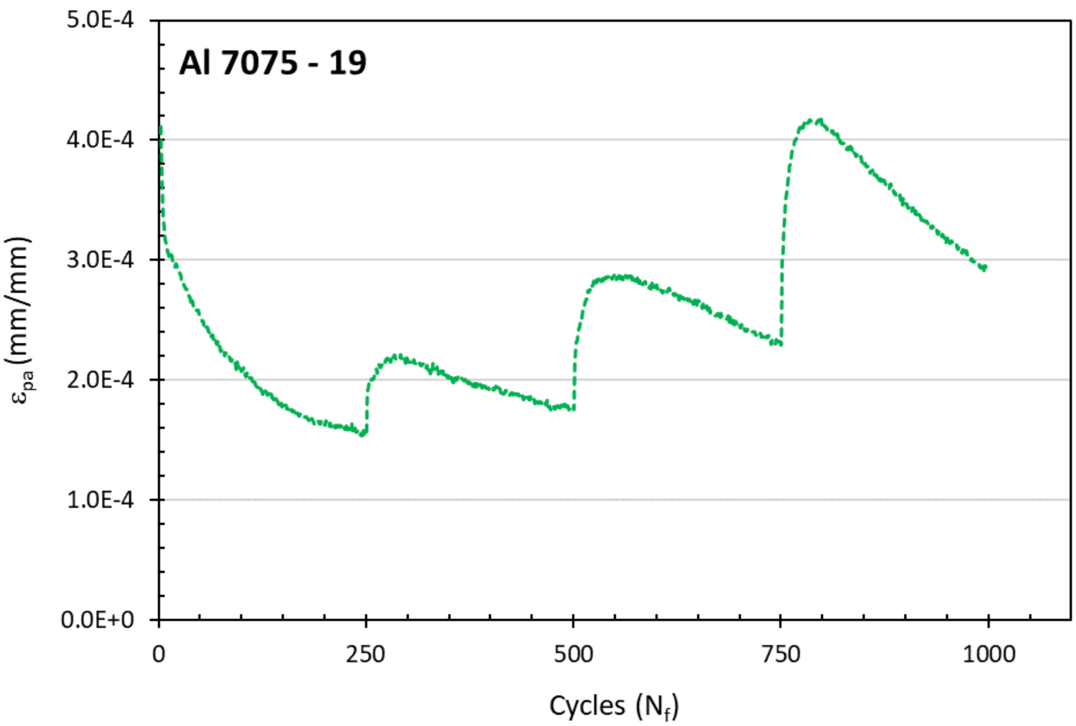

Figure 3.39 Plastic strain amplitude vs. the number of cycles (N_f) for Al 7075 – 19.

For the present test setup, a total of 1000 cycles were applied. As displayed in figure 3.38, when an initial 250 cycles applied, a substantial change in strain has been seen. Nevertheless, with an increase in the applied number of cycles, a little change was detected. Figure 3.39 outlines plastic strain amplitude "ε_{pa}" as a function of an applied number of cycles. By the end of every stress level, a spike in "ε_{pa}" has been witnessed, later that starts falling and eventually gets stabilized. The acquired information has been used for additional analysis, and results are discussed in chapter 4.

3.3.3 Fatigue damage characterization based upon the surface parameters for Al 7075

Two Al 7075 alloy samples have been selected and prepared, as described in section 3.2.3. Fully reversed strain-controlled fatigue tests using axial extensometer at 0.5 Hz frequency were demonstrated. Tests were conducted at strain amplitudes of 0.005, and 0.01 mm/mm, and details are explained in the following sections.

3.3.3.1 Damage test with fully reversed 0.005 mm/mm strain amplitude for Al 7075

As explained above and in section 3.2.3.1, an intermittent fatigue test was performed. Before running the fatigue test, benchmark measurements for "Ra" and micro-indentations have been taken. Following the measurements, a damage test was carried out and terminated at a predefined interval. The details of predefined intervals are presented in Table 3.7.

After every loading interval, Al 7075 - 30 sample was unloaded from peak stress/strain to approximately zero stress/strain. However, at this strain amplitude, the resulted hysteresis loop was not symmetric, as presented in figure 3.40, that prevented to unload sample to the desired zero stress and strain point. In this case, 7075-30 sample unloaded to nearly zero stress that generated plasticity in the material.

Once the sample was unloaded, surface roughness and instrumented micro-indentation measurements carried out, and a similar process had been followed until the failure.

Table 3.7 Pre-defined life intervals for Al 7075 – 30 at 0.005 mm/mm strain amplitude showing the number of reversals/cycles to apply.

Al 7075 - 30		
Life Interval (%)	Life in cycles (N_f)	Life in reversals ($2N_f$)
10	650	1300
25	1625	3250
50	3250	6500
80	5200	10400
90	5850	11700
95	6175	12350
100	6500	13000
until failure	-	-

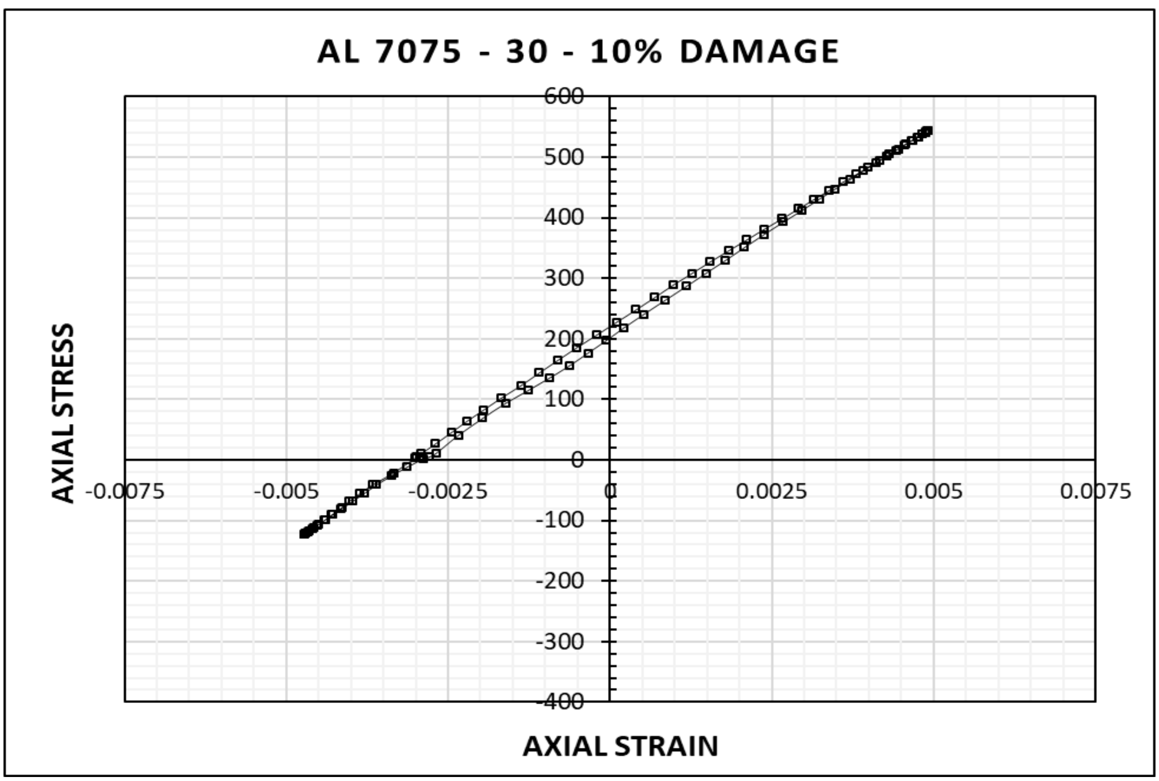

Figure 3.40 Hysteresis loop for Al 7075 – 30 showing the 10th cycle.

Stress and fatigue life (%) information received from an intermittent fatigue damage test was plotted and contrasted with a cyclic strain-controlled test from section 3.3.2.2, as demonstrated in figure 3.41. A somewhat similar trend in stress response has been seen in the curves of fatigue damage and cyclic strain-controlled test.

The following figure displays strain hardening in the material at the first few cycles and continues until it reaches the maximum stress and subsequently remains roughly constant. A comparable pattern has been noticed at every stress level. The fatigue damage test continued for up to 46% of the total fatigue life, and afterward, the sample failed.

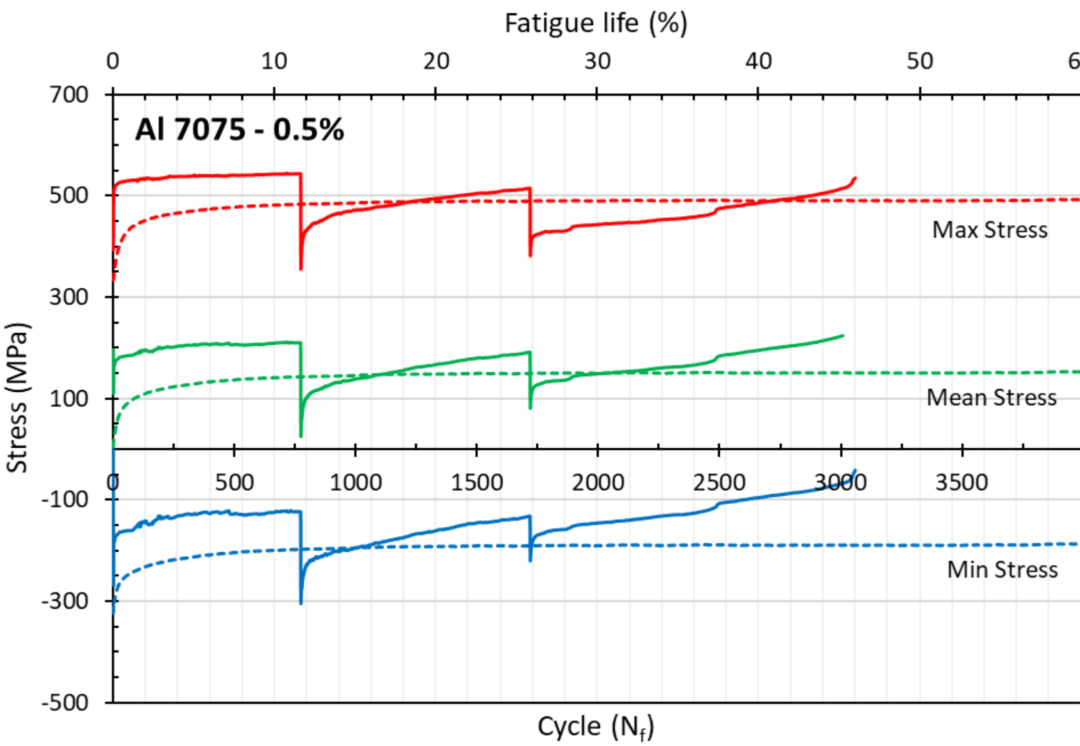

Figure 3.41 Stress (MPa) versus fatigue life (%) for Al 7075 – 30 at 0.005 mm/mm strain amplitude.

Following the fatigue damage test, the micro-indentation measurements were carried out. All measurements performed at 1250 mN peak indentation load at the rate of 50 mN/sec and achieved results are illustrated in figure 3.42. The figure shows the combined indentation response at different fatigue life (%). A significant change in the maximum penetration depth (h_{max}) has been seen following the sample failure.

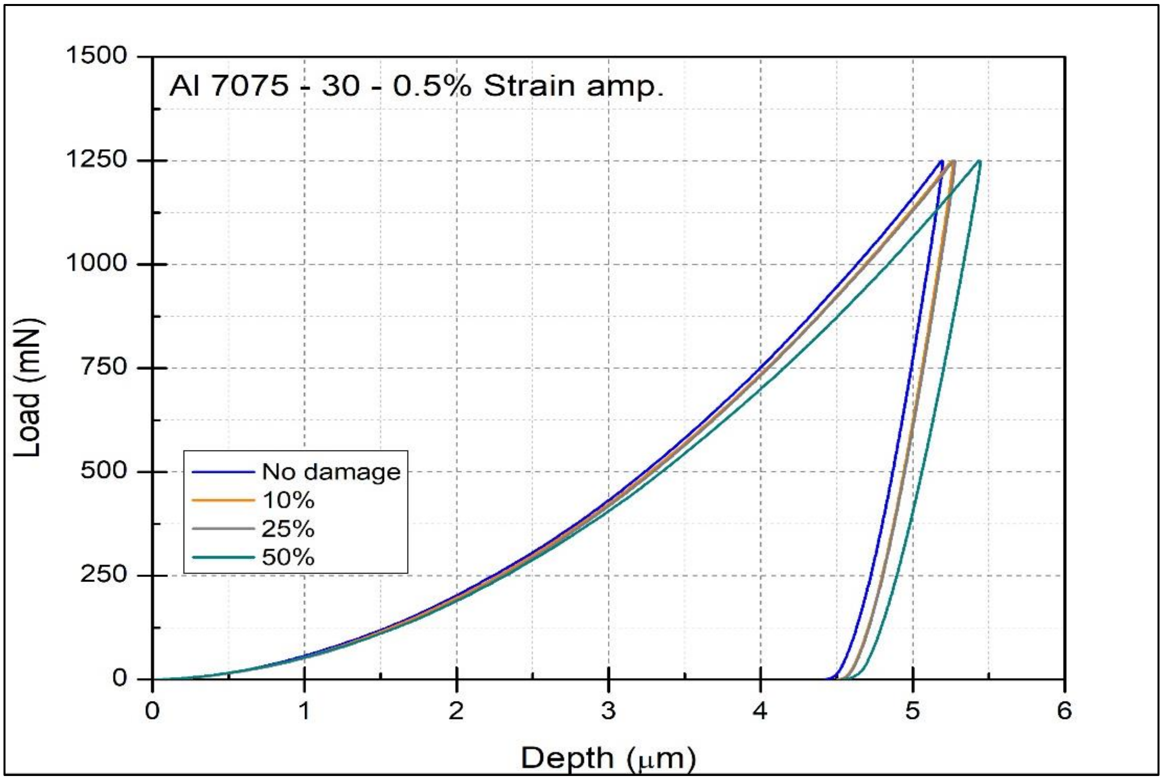

Figure 3.42 Indentation load (mN) versus the mean indentation depth (μm) curves at different fatigue life (%) levels for Al 7075 – 30 at peak load of 1250 mN.

3.3.3.2 Damage test with fully reversed 0.01 mm/mm strain amplitude for Al 7075

As explained in the earlier section, a similar fatigue damage test has been designed and executed at 0.01 mm/mm strain amplitude. The calculated stress intervals are detailed in Table 3.8. After each loading condition, a sample was unloaded, as described in section 3.2.3.1. After applying the initial 10% of fatigue life hysteresis loop for 10th cycle is plotted in figure 3.43, which shows the unloading pattern for Al 7075 – 31 sample.

Figure 3.44 demonstrates the information gained from the fatigue damage test, and cyclic strain-controlled test explained in section 3.2.2.2. Stress – fatigue life (%) and the stress – cycle (N_f) data are plotted collectively in figure 3.44.

Table 3.8 Pre-defined life intervals for Al 7075 – 31 at 0.01 mm/mm strain amplitude showing the number of reversals/cycles to apply.

Al 7075 - 31		
Life Interval (%)	Life in cycles (N_f)	Life in reversals ($2N_f$)
10	60	120
25	150	300
50	300	600
80	480	960
90	540	1080
95	570	1140
100	600	1200
until failure	-	-

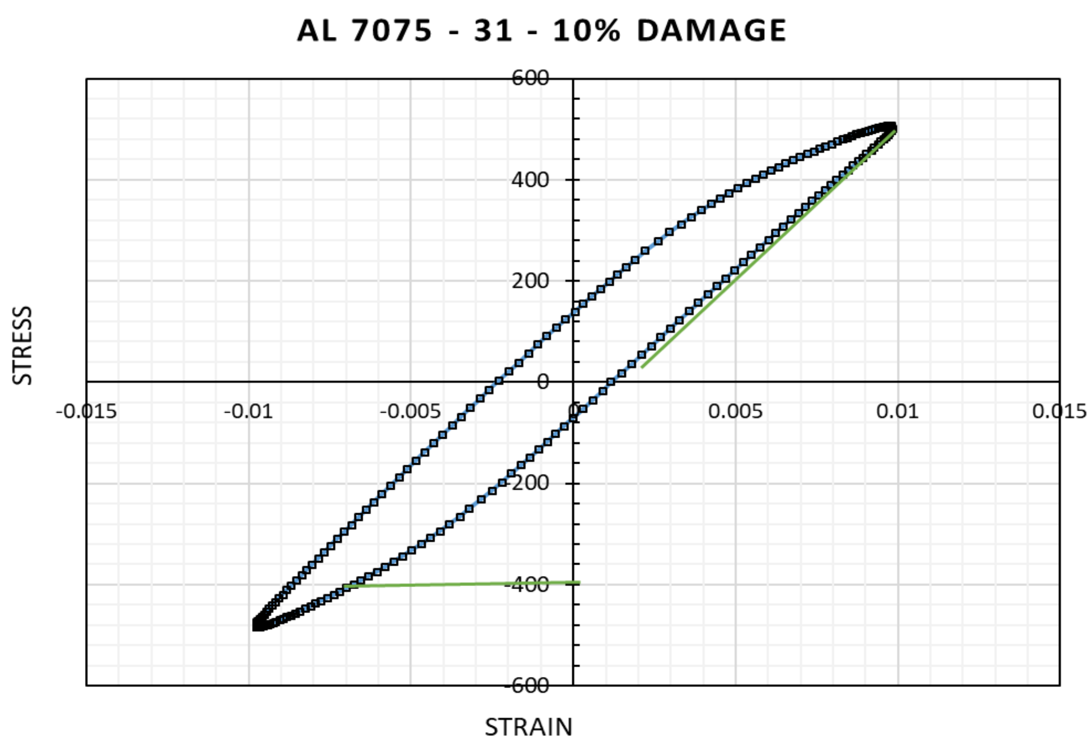

Figure 3.43 Unloading of a sample from peak stress to zero stress and strain for Al 7075 – 31.

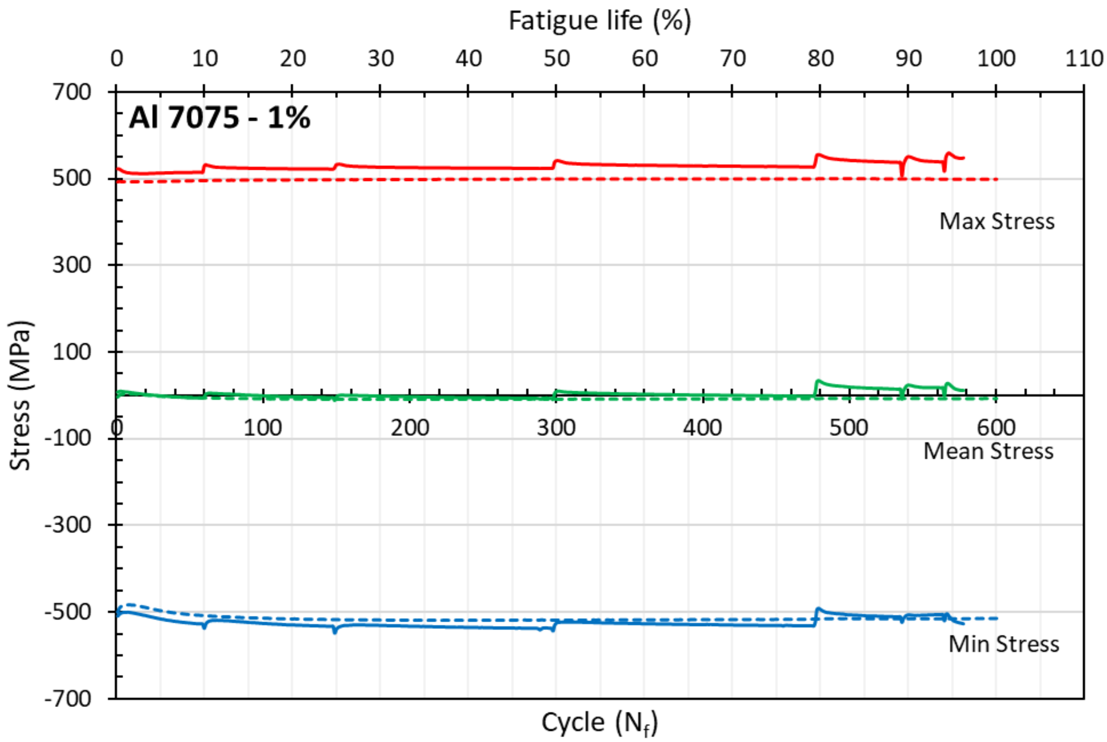

Figure 3.44 Stress (MPa) versus fatigue life (%) for Al 7075 – 31 at 0.01 mm/mm strain amplitude.

The above figure demonstrates the stress response for a number of cycles applied. It is evident that fatigue damage test performs in a similar pattern as in the cyclic strain-controlled test. Nevertheless, Al 7075 - 31 sample fails after applying 98% of the total life cycles.

Following the fatigue test, instrumented micro-indentations were carried out and recorded. Simultaneously, surface roughness measurements were also taken. The mean indentation depth data is displayed below. Figure 3.45 illustrates a load versus mean indentation depth curves at different fatigue life (%) levels. With an increase in a number of cycles, a change in max penetration depth (h_{max}) has been detected. The outcomes of all the above tests were put together and received results are described in chapter 4.

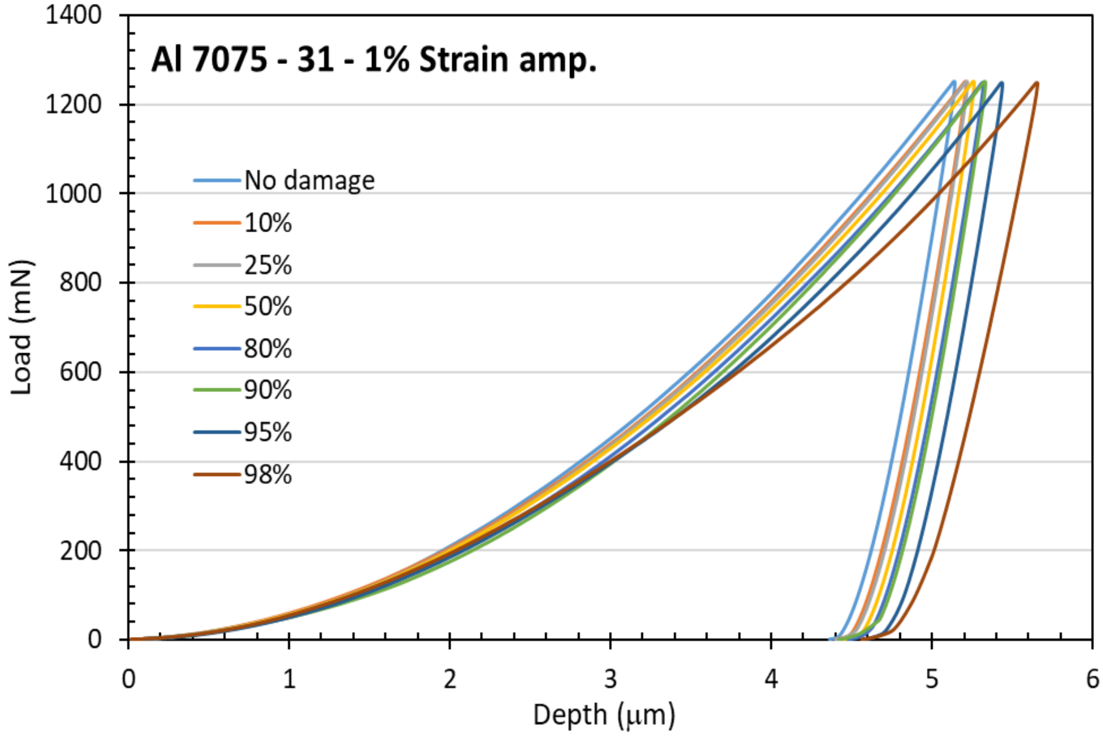

Figure 3.45 Indentation load (mN) versus the mean indentation depth (μm) curves at different fatigue life (%) levels for Al 7075 – 31 at peak load of 1250 mN.

4 EXPERIMENTAL FINDINGS

4.1 Introduction

This chapter details the key findings based on the results obtained from various tests described in the previous chapter. The resulted information is categorized based on the material and grouped into three different sections; 1) influence of surface roughness on Vickers micro-hardness, 2) correlation in the cyclic elastoplastic behavior of materials during the work hardening obtained from instrumented micro-indentations and strain-controlled fatigue tests, and 3) variation in the surface quality parameters such as roughness and micro-hardness of the material with the increase in fatigue damage.

4.2 Experimental analysis for Al 6061

4.2.1 Influence of surface roughness on Vickers micro-hardness

Instrumented micro-hardness indentation and surface roughness measurement techniques performed in section 3.2.1.2 demonstrate the effect of surface roughness on Vickers micro-hardness. It has been noted that specimen's ground/ polished with fine-grit sizes show an excellent surface roughness/waviness results than with the coarse grit sizes.

Figure 4.1 depicts the influence of surface roughness on the micro-hardness, where resulting values for Vickers micro-hardness (*HV*) mapped with the arithmetic mean roughness (*Ra*) for Al 6061 alloy. At "*Ra*" of 12 nm, the Vickers hardness was found to be HV/130. An almost no change in HV is seen until roughness "Ra" of 200 nm. However, after 200 nm roughness reduction in the Vickers hardness has been witnessed. The following plots also exhibit the scatter in the Vickers micro-hardness.

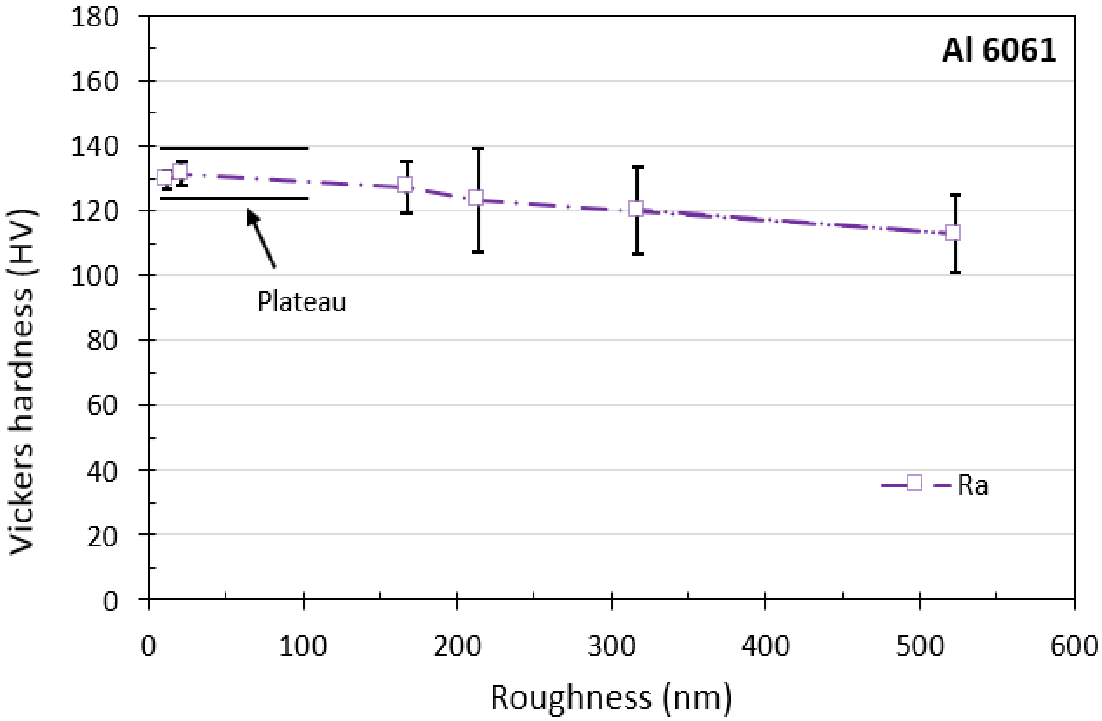

Figure 4.1 Vickers micro-hardness (HV) plotted as a function of the Arithmetic mean roughness "Ra" for Al 6061 alloy for a peak load of 1250 mN at 50mN/sec.

It is established that for aluminum 6061 alloy, the Arithmetic mean roughness "*Ra*" is inversely proportional to the Vickers micro-hardness until it achieves the plateau. Furthermore, when it reaches the plateau, additional change in the surface roughness "*Ra*" has no considerable effect on the Vickers micro-hardness.

As depicted in the above figure, It is also worth noting that the surface roughness "Ra" has a significant influence on the scatter in micro-hardness. Even though the observed scatter has no noticeable effect, but it is clear that as surface roughness starts lessening, the scatter begins to diminish.

While the arithmetic mean roughness "*Ra*" was measured, the root mean square (RMS) roughness "*Rq*" was also noted. The resulting values of RMS "*Rq*" are likewise plotted in Figure 4.2. As mentioned above, an analogous response has observed in Vickers micro-hardness with

RMS "Rq" roughness. The above figure also displays the scatter in Vickers micro-hardness (*HV*) to the root mean square (RMS) roughness "*Rq*" for Al 6061 alloy.

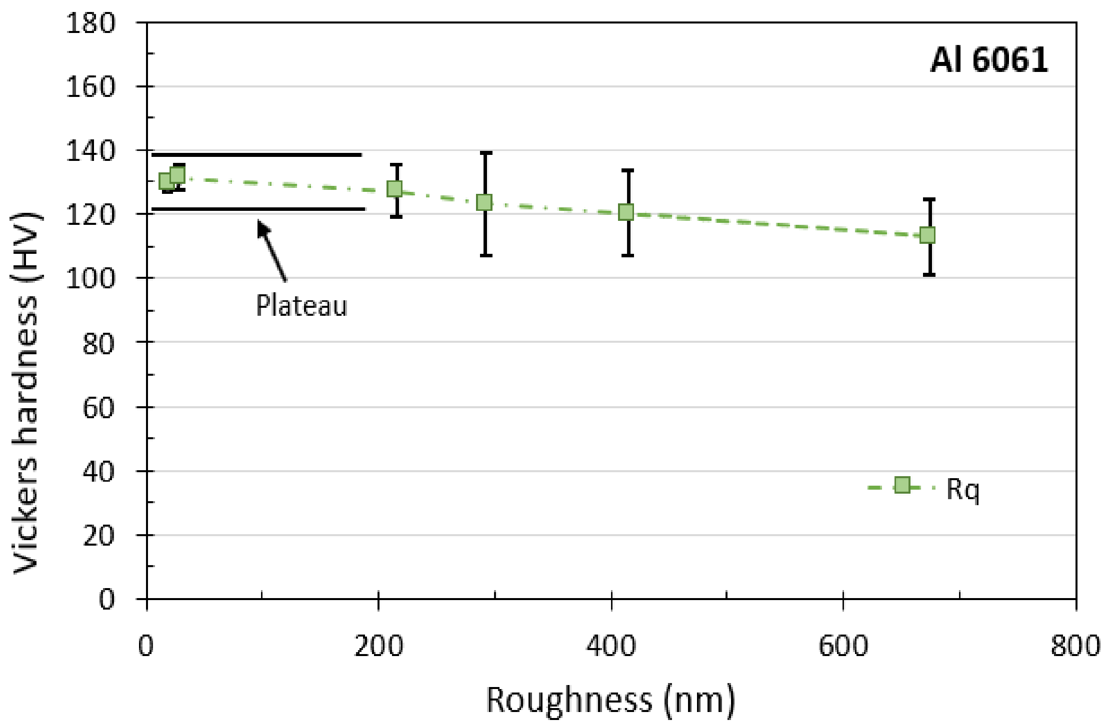

Figure 4.2 Vickers micro-hardness (HV) plotted as a function of the root mean square roughness "Rq" for Al 6061 alloy for a peak load of 1250 mN at 50 mN/sec.

In summary, the surface roughness of the material has a significant influence on the Vickers micro-hardness. However, it is worth to know the roughness values where micro-hardness attains a plateau; therefore, for the future micro-indentation tests, aluminum specimens could be prepared until the desired surface roughness. It is taken into account that for aluminum 6061 alloy, surface roughness "*Ra*," "*Rq*" values of 200 nanometers or lower are excellent for instrumented micro-indentations. To do so, the samples should be ground and polished until 800 grit silicon carbide paper.

4.2.2 Relationship in the destructive and non-destructive test method for Al 6061

4.2.2.1 Cyclic micro-hardness indentation results (Non-destructive test method)

As explained in chapter 3, load-controlled cyclic micro-hardness indentations were carried out, and plastic deformation for every hysteresis loop has been measured. The calculated plastic deformation in termed as the width of the loop and evaluated in microns. The resulted width (μm) for stress levels ranging from 500 to 1750 mN is plotted against a number of cycles applied, as demonstrated in figure 4.3.

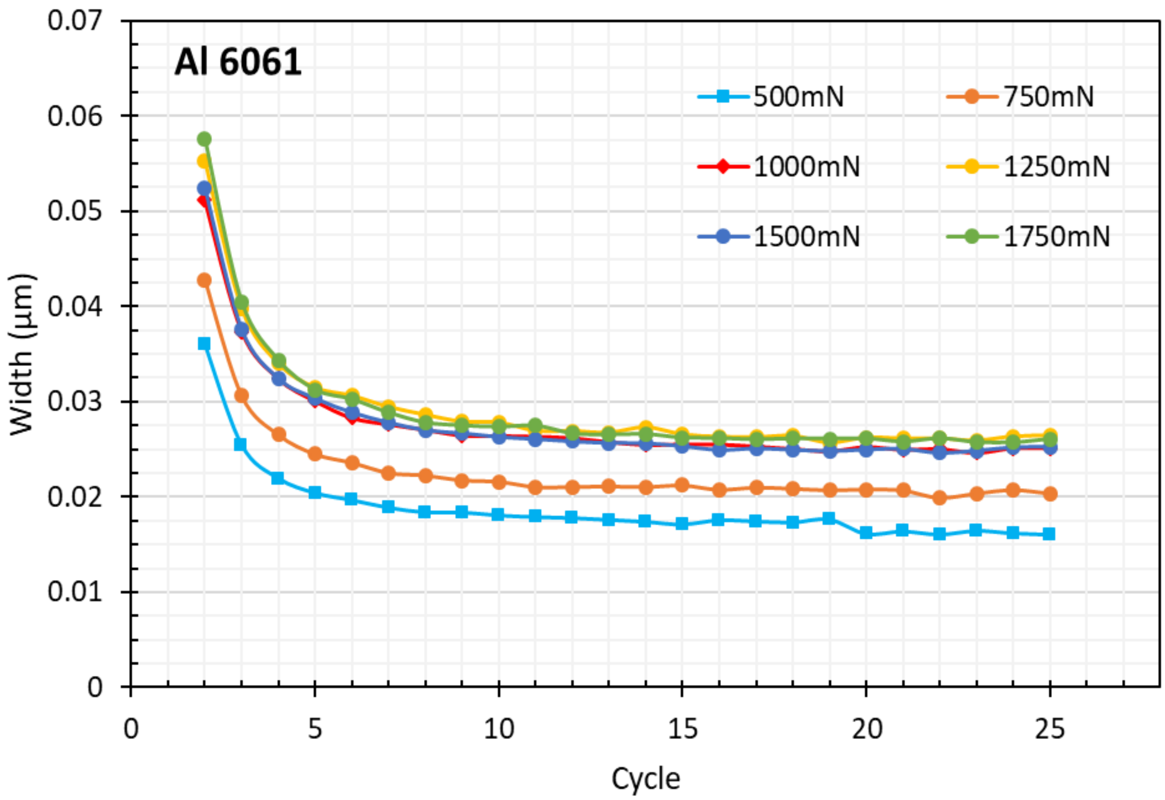

Figure 4.3 Plastic deformation (width) calculated at each hysteresis loop plotted as a function of cycles for Al 6061, applied at stress levels ranging from 500 mN to 1750 mN at the load rate of 50 mN/sec.

Figure 4.3 illustrates the change in the width of a hysteresis loop, with an increasing number of cycles. With the increasing cycles, a reduction in the width of the loop was noticed. The decrease in the width of the loop (μm) continued till it reaches a plateau. In Al 6061 alloy, for every single load level, it was determined that approximately after 12-13 cycles, no change or equilibrium was evident in width. The width of the stabilized hysteresis loop for each stress level has been computed for further analysis.

Figure 4.4 displays the calculated stabilized hysteresis loop width (μm) plotted as a function of maximum load applied at each load level. The information is mapped on a log-log plot, and the power-law trendline used to determine if there is any relationship or not.

In the case of Al 6061 alloy, it was noted that on a log-log scale, a power-law relationship between the maximum load and the width of the loop has been witnessed. The resulted equation for the given relation is demonstrated in figure 4.4, as below. The equation delivers a strain hardening exponent "n" and strain hardening coefficient "A" from cyclic micro-indentation. This power-law relationship will be used to determine the strain hardening behavior of investigated material and the existing correlation between them.

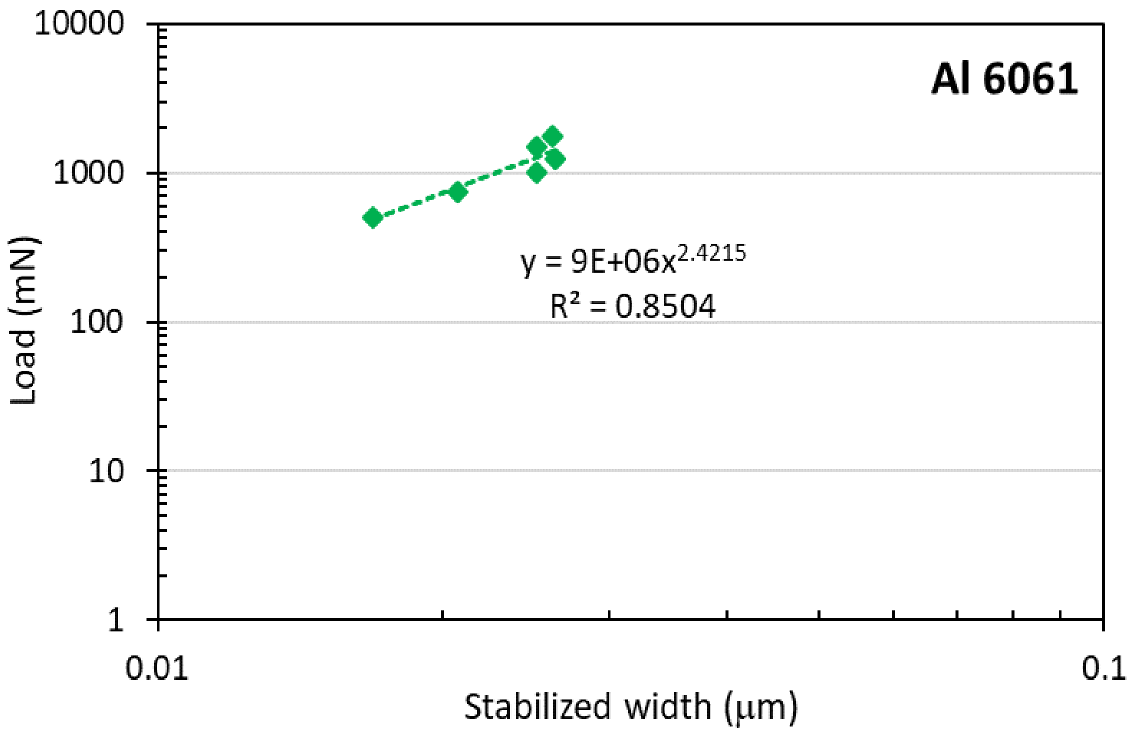

Figure 4.4 Power-law relationship on a log-log scale between the width (μm)of the stabilized hysteresis loop and the maximum load applied (mN) for load-controlled cyclic indentations on Al 6061 alloy.

4.2.2.2 Destructive test results

Strain-controlled fatigue tests at various strain amplitudes were performed, and details for the same are provided in Chapter 3. The obtained hysteresis loop data has been analyzed to calculate plastic strain (ε_p) at mean stress in the material that occurred during each test. The hysteresis loops show a significantly higher amount of plasticity in a 0.02 mm/mm strain amplitude test than 0.005 mm/mm.

The resulted information from 0.005, 0.01, and 0.02 mm/mm strain amplitude fatigue experiments are plotted in the below figures.

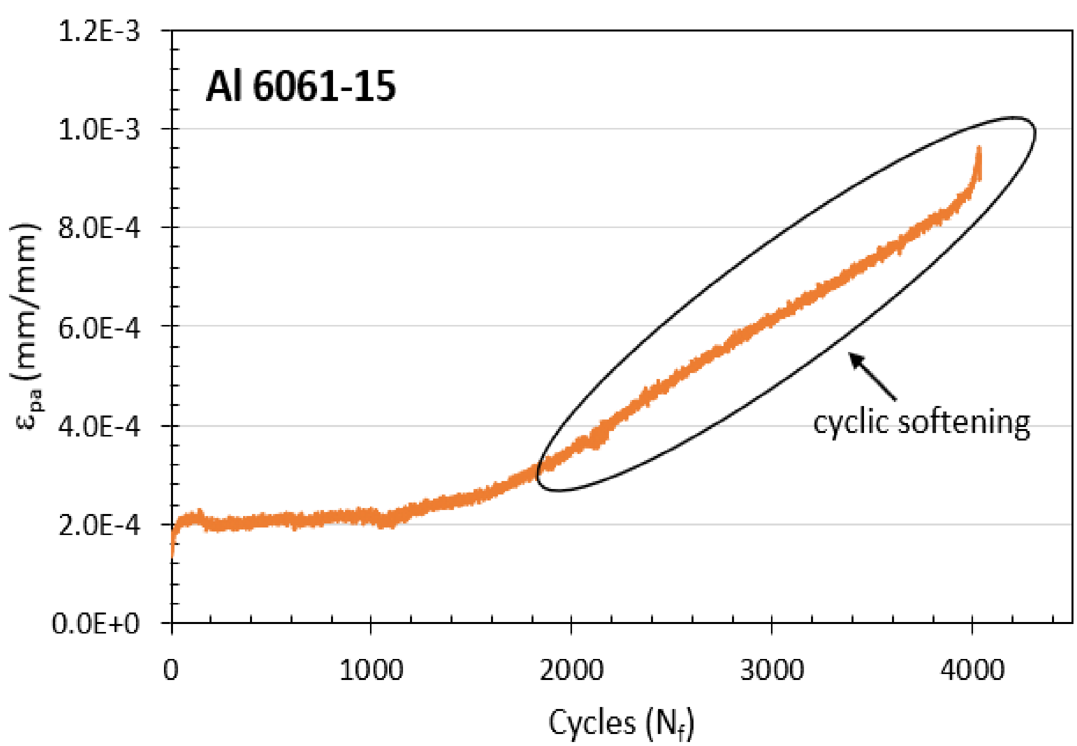

Figure 4.5 Plastic strain amplitude (ε_{pa}) as a function of a number of cycles (N_f) applied for Al 6061 – 15 at 0.005mm/mm strain amplitude and 0.5 Hz frequency.

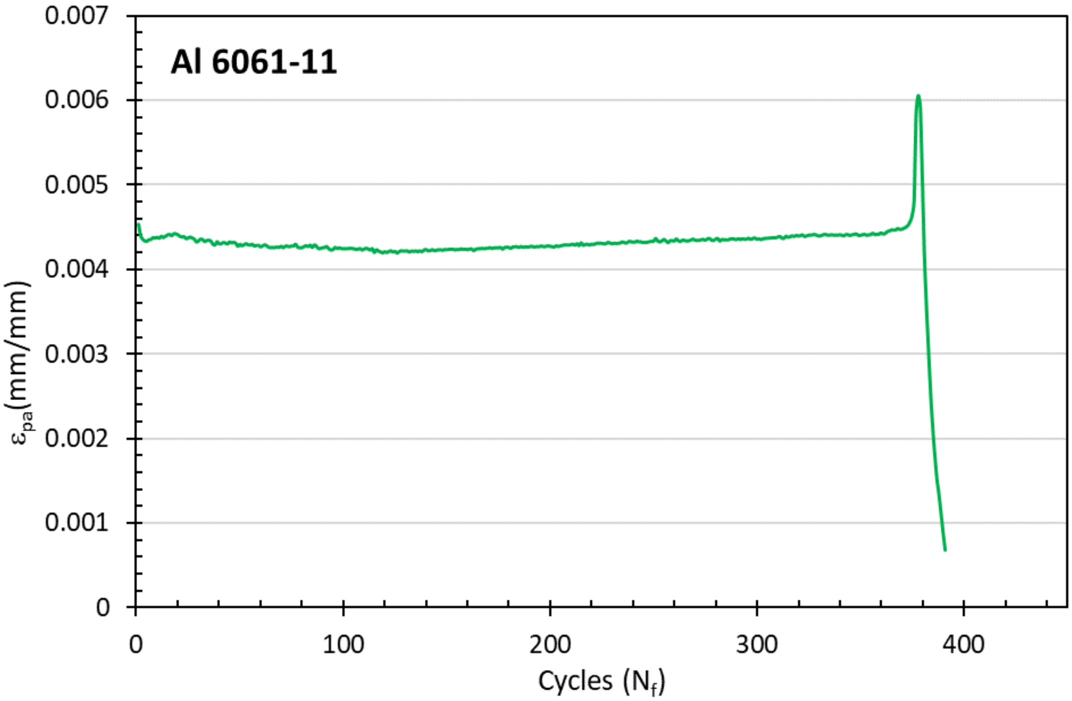

Figure 4.6 Plastic strain amplitude (ε_{pa}) as a function of a number of cycles (N_f) applied for Al 6061 – 11 at 0.01mm/mm strain amplitude and 0.5 Hz frequency.

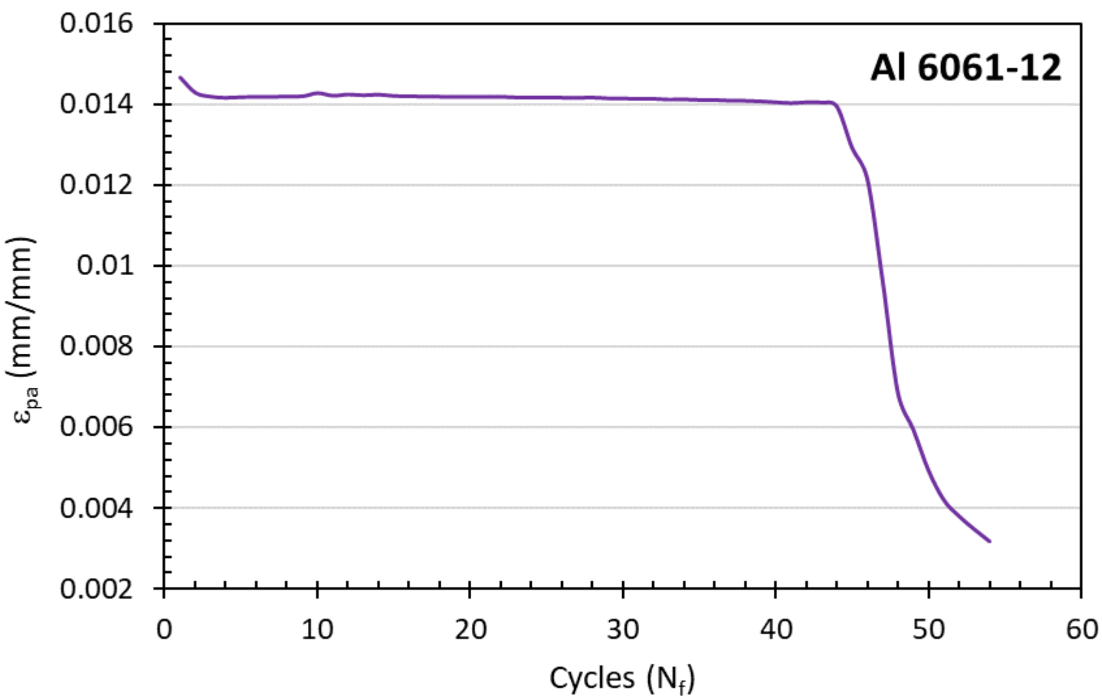

Figure 4.7 Plastic strain amplitude (ε_{pa}) as a function of a number of cycles (N_f) applied for Al 6061 – 12 at 0.02mm/mm strain amplitude and 0.5 Hz frequency.

Figures 4.5, 4.6, and 4.7 illustrates a plastic strain amplitude (ε_{pa}) as a function of fatigue life (N_f) for Al 6061 alloys. Figs. 4.6.and 4.7 indicates considerable values of plastic strain amplitude (ε_{pa}). Additionally, it has been noted that "ε_{pa}" shows a stable response until 90 – 95% of the total fatigue life. However, in figure 4.5 for Al 6061 – 15 marginally small values of plastic strain amplitude (ε_{pa}) have been observed, and a stable "ε_{pa}" response was foreseen until 25% of the total fatigue life. From that point onward, plastic strain amplitude (ε_{pa}) was monotonically increasing until failure occurs.

Leveraging Figs. 4.5 – 4.7, a plastic strain amplitude (ε_{pa}) at a steady-state or half-life for all strain amplitude is determined and employed for further analysis. The obtained values for all specimens are detailed in the following table.

Table 4.1 Specifics of stress amplitude and plastic strain amplitude at steady state/half-life for Al 6061.

Specimen	**Stress amplitude (MPa)**	**Plastic strain amplitude (mm/mm)**	**Half-life cycle**
Al 6061 – 15	278	2.06E-04	500th
Al 6061 – 11	297	4.24E-03	250th
Al 6061 – 12	318	1.42E-02	20th

The resulting plastic strain amplitude and stress amplitude values at steady-state/half-life are drawn on a log-log plot, as displayed in figure 4.8. The findings demonstrate that there is a power-law relationship on a log-log scale. The equation attained from the power-law is also shown in the below chart. The equation yields a strain hardening exponent "n" and a strain hardening coefficient "A".

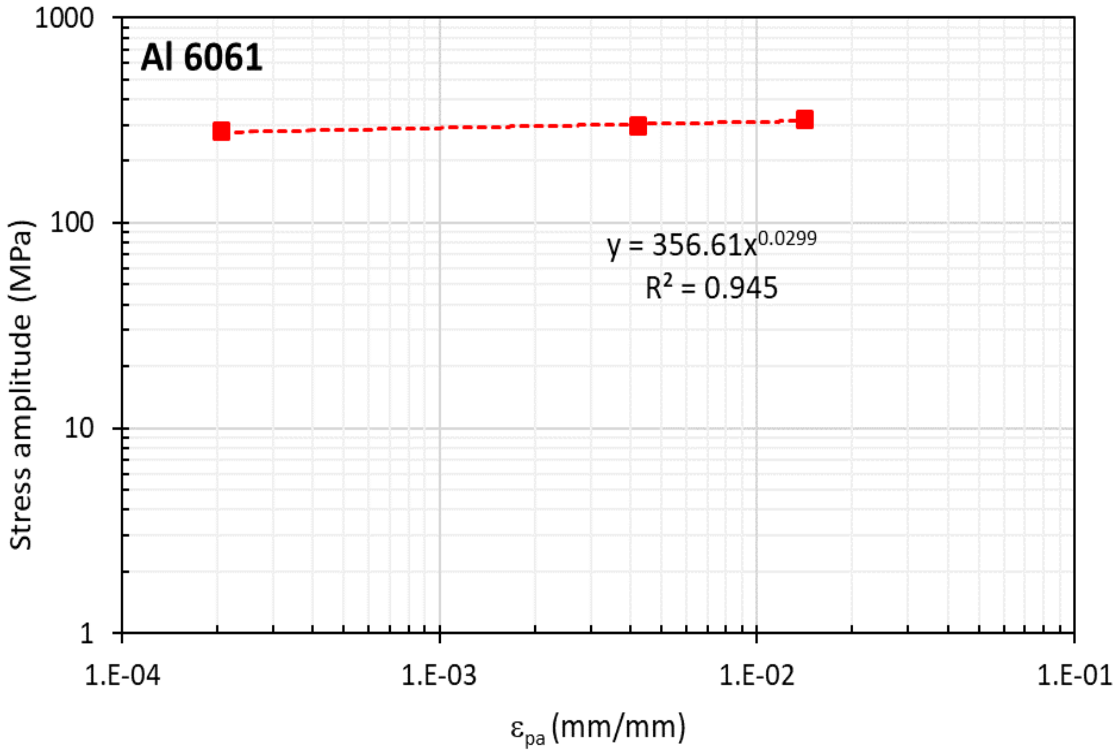

Figure 4.8 Plastic strain amplitude (ε_{pa}) as a function of stress amplitude (MPa) gained from cyclic strain-controlled tests for Al 6061 alloy.

As described in chapter 3, the cyclic compression experiment (destructive test method) was carried out. Plastics strain amplitude (ε_{pa}) versus the fatigue life chart was plotted from the response of the hysteresis loop. As mentioned above, the steady-state values for plastic strain amplitude at each stress level have been noted, and details provided in Table 4.2.

Table 4.2 Specifics of stress amplitude and plastic strain amplitude at steady-state for Al 6061 – 22.

Stress amplitude (MPa)	**Plastic strain amplitude (mm/mm)**	**Half-life cycle**
242	2.90E-05	150th
252	3.89E-05	300th
262	6.56E-05	450th
272	1.34E-04	600th

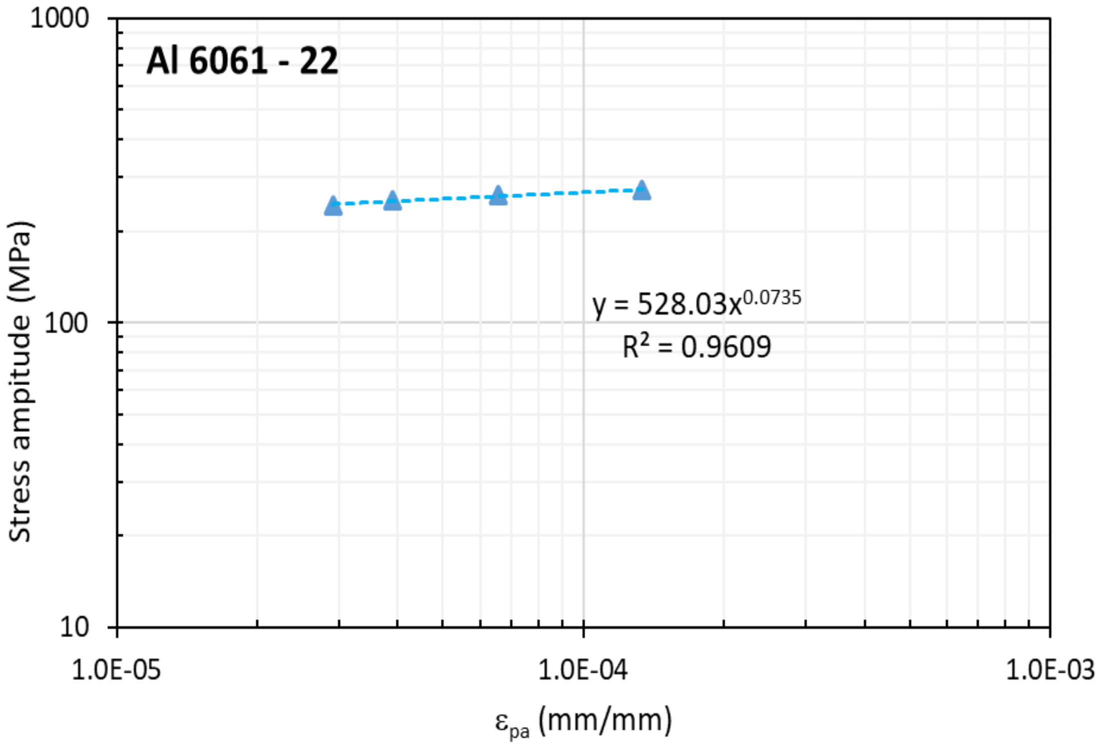

Figure 4.9 Plastic strain amplitude (ε_{pa}) mapped versus the stress amplitude (MPa) gained from the cyclic compression test for Al 6061 - 22.

Figure 4.9 demonstrates stress amplitude and plastic strain amplitude (ε_{pa}) mapped on a log-log chart. The plotted data points for Al 6061 – 22 display a power-law relationship on a log-log scale, and the equation derived from the association shown in the above chart provides a strain hardening exponent "n" and a strain hardening coefficient "A".

4.2.2.3 Discussion

As explained and demonstrated in the above sections, 4.2.2.1 and 4.2.2.2, the attained power-law relationship charts are compared to find the similarities or any existing correlation between them. To do so, the resulted data from strain-controlled fatigue tests and stress-controlled cyclic compression is plot altogether. The acquired information has been exhibited in figure 4.10, which indicates the stress amplitude on the y-axis and plastic deformation on X-axis.

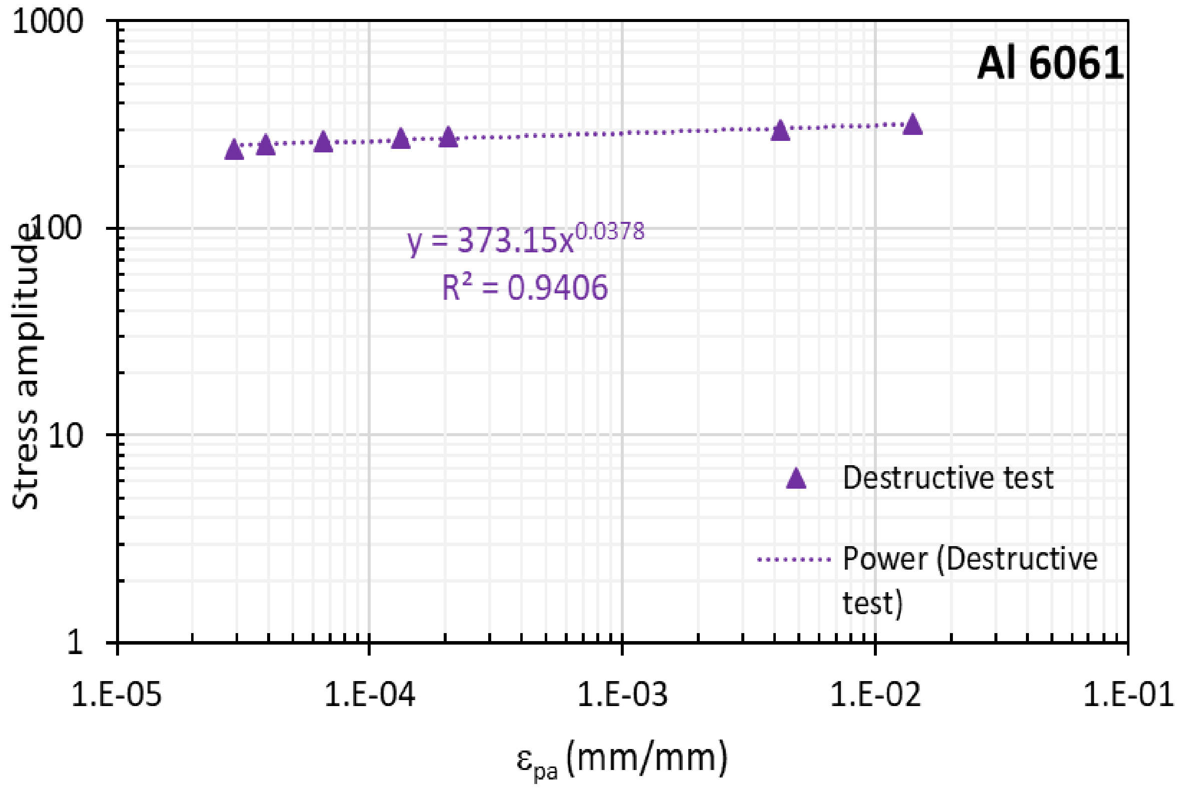

Figure 4.10 Combination of data gained from cyclic strain-controlled tests and the cyclic compression test for Al 6061 alloy.

Figure 4.10 demonstrates a correlation between the information received from cyclic strain-controlled tests and the cyclic compression test. The resulted equation gives the strain hardening exponent "n" of 0.0378 and strain hardening coefficient "A" of 373. The acquired outcomes will be assessed with the data gained from cyclic micro-indentation to discover an existing relationship between them.

4.2.3 Characterization of fatigue damage for Al 6061 alloy

4.2.3.1 Damage test results for 0.005 mm/mm strain amplitude

In chapter 3, a detailed explanation of the damage testing has been provided. This section focuses on results yielded from performed damage experiments. The experimental outcomes have been utilized to demonstrate the fatigue life (%) behavior under various surface parameters like Vickers micro-hardness (HV), surface roughness (Ra), rate of change in slopes (%), and the instrumented elastic modulus "EIT" (GPa).

As mentioned above, the data obtained from Al 6061 – 26 for the surface parameters as a function of fatigue life (%) mapped in the figures 4.11 – 4.13, as displayed below. The surface roughness "Ra" (nm) and scatter in "Ra" plotted against fatigue life (%) as exhibited in the following figure 4.11.

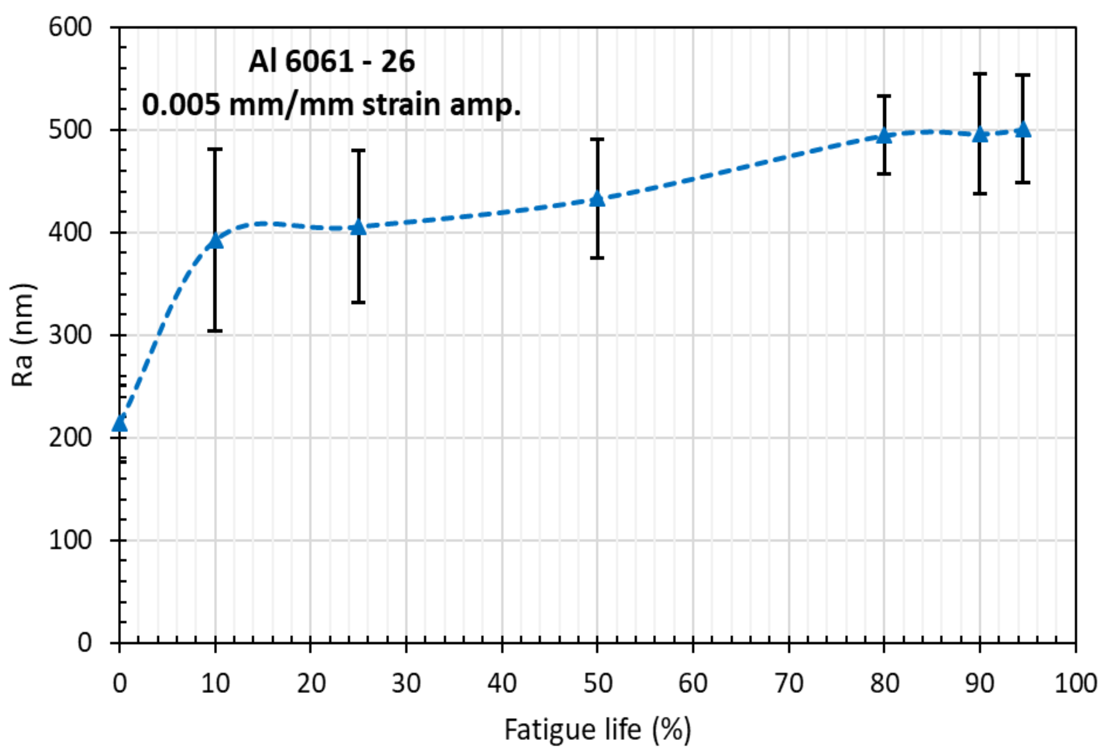

Figure 4.11 Surface roughness (Ra) and scatter in "Ra" versus fatigue life (%) for 6061 – 26 under fully reversed 0.005 mm/mm strain amplitude.

In the case of Al 6061 – 26 at fully reversed 0.005 mm/mm strain amplitude, figure 4.10 demonstrates the sudden upswing in roughness "Ra" (nm) within an initial 10% of applied fatigue life. Moreover, a considerable increase in "Ra" has been viewed from 10% to 80% of total life. Nonetheless, with an additional applied life after 80%, very little or no variation in "Ra" has been noticed. Also, it has been observed that scatter in "Ra" has no apparent relation to fatigue life.

Following to the surface roughness plot, the obtained hysteresis loops and micro-indentations curves from fatigue damage test are used to calculate the unloading slopes. As shown in figure 4.12, for calculating the unloading slope, two points (80% and 25%) on the unloading curve were selected for which the values were extracted from the experimental data. Similar to the unloading slope for hysteresis, the micro-indentation unloading slope was also calculated.

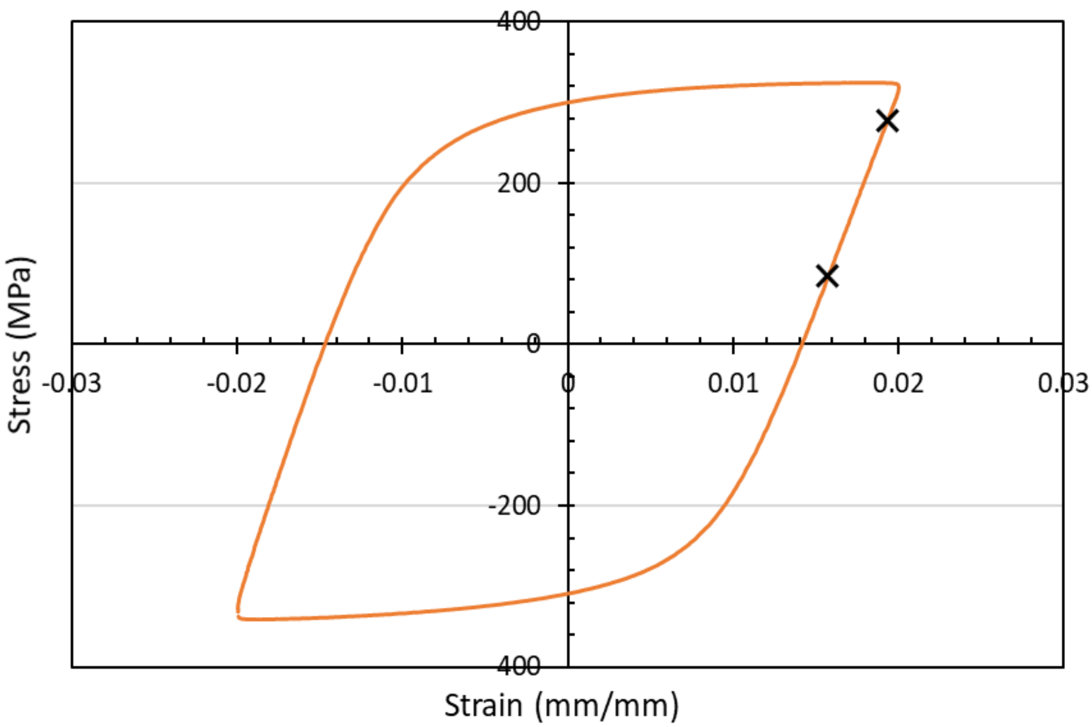

Figure 4.12 Schematics for calculation of unloading slope.

The obtained unloading slopes were then used to calculate the normalized slopes. The normalized hysteresis slope is defined as the unloading slope (E) found after each cyclic load intervals over the initial unloading slope (E_o) found before applying any cyclic load intervals. Similarly, the normalized unloading slope for micro-indentation "C/C_o" is defined where "C_o" is the initial micro-indentation slope, and "C" is the slope measured after each cyclic loading interval.

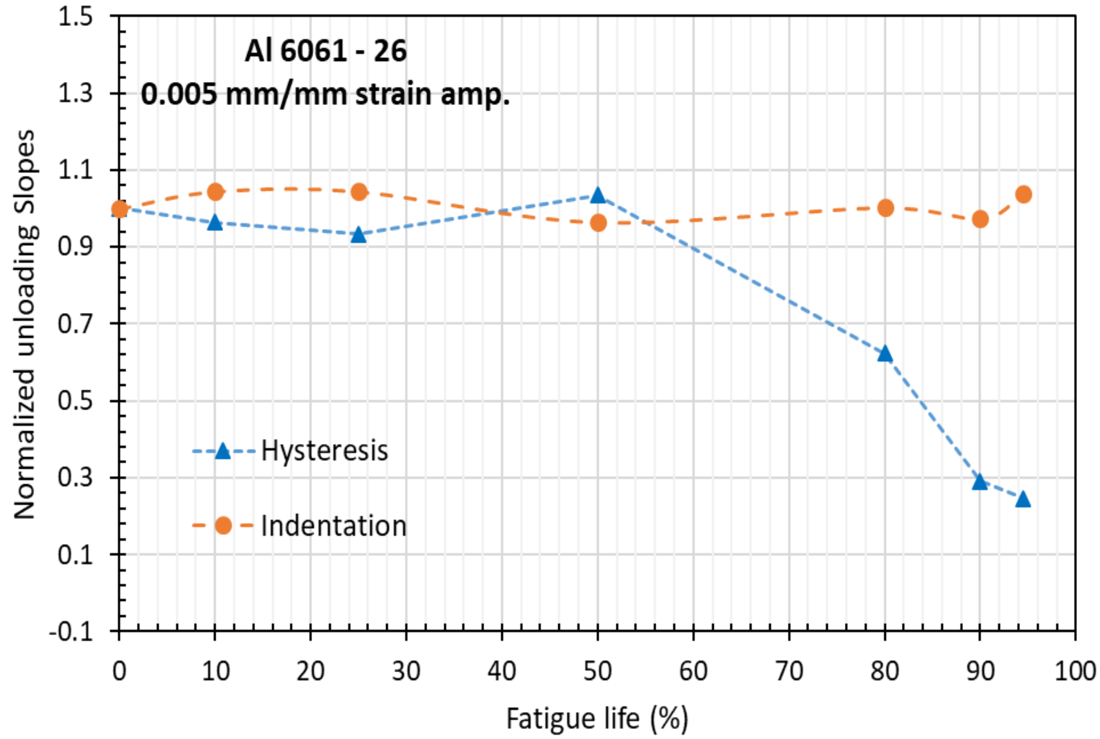

Figure 4.13 Normalized unloading slopes for hysteresis and micro-indentation as a function of fatigue life (%) for Al 6061 – 26 under fully reversed 0.005 mm/mm strain amplitude.

Figure 4.13 demonstrates the normalized slopes versus fatigue life (%). Evidently, as fatigue life was applied, until 50% of the total life, a slight increase in the normalized hysteresis slope is observed. However, after that, an exorbitant reduction has been seen until specimen failure. At the same time, the normalized unloading slope achieved from micro-indentations doesn't change much.

In contrast, the normalized unloading slopes for Hysteresis (E/E_o) and indentation (C/C_o) show a similar trend in the beginning. Nevertheless, as more fatigue life intervals were applied, the normalized slope for hysteresis demonstrates a sudden decrease, whereas no significant variations in the micro-indentation.

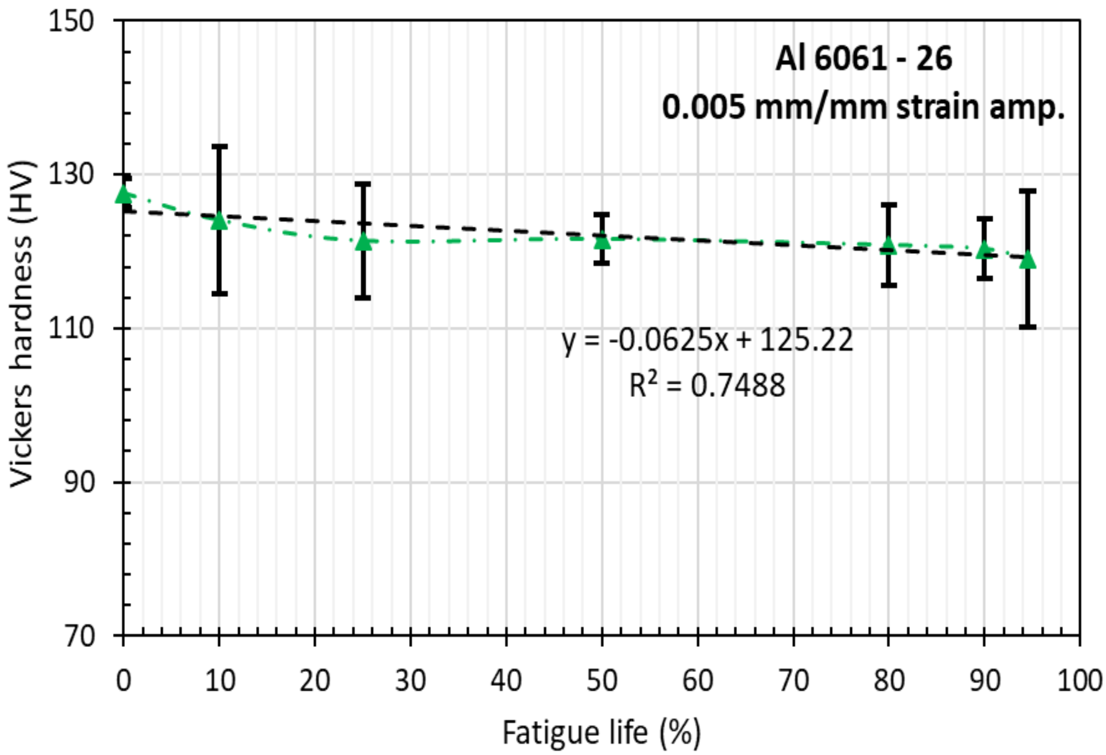

Figure 4.14 Vickers micro-hardness (HV) and scatter in "HV" against fatigue life (%) for Al 6061 – 26 under fully reversed 0.005 mm/mm strain amplitude.

As discussed in Chapter 3, after every cyclic loading interval, micro-hardness indentations were performed. The resulted data has been plotted in figure 4.14 also shows the best fit line and the obtained equation. Prior to applying any fatigue life, the Vickers micro-hardness (HV) found to be 127.5/HV. As the fatigue life was applied, a sizeable reduction in "HV" has been witnessed. However, a decrease in "HV" is noticed until 25% of total life after that up to 80% a negligible, or no change is seen whereas following 80% to a specimen failure, a slight decrease has been viewed. Eventually, the Vickers micro-hardness at specimen failure is recorded to be 119/HV.

4.2.3.2 Damage test results for 0.01 mm/mm strain amplitude

Parallel to the 0.005 mm.mm strain amplitude, experiments with a fully reversed 0.01 mm/mm strain amplitude were carried out and had described in chapter 3. The experimental findings for Al 6061 – 31 are discussed in this section as below.

The surface roughness "Ra" (nm) has been mapped against fatigue life (%), as demonstrated in figure 4.15. A rapid increase from 250 nm to 524 nm in roughness "Ra" (nm) has been noted within an initial 10% of fatigue life. Likewise, for an applied fatigue life from 10% to 100%, an escalation in "Ra" has been noted but not as abrupt as seen earlier.

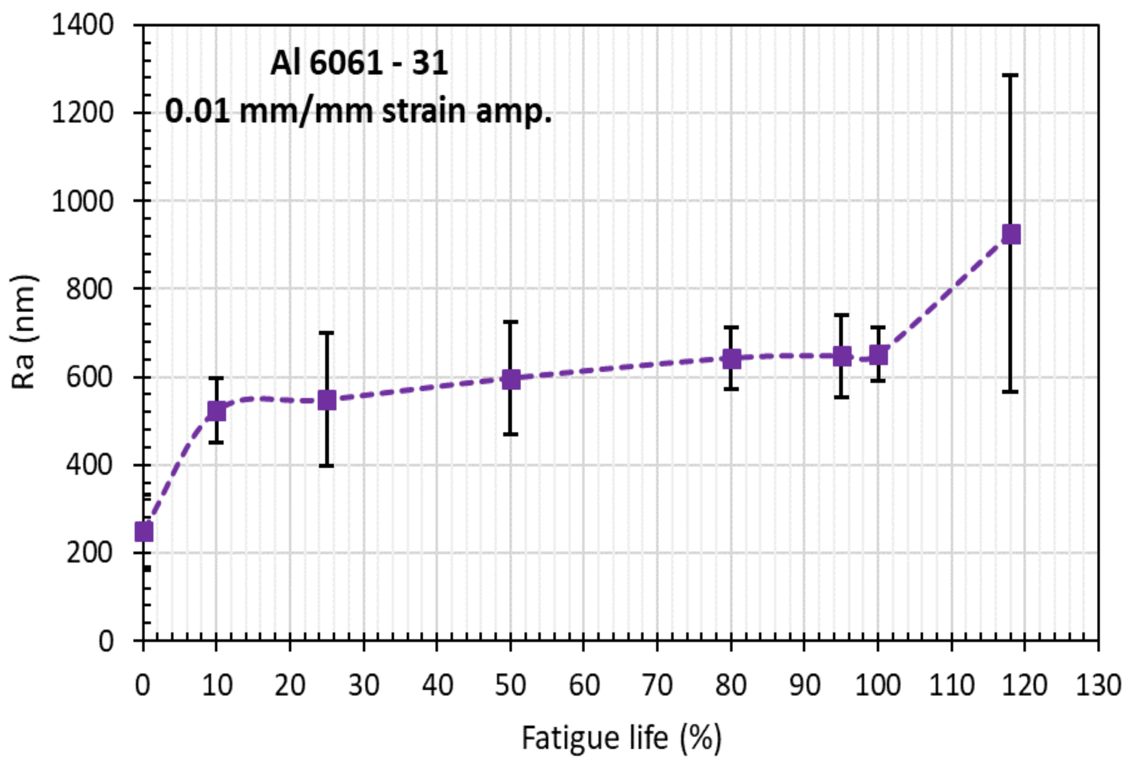

Figure 4.15 Surface roughness (Ra) and scatter in "Ra" versus fatigue life (%) for 6061 – 31 under fully reversed 0.01 mm/mm strain amplitude.

However, during the very last cyclic loading interval, "Ra" found to be as sharp as spotted in the initial 10% of total life. Scatter in "Ra" is recorded, and a minimal variation in scatter over the entire life applied has been perceived, although when there was a failure, huge scatter has been detected.

Following the surface roughness graph, and as explained in the earlier section, the normalized slopes were calculated. The normalized unloading slopes for hysteresis (E/E_o) and micro-indentation (C/C_o), as displayed in figure 4.16, has been mapped as a function of fatigue life (%). During an initial 25% of total life, the normalized micro-indentation slope expresses a decrease, but after that, no change has been seen until 90% of the fatigue life. However, a small increment is seen up to 100% of fatigue life, and then a sudden drop until sample failure is seen. At the same time, the normalized hysteresis slope showed a sharp increase at 50%, and then a fall at 80%. Furthermore, a similar pattern like a little increment through 80 – 100% of fatigue life, and consequently, a steady fall has been noticed in both normalized slopes.

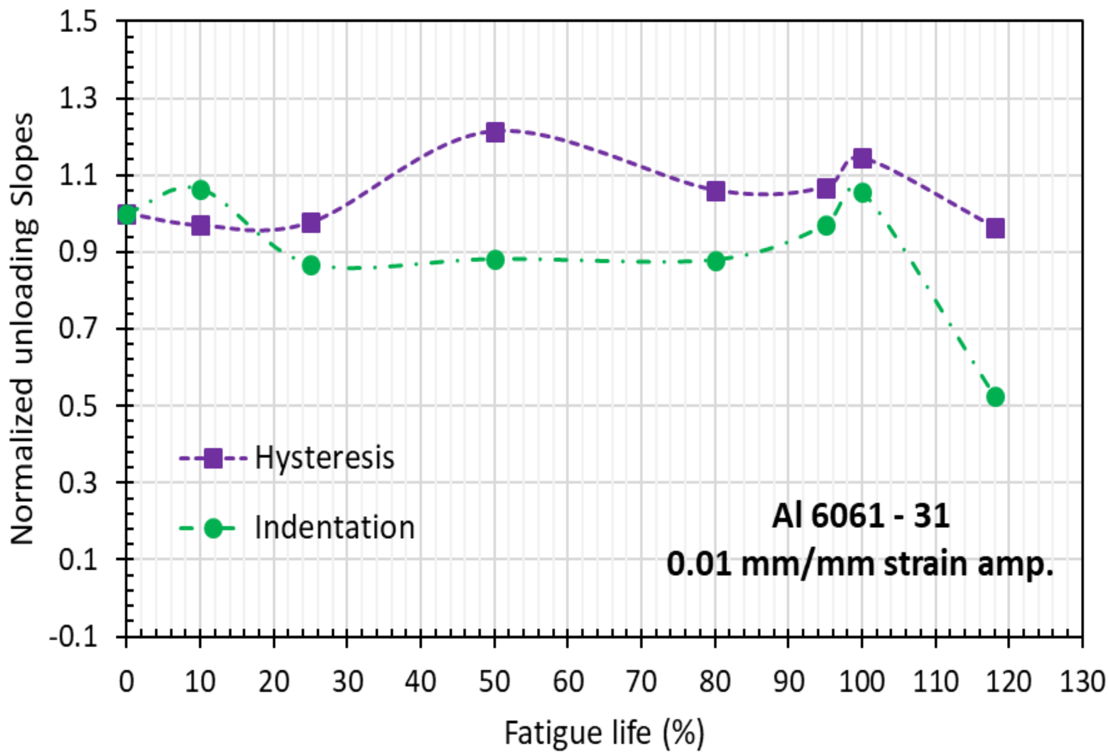

Figure 4.16 Normalized unloading slopes for hysteresis and micro-indentation as a function of fatigue life (%) for Al 6061 – 31 under fully reversed 0.01 mm/mm strain amplitude.

As discussed in the previous section, a similar type of figure has been plotted for Al 6061 – 31, where the horizontal axis displays the fatigue life (%) of material and vertical axis shows a Vickers micro-hardness (HV) and scatter in "HV" for a fully reversed 0.01 mm/mm strain amplitude. Also, the best fit line is drawn, and the equation for it is given in figure 4.17.

As illustrated in figure 4.17, before applying any fatigue life, the Vickers micro-hardness (HV) was measured and discovered to be 134.5/HV with a reasonable scatter. Throughout the entire fatigue life (%), as cyclic loading intervals were applied, a gradual decrease in the "HV" has been noticed. Simultaneously, the scatter in Vickers micro-hardness has retrieved marginally similar response until 100% of fatigue life, but after specimen failure, more scatter observed. The micro-hardness has been reduced by 25% from 134.5/HV to 100.5/HV over an entire fatigue life for Al 6061 – 31 under fully reversed 0.01 mm/mm strain amplitude.

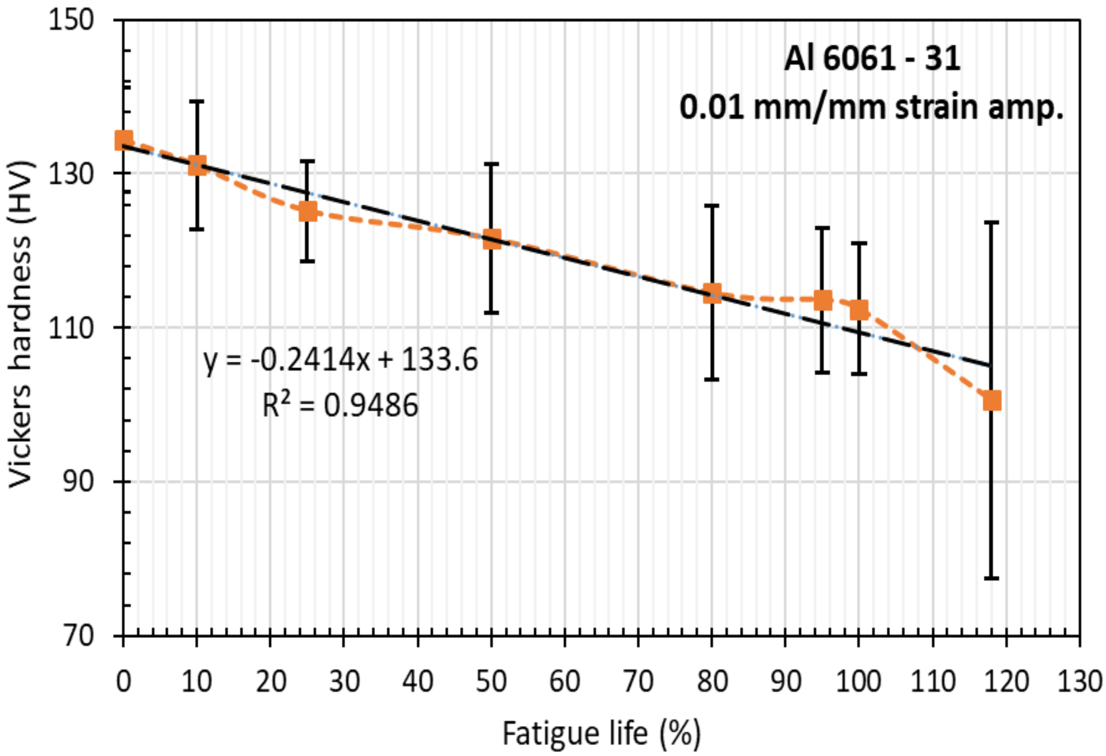

Figure 4.17 Vickers micro-hardness (HV) and scatter in "HV" against fatigue life (%) for Al 6061 – 31 under fully reversed 0.01 mm/mm strain amplitude.

4.3 Experimental analysis for Al 7075

4.3.1 Influence of surface roughness on Vickers micro-hardness

Experimental details for the surface roughness measurements and instrumented micro-indentations are provided in chapter 3. The outcomes for performed experiments have been mapped in this section, demonstrating the Vickers micro-hardness (HV) as a function of arithmetic mean roughness “Ra” and root mean square (RMS) roughness “Rq” in following Figs. 4.18 and 4.19.

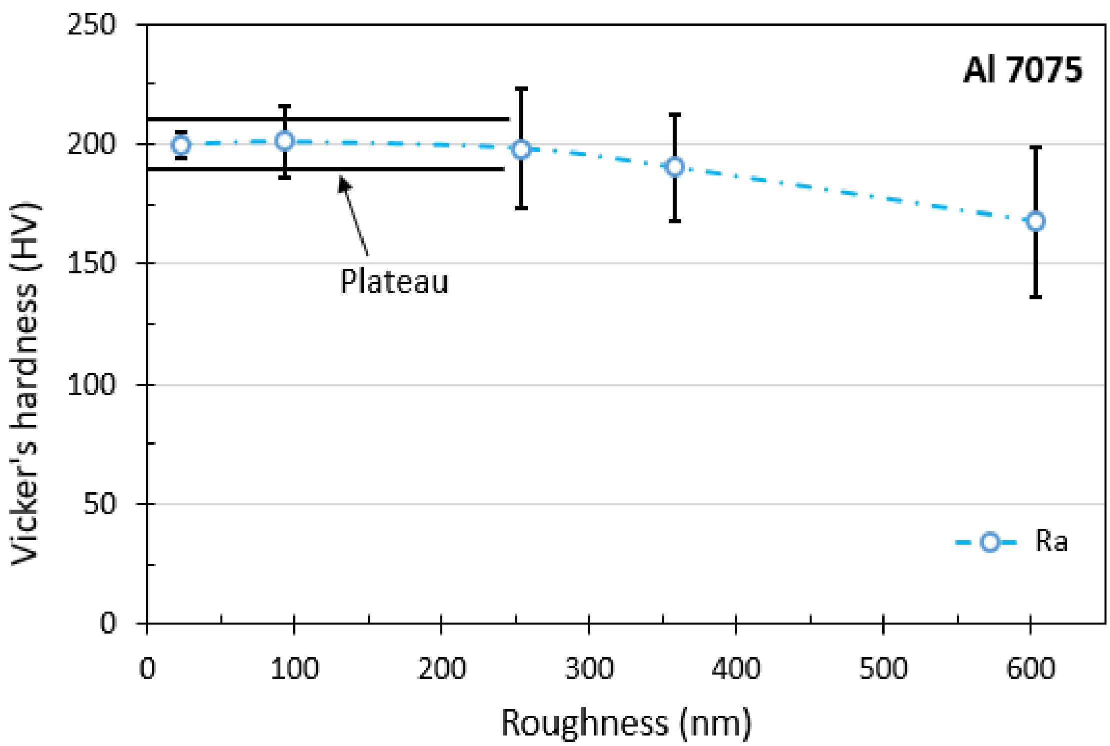

Figure 4.18 Vickers micro-hardness (HV) plotted as a function of the Arithmetic mean roughness “Ra” for Al 7075 alloy for a peak load of 1250 mN at 50mN/sec.

As mentioned above, Vickers micro-hardness (HV) and scatter in “HV” is plotted versus the roughness “Ra” for Al 7075 alloy, as shown in below figure 4.18. It has been noted that at surface roughness “Ra” of 20 nm hardness found to be 212/HV and minimal scatter was seen. Furthermore, no variation in “HV” has been viewed despite the “Ra” was raised to 250 nm, but higher scatter is spotted. However, additional increments in “Ra” like as to 350nm and 600nm “HV” observed to be falling with a higher scatter.

Figure 4.19 displays the roughness “Rq” plotted against Vickers micro-hardness “HV” for Al 7075 alloy. As described above, an analogous development in “HV” has been witnessed with an escalating “Rq” roughness.

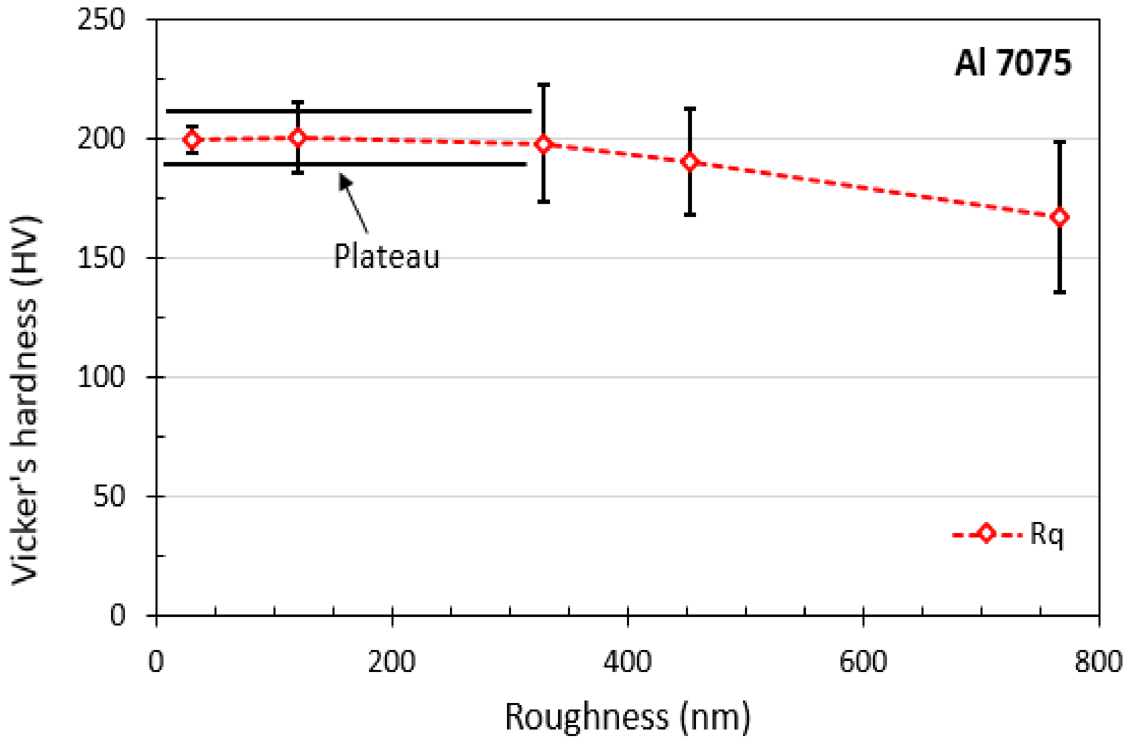

Figure 4.19 Vickers micro-hardness (HV) plotted as a function of the root mean square roughness “Rq” for Al 7075 alloy for a peak load of 1250 mN at 50 mN/sec.

In short, the Vickers micro-hardness “HV” highly depends on the surface roughness of the material. On the other hand, the roughness values for “Ra” and “Rq” below 250 nm do not exhibit marginal alterations in “HV,” as a result, roughness values below 250 nm are perfect for instrumented micro-indentations, and this surface roughness could be achieved by polishing sample to 800 – 1000 grit size silicon carbide papers.

4.3.2 Relationship in the destructive and non-destructive test method for Al 7075

4.3.2.1 Cyclic micro-hardness indentation results (Non-destructive test method)

Load-controlled cyclic micro-hardness indentations, as described in the previous section 4.2.2.1, have been performed. At each peak load, 25 cycles applied, and the acquired outcomes have been analyzed and plotted in the below figure.

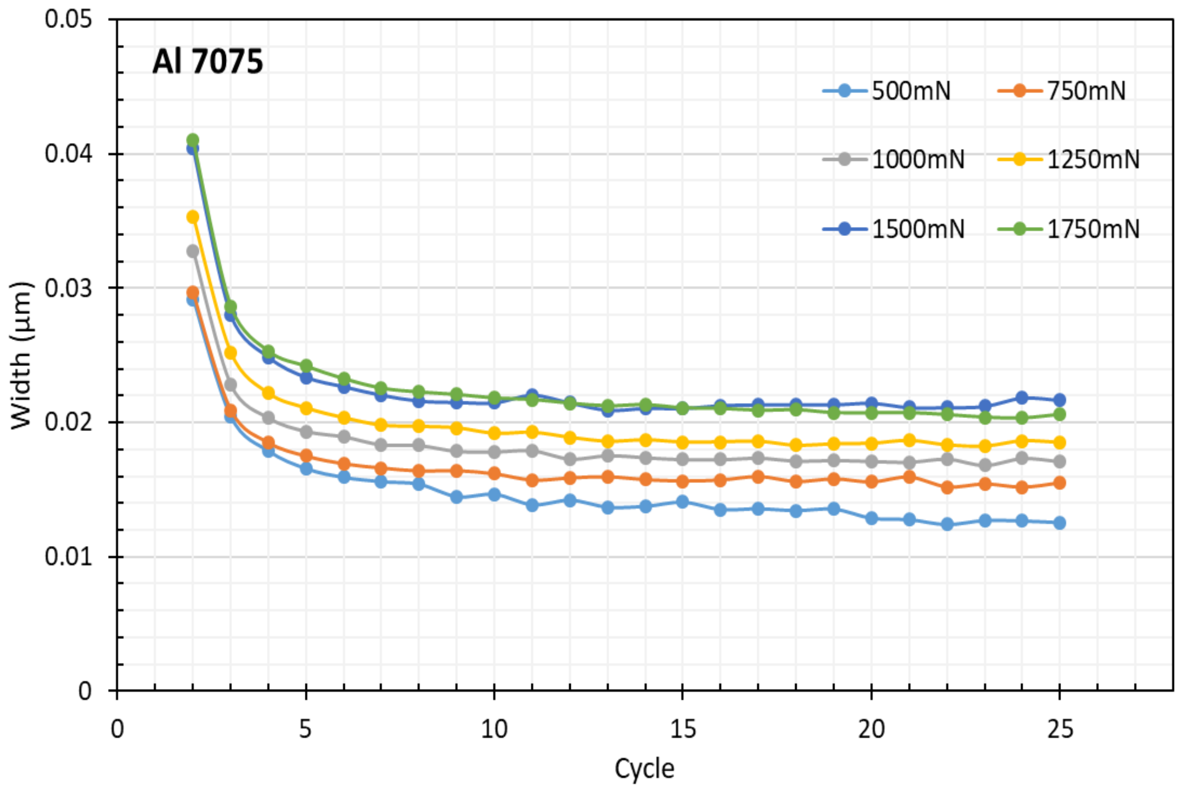

Figure 4.20 Plastic deformation (width) calculated at each hysteresis loop plotted as a function of cycles for Al 7075, applied at stress levels ranging from 500 mN to 1750 mN at the load rate of 50 mN/sec.

For every hysteresis loop width at a mean indentation load was determined and has been plotted against the applied number of cycles, as illustrated in figure 4.20. From the above figure, it is understandable that as more cycles were applied, the reduction in plastic deformation has been noticed. After specific cycles like as on or after the 13th cycle, the plasticity in the material expresses a negligible impact. Comparable pattern found for all peak indentation loads ranging from 500 – 1750 mN.

For all peak indentation load levels, the width of a stabilized hysteresis loop is determined and noted. The attained values for Al 7075 have been mapped with the applied indentation loads, as displayed in figure 4.21.

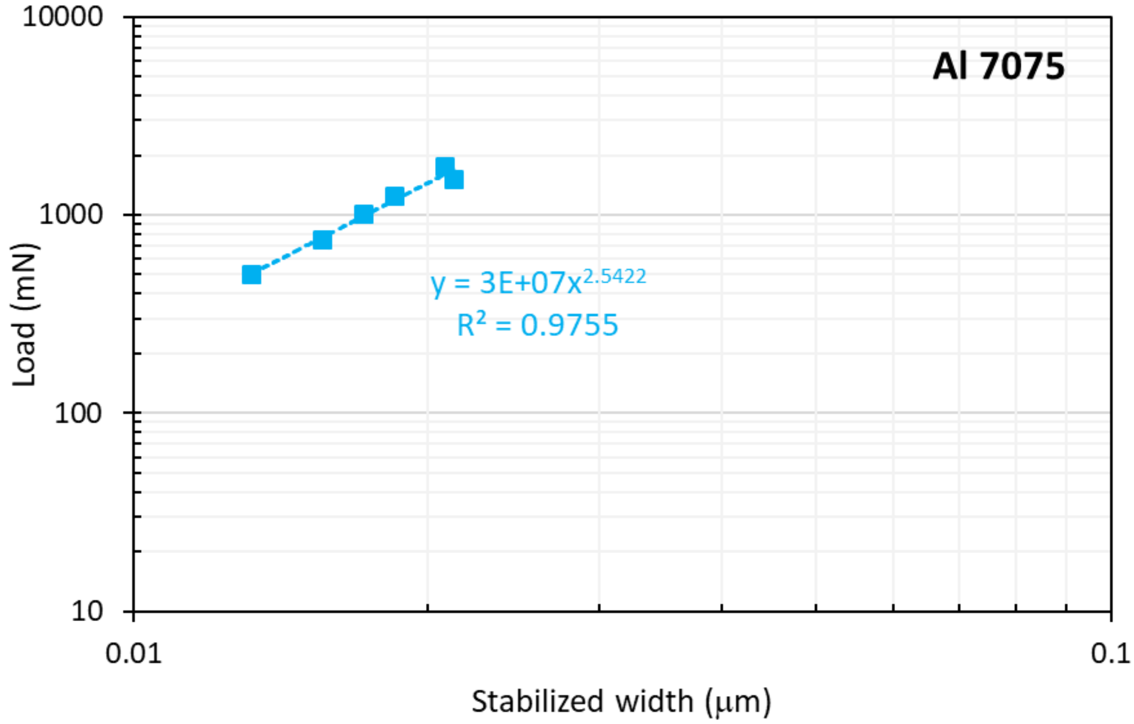

Figure 4.21 Plastic strain amplitude (ε_{pa}) as a function of stress amplitude (MPa) gained from cyclic strain-controlled tests for Al 7075 alloy.

Figure 4.21 shows a log-log scale with the width (μm) of a stabilized hysteresis loop on a horizontal axis and peak indentation load on a vertical axis for Al 7075 alloy. The above plot demonstrates a power-law relationship amongst a width of the hysteresis loop and the maximum indentation load. The correlation presented in terms of an equation that has been disclosed in the above figure. The extracted equation provides a strain hardening exponent "n" and strain hardening coefficient "A" from cyclic micro-indentation.

4.3.2.2 Destructive test results

Chapter 3 describes the experimental details of a strain-controlled fatigue test performed for Al 7075 alloy at different strain amplitudes. The experimental outcomes are presented in the following Figs. 4.22 – 4.24. The resulting figures show that plastic strain amplitude (ε_{pa}) mapped against fatigue life (N_f).

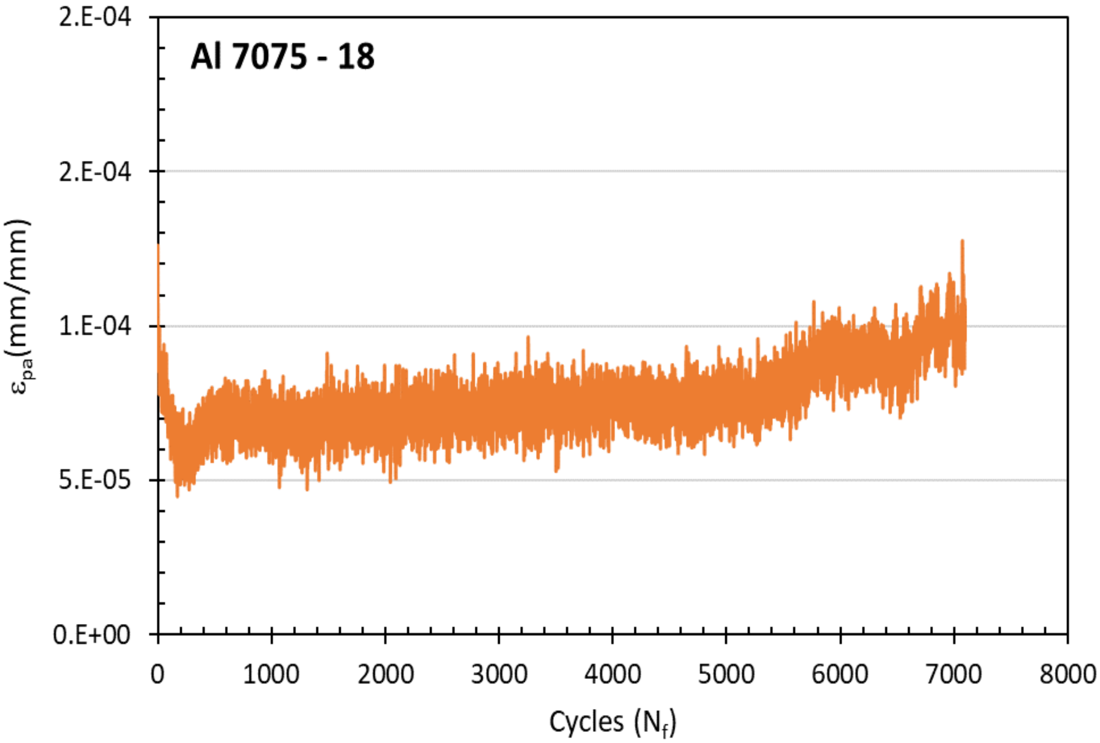

Figure 4.22 Plastic strain amplitude (ε_{pa}) as a function of a number of cycles (N_f) applied for Al 7075 – 18 at 0.005mm/mm strain amplitude and 0.5 Hz frequency.

In figure 4.22, for Al 7075 – 18 at 0.005mm/mm strain amplitude, an initial falloff in "ε_{pa}" has been observed until 200 cycles, and subsequently, the plastic strain amplitude becomes stable, and stabilization is seen up to roughly around 4000 cycles. However, after that, with increasing cycles, a rise in "ε_{pa}" has been recorded, and it lasted until specimen failure.

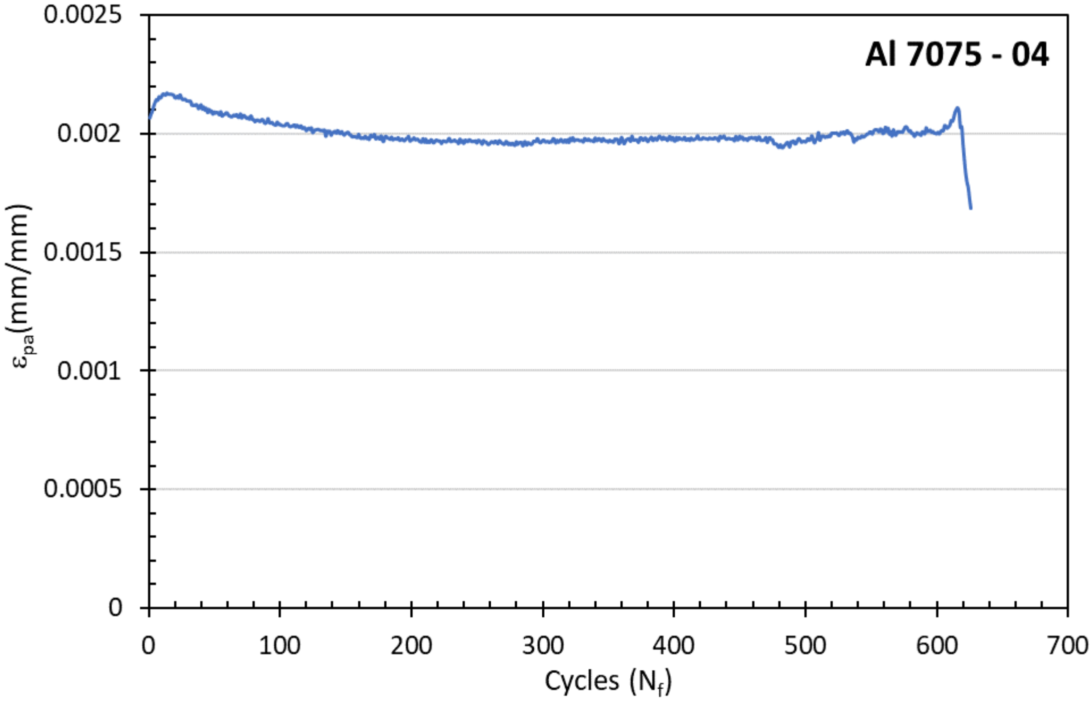

Figure 4.23 Plastic strain amplitude (ε_{pa}) as a function of a number of cycles (N_f) applied for Al 7075 – 04 at 0.01mm/mm strain amplitude and 0.5 Hz frequency.

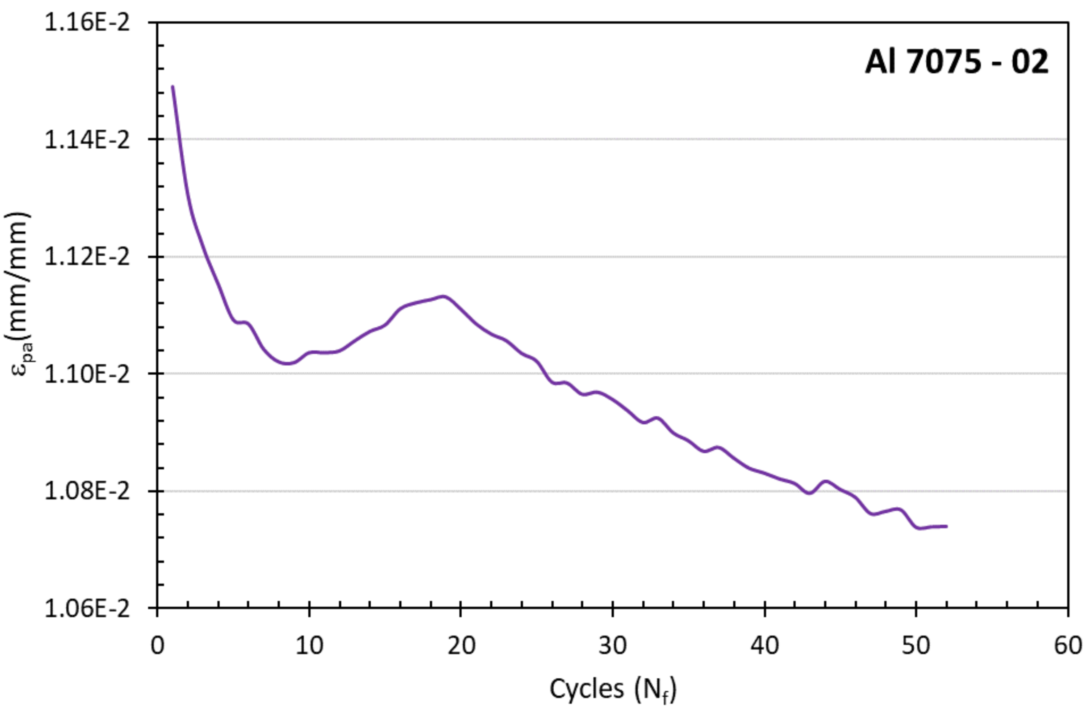

Figure 4.24 Plastic strain amplitude (ε_{pa}) as a function of a number of cycles (N_f) applied for Al 7075 – 02 at 0.02mm/mm strain amplitude and 0.5 Hz frequency.

Furthermore, figure 4.23 reveals an initial rise, followed by a drop in plastic strain amplitude (ε_{pa}). After 150 cycles, the "ε_{pa}" demonstrates a steady response up until 90 – 95% of the total fatigue life. As shown in figure 4.24, the Al 7075 – 03 under 0.02 mm/mm strain amplitude the "ε_{pa}" is observed to decreasing in the first eight cycles, and after that, a growth up to 20 cycles has been watched. With additional cycles, the plastic strain amplitude starts falling until the specimen fails.

Utilizing Figs. 4.22 – 4.24, a plastic strain amplitude (ε_{pa}) at a steady-state or half-life for all strain amplitude is determined and utilized for further analysis. The gained values for all specimens are detailed in the following table.

Table 4.3 Specifics of stress amplitude and plastic strain amplitude at steady state/half-life for Al 7075.

Specimen	**Stress amplitude (MPa)**	**Plastic strain amplitude (mm/mm)**	**Half-life cycle**
Al 7075 – 18	340	2.30E-05	1500th
Al 7075 – 04	508	1.96E-03	250th
Al 7075 – 02	551	1.10E-02	10th

The above data has been plotted on a log-log scale, as displayed in figure 4.25. The plot demonstrates stress amplitude (MPa) as a function of plastic strain amplitude "ε_{pa}" (mm/mm) for Al 7075 alloy under 0.005, 0.01, 0.02 mm/mm strain amplitudes. The power-law relationship has been discovered, and the developed relation is exhibited in the following equation.

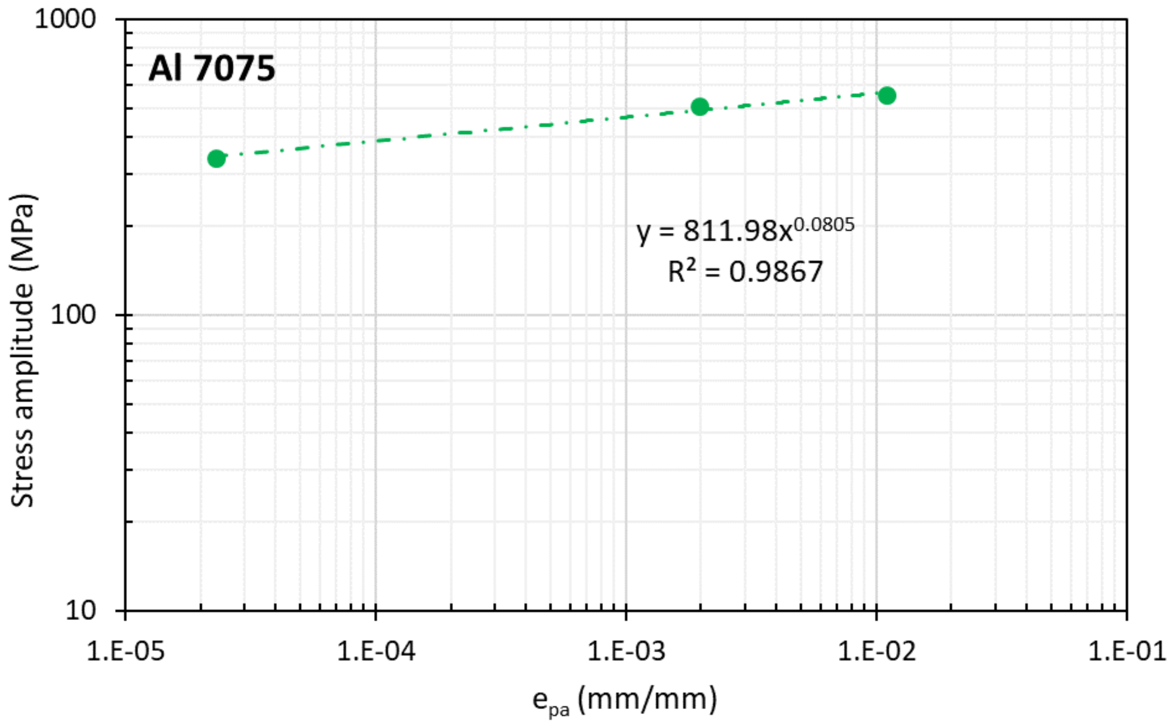

Figure 4.25 Plastic strain amplitude (ε_{pa}) as a function of stress amplitude (MPa) gained from cyclic strain-controlled tests for Al 7075 alloy.

Table 4.4 Specifics of stress amplitude and plastic strain amplitude at steady-state for Al 7075 – 19.

Al 7075 - 19		
Stress amplitude (MPa)	**Plastic strain amplitude (mm/mm)**	**Half-life cycle**
435	1.56E-04	250th
460	1.76E-04	500th
473	2.29E-04	750th
485	2.93E-04	1000th

Following the cyclic strain-controlled tests, the cyclic compression test for Al 7075 – 19 was performed as described in chapter 3. The obtained "ε_{pa}" and stress amplitudes are listed in table 4.4. The table data has been plotted on a log-log scale, as presented in figure 4.26. The following plot displays a power-law relationship, and it has been represented in the form of an equation, as in figure 4.26.

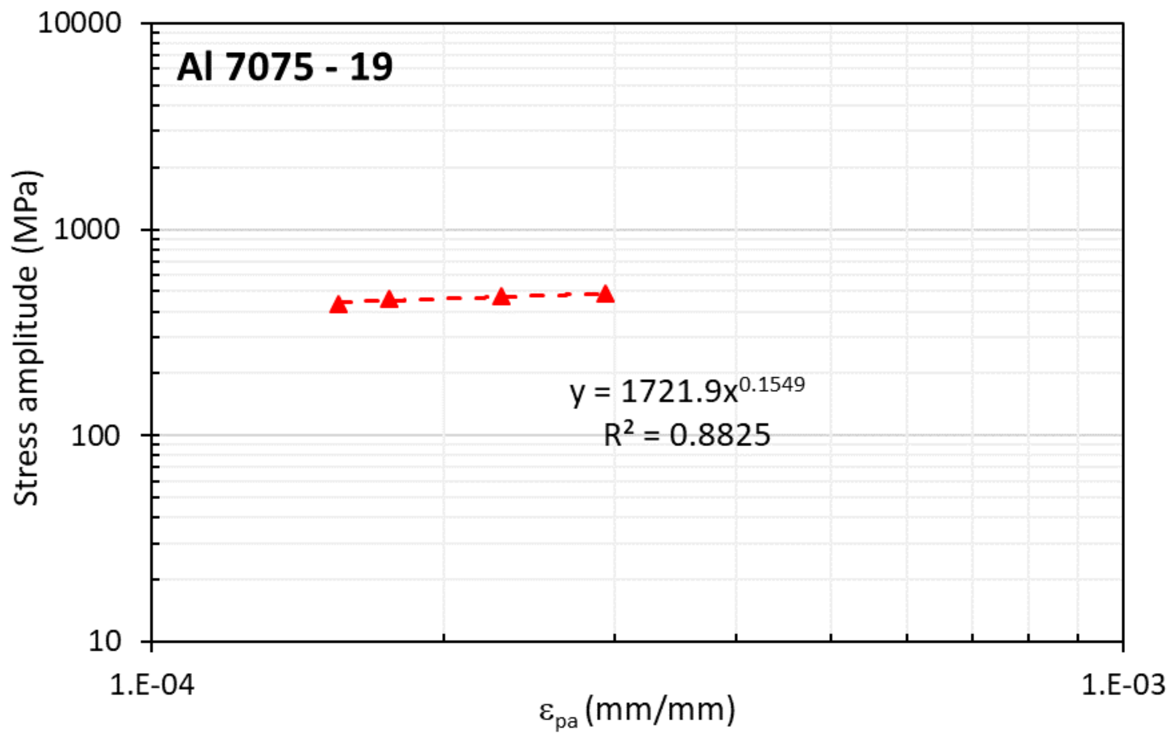

Figure 4.26 Plastic strain amplitude (ε_{pa}) mapped versus the stress amplitude (MPa) gained from the cyclic compression test for Al 7075 - 19.

4.3.2.3 Discussion

As clarified and exhibited in the above segments, 4.3.2.1 and 4.3.2.2, the achieved power-law relationship outlines are contrasted to discover the resemblances or any contemporary connection between them. The gained information from strain-controlled fatigue tests and stress-controlled cyclic compression is plot together. The collected data appears in figure 4.27, indicating the stress amplitude on a vertical axis and plastic deformation on a horizontal axis.

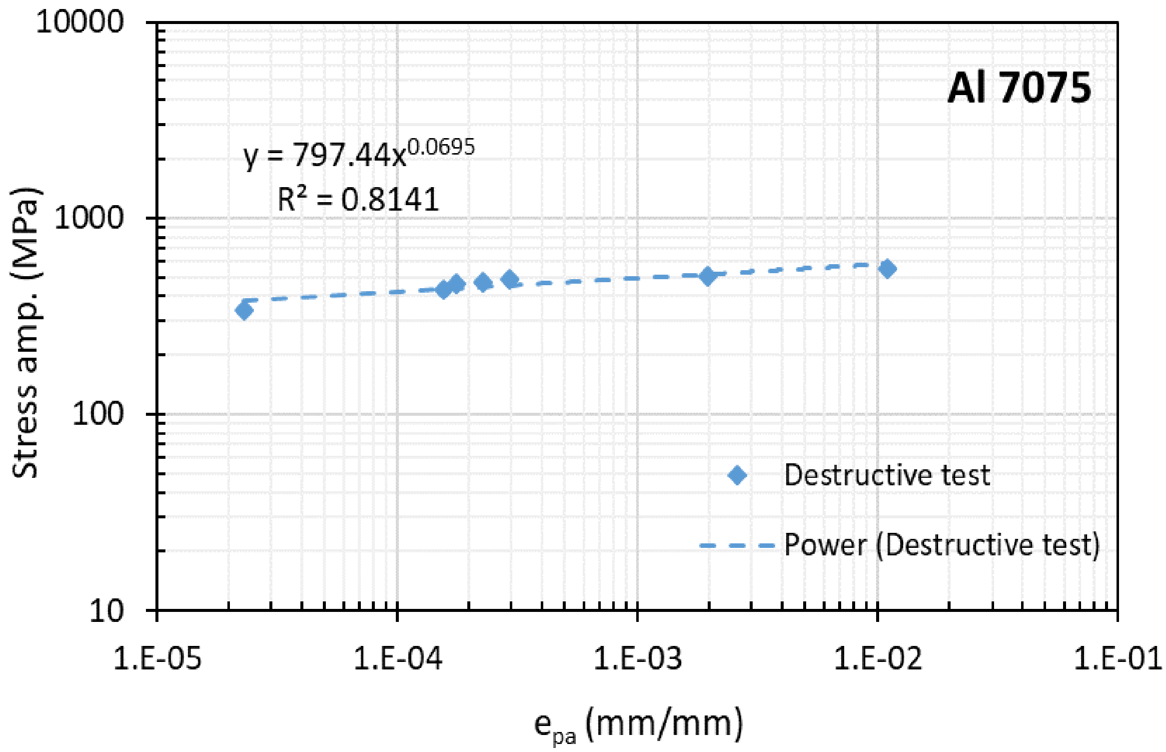

Figure 4.27 Combination of data gained from cyclic strain-controlled tests and the cyclic compression test for Al 7075 alloy.

Figure 4.27 demonstrates a correlation between the information received from cyclic strain-controlled testing and the cyclic compression testing. The resulted equation gives 0.0695 for strain hardening exponent “n” and 797 for strain hardening coefficient “A”. The results obtained will be compared with the information gained from cyclic micro-indentation in order to establish an existing relationship between them.

4.3.3 Characterization of fatigue damage for Al 7075 alloy

4.3.3.1 Damage test results for 0.005 mm/mm strain amplitude

Chapter 3 discusses the experimental details of an intermittent fatigue damage test method carried out at 0.005 mm/mm strain amplitude for Al 7075. The accomplished outcomes are exhibited and described below.

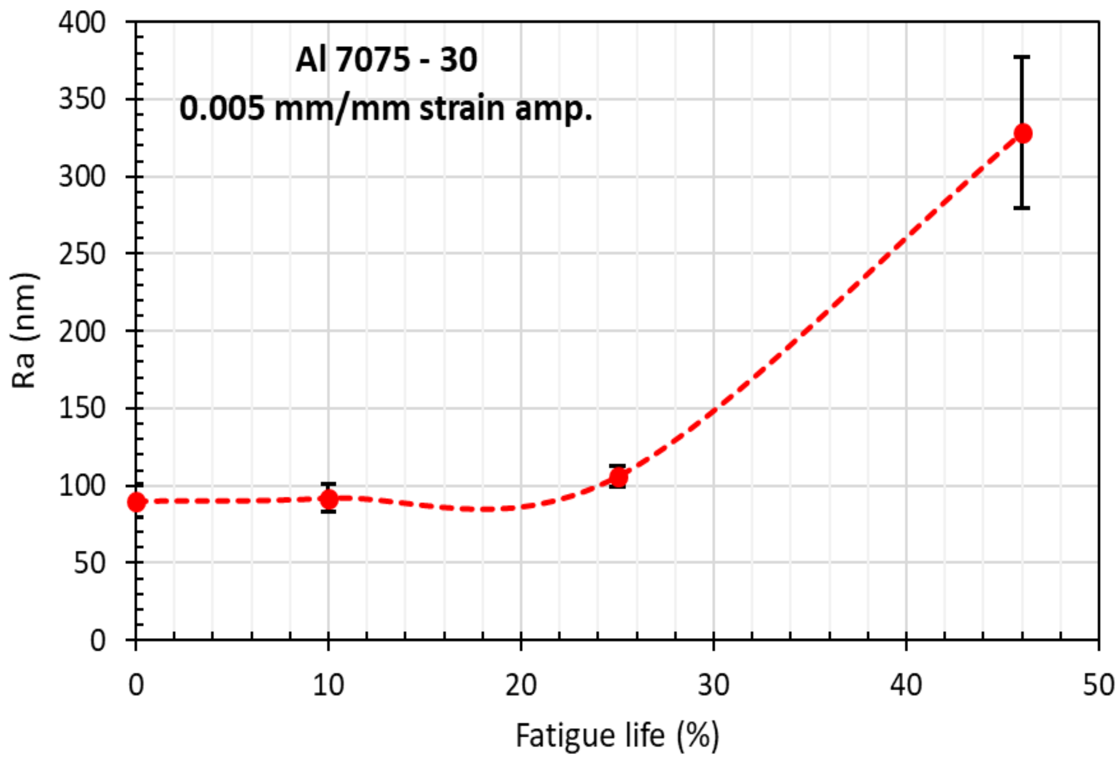

Figure 4.28 Surface roughness (Ra) and scatter in "Ra" versus fatigue life (%) for Al 7075 – 30 under fully reversed 0.005 mm/mm strain amplitude.

The above figure 4.28 illustrates, arithmetic surface roughness "Ra" (nm) and scatter in "Ra" mapped as a function of fatigue life (%). As revealed in the above figure, surface roughness and the scatter shows a steady response following 10% of fatigue life. Subsequent to the 10% when a specimen was loaded, and 25% of life applied. A small increase in "Ra" from 92 nm to 106 nm has been noted, and at the same time, the scatter lessened. The specimen was failed after applying 46% of fatigue life, and the "Ra" found at failure is 210% higher. Additionally, the scatter in "Ra" at failure found to be massive.

Similarly, in figure 4.29, the normalized slopes for hysteresis and micro-indentation are being plotted and compared with varying fatigue life (%). It has been noted that with an initial increase in fatigue life from 10% to 25%, normalized hysteresis and micro-indentation slopes do not show any changes. However, as more cycles were applied, normalized slopes for hysteresis and micro-indentation are seen to be decreasing. In conclusion, the normalized hysteresis and micro-indentation slopes demonstrate a similar response under the increasing fatigue life.

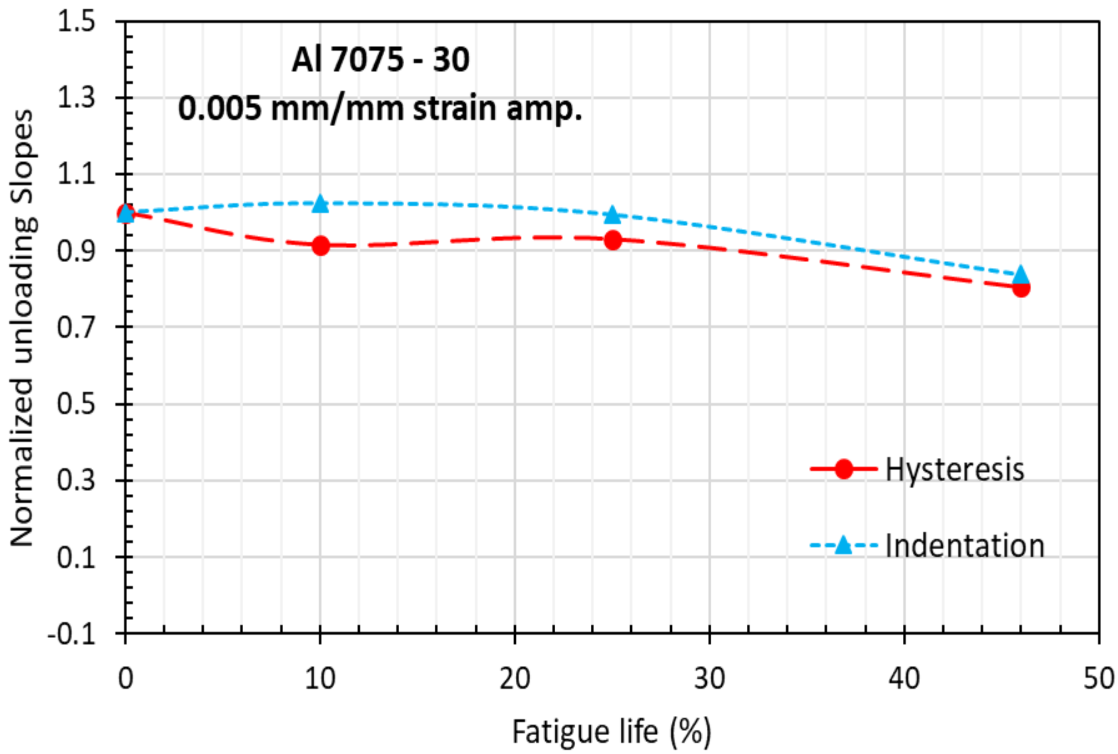

Figure 4.29 Normalized unloading slopes for hysteresis and micro-indentation as a function of fatigue life (%) for Al 7075 – 30 under fully reversed 0.005 mm/mm strain amplitude.

Vickers micro-hardness (HV) and scatter in it against fatigue life (%) has been shown in figure 4.30. The best fit line for the plotted data is drawn, and the obtained equation is also shown in the below figure. Before applying any loading intervals, the hardness measurements have been taken, and hardness found to be 208/HV. As 10% of fatigue life was applied, hardness decreased to 201/HV. Following that, no improvement in hardness was reported until 25% of fatigue life was applied, although it was noted that the hardness decreased after that. In particular, the Vickers hardness reduced from the original value by 6.5%.

Instantaneously, no modification was reported in the scatters until 25% of fatigue life, but after the failure of a specimen at 46% of fatigue life, scatters in HV were found to be elevated.

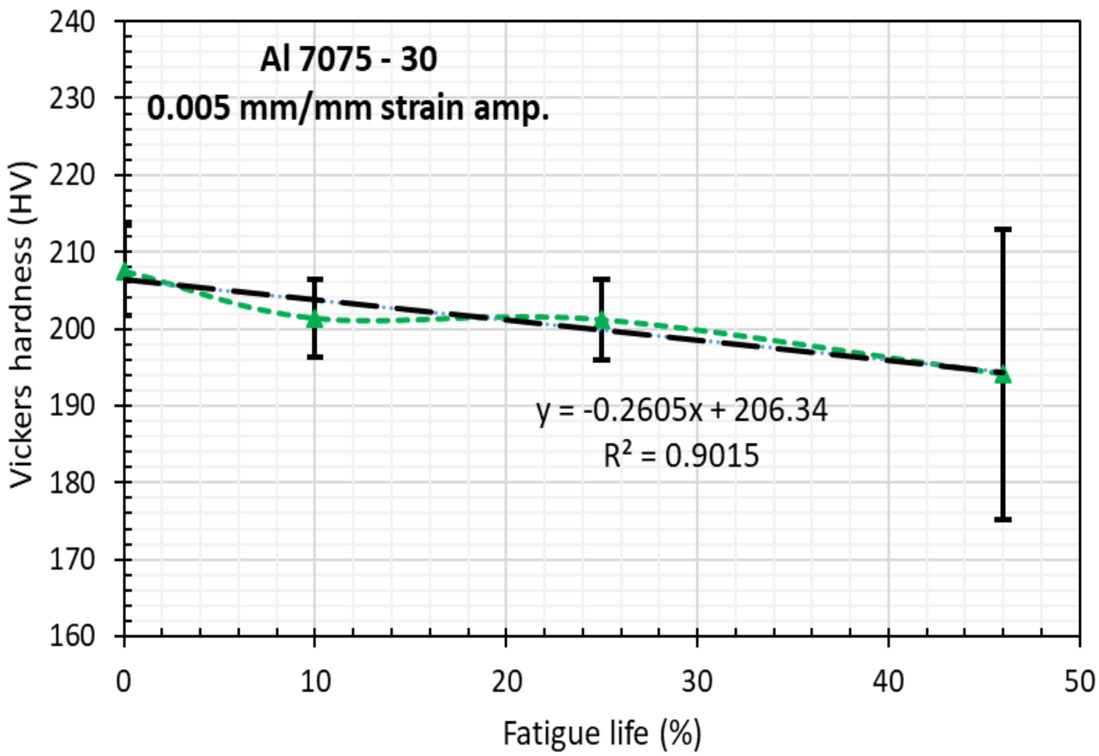

Figure 4.30 Vickers micro-hardness (HV) and scatter in "HV" against fatigue life (%) for Al 7075 – 30 under fully reversed 0.005 mm/mm strain amplitude.

4.3.3.2 Damage test results for 0.01 mm/mm strain amplitude

Similar to section 4.3.3.1, the fatigue damage test with 0.01 mm/mm strain amplitude has been carried out on Al 7075 – 31, and the resulting findings are described in detail in this section as below.

Roughness "Ra" (nm) mapped as displayed in figure 4.31 with fatigue life (%). As exhibited below, an increment in arithmetic roughness of 80 nm to 210 nm within an initial 10% of applied life was noticed. Nonetheless, a marginal rise in "Ra" was detected with an additional increase in fatigue life from 10 percent – 80 percent. The further rise in fatigue damage shows a significant change in "Ra" roughness until the failure has occurred. At the same time, no significant difference in scatter was recorded for entire fatigue life.

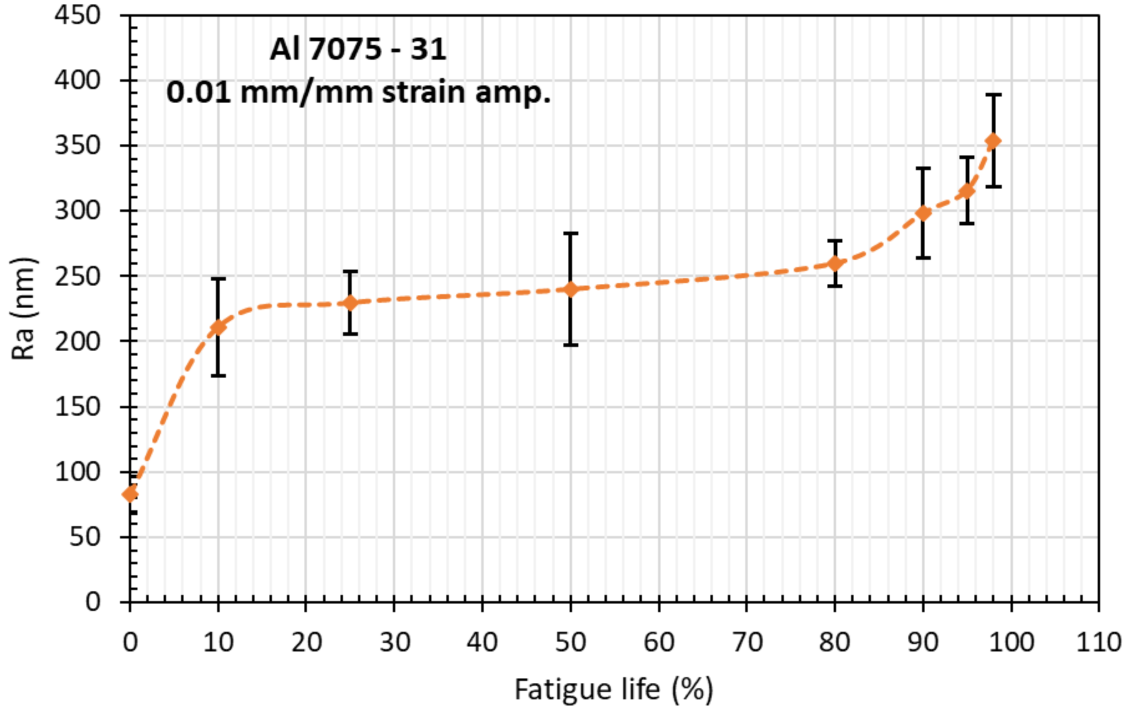

Figure 4.31 Surface roughness (Ra) and scatter in "Ra" versus fatigue life (%) for Al 7075 – 31 under fully reversed 0.01 mm/mm strain amplitude.

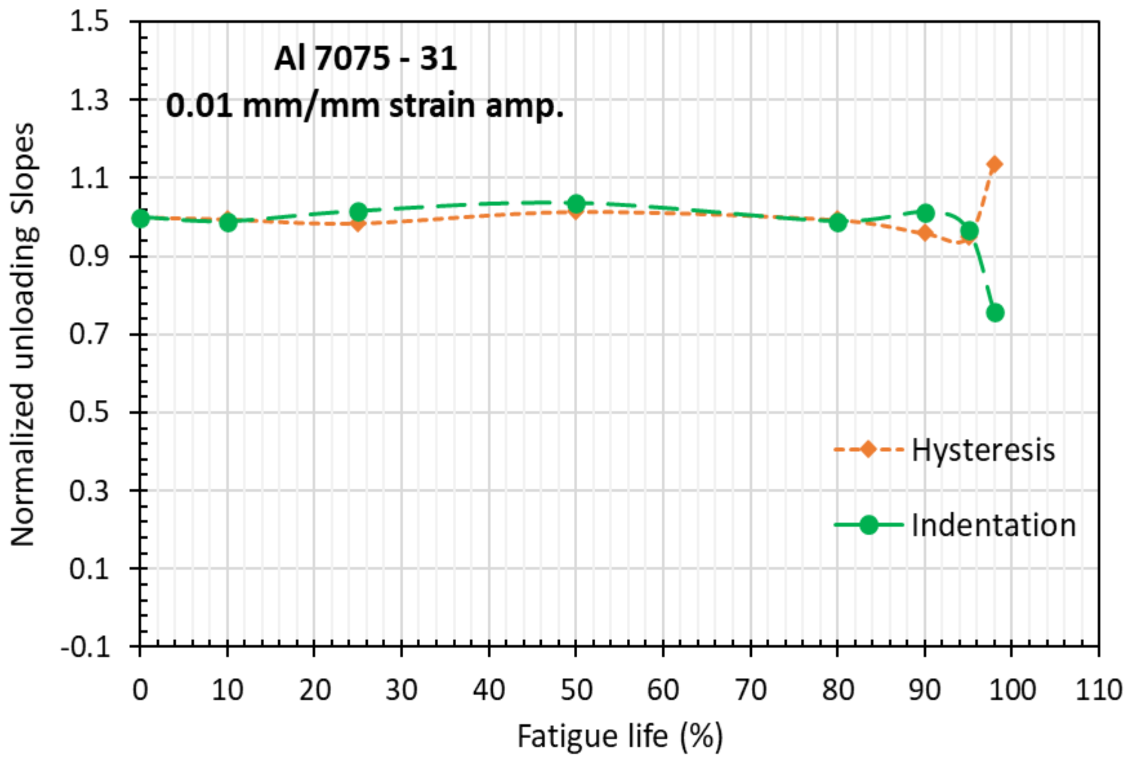

Figure 4.32 Normalized unloading slopes for hysteresis and micro-indentation as a function of fatigue life (%) for Al 7075 – 31 under fully reversed 0.01 mm/mm strain amplitude.

In figure 4.32, the normalized unloading slopes for hysteresis and micro-indentation has been mapped as a function of fatigue life (%). Normalized hysteresis and micro-indentation slopes are seen to be less influenced until 90% of fatigue life. However, after 90% of fatigue life until the failure of the sample, an abrupt increase in the normalized hysteresis slope is noticed. At the same time, the normalized micro-indentation slope is observed to be decreasing.

Following to the normalized micro-indentation and hysteresis unloading slopes, the Vickers micro-hardness for Al 7075 – 23 has been plotted versus the fatigue life. Figure 4.33 indicates fatigue life (%) on the horizontal axis, and the vertical axis shows a Vickers micro-hardness (HV) and scatter in “HV” for a fully reversed 0.01 mm/mm strain amplitude. A best-fit line for a given figure has been drawn, and the obtained best-fit equation is displayed in the following figure 4.33.

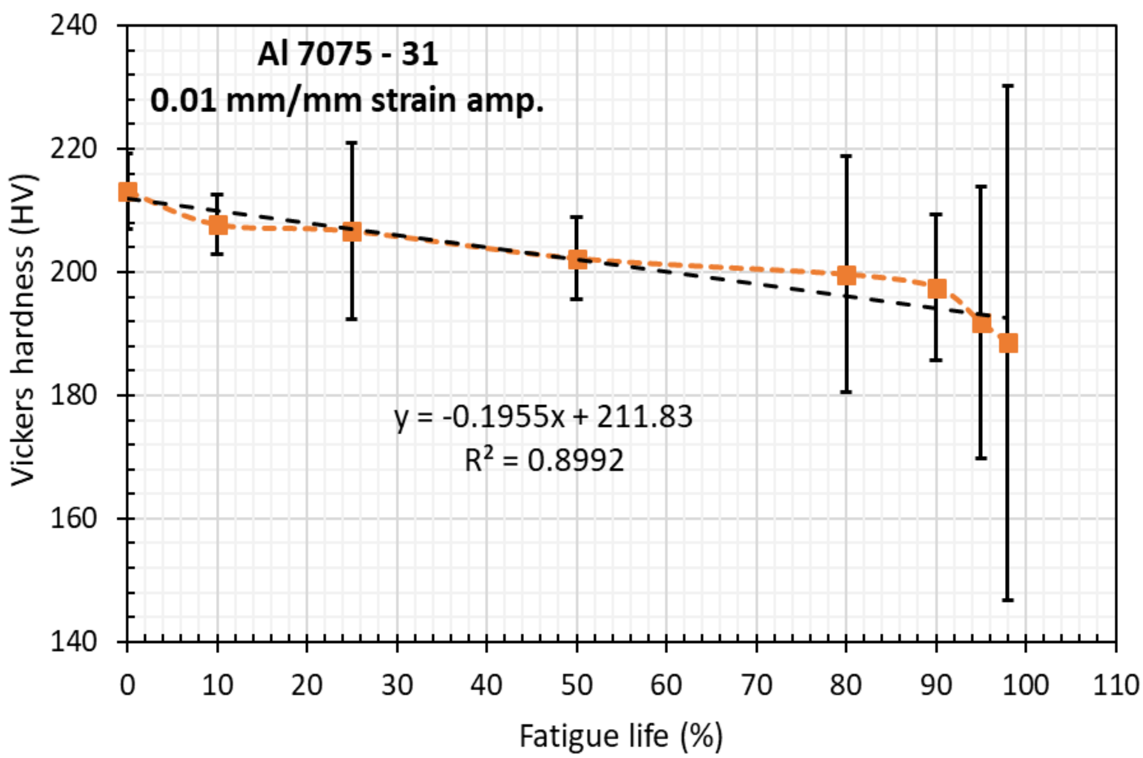

Figure 4.33 Vickers micro-hardness (HV) and scatter in “HV” against fatigue life (%) for Al 7075 – 31 under fully reversed 0.01 mm/mm strain amplitude.

As demonstrated in figure 4.33, similar to the previous section, before applying any fatigue life, the Vickers micro-hardness (HV) was measured. Initially, the hardness discovered to be 213/HV with some scatter. As cyclic loading intervals were applied, a gradual decrease in the "HV" has been noticed until 90% of fatigue life. At the same time, a marginal rise in the scatter has been observed. Further increase in cyclic loading interval indicates a significant decrease in Vickers micro-hardness. Besides, a decrease in Vickers micro-hardness, a substantial increase in scatter, was found as the fatigue damage was increased. Overall the Vickers hardness is decreased by 11.5 percent from 213/HV to 188/HV.

4.4 Discussion

The above sections examine the experimental results for Al 6061 and Al 7075 individually. End results from the above-described sections, when merged, the following interpretation has been made.

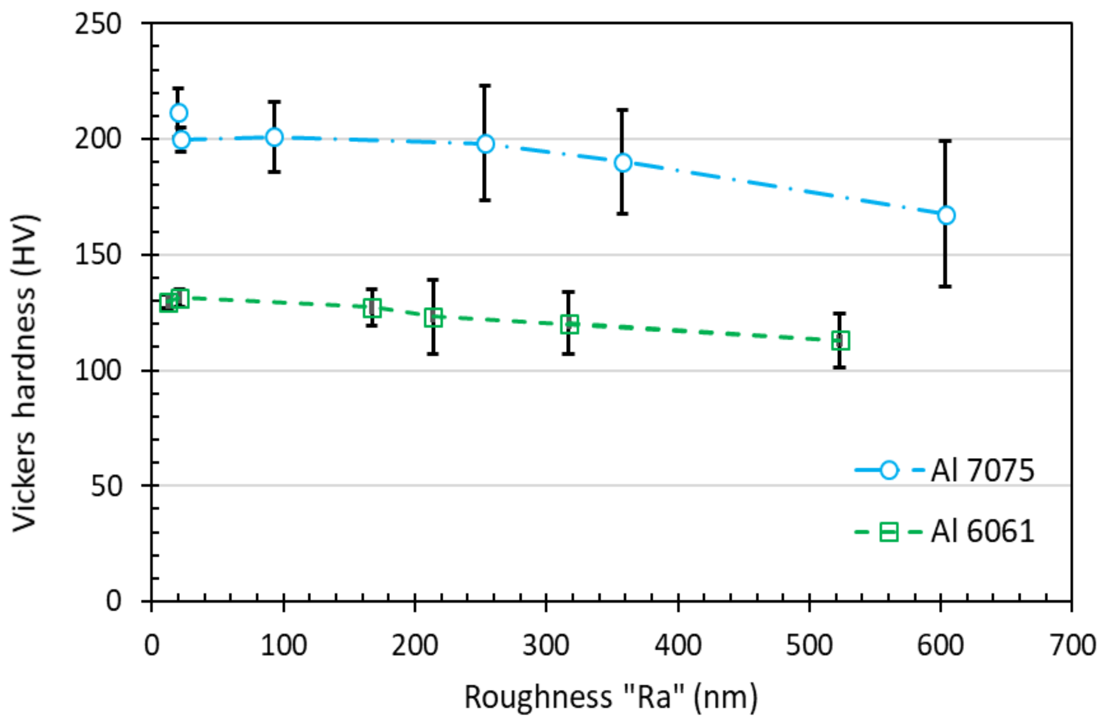

Figure 4.34 Vickers micro-hardness (HV) and scatter plotted as a function of the Arithmetic mean roughness "Ra" for Al 6061 and Al 7075 alloy for a peak load of 1250 mN at 50mN/sec.

Figure 4.34 outlines the findings for both aluminum alloys under sections 4.2.1 and 4.3.1. The Vickers micro-hardness "HV" plotted on a vertical axis and the average arithmetic surface roughness "Ra" on the horizontal axis. Based on the plot, it can be concluded that both aluminum alloys demonstrate a comparable trend, that with rising roughness "Ra" Vickers micro-hardness "HV" reduces. However, for both materials, scatter in Vickers hardness does not give any clear response. It can also be noticed that the very marginal scatter observed for small roughness values, and scatter appears to be increasing and decreasing for higher roughness values.

As described in section 4.2.2 and 4.3.2, the obtained plastic strain amplitudes for different experiments at distinct strain amplitudes are plotted together for both aluminum alloys, as displayed in Figs. 4.35 and 4.36. The following figures show a material response under three different strain amplitudes.

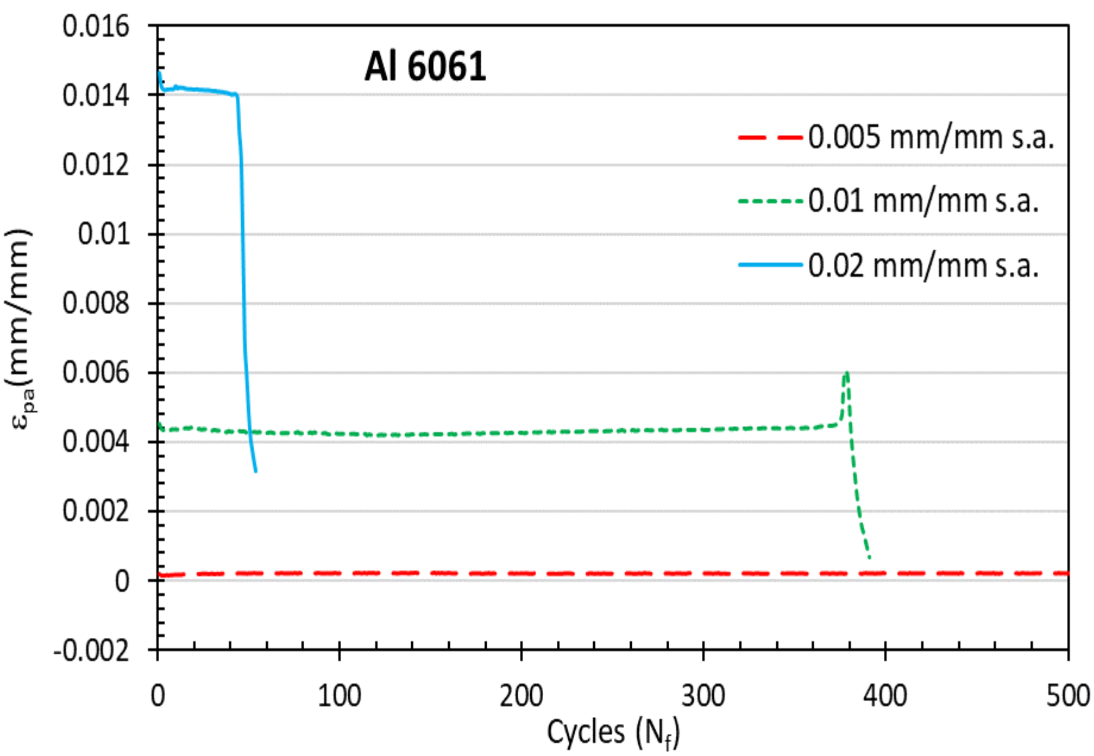

Figure 4.35 Plastic strain amplitude (ε_{pa}) as a function of a number of cycles (N_f) applied at 0.005 mm/mm, 0.01 mm/mm, and 0.02 mm/mm strain amplitude for Al 6061 alloy.

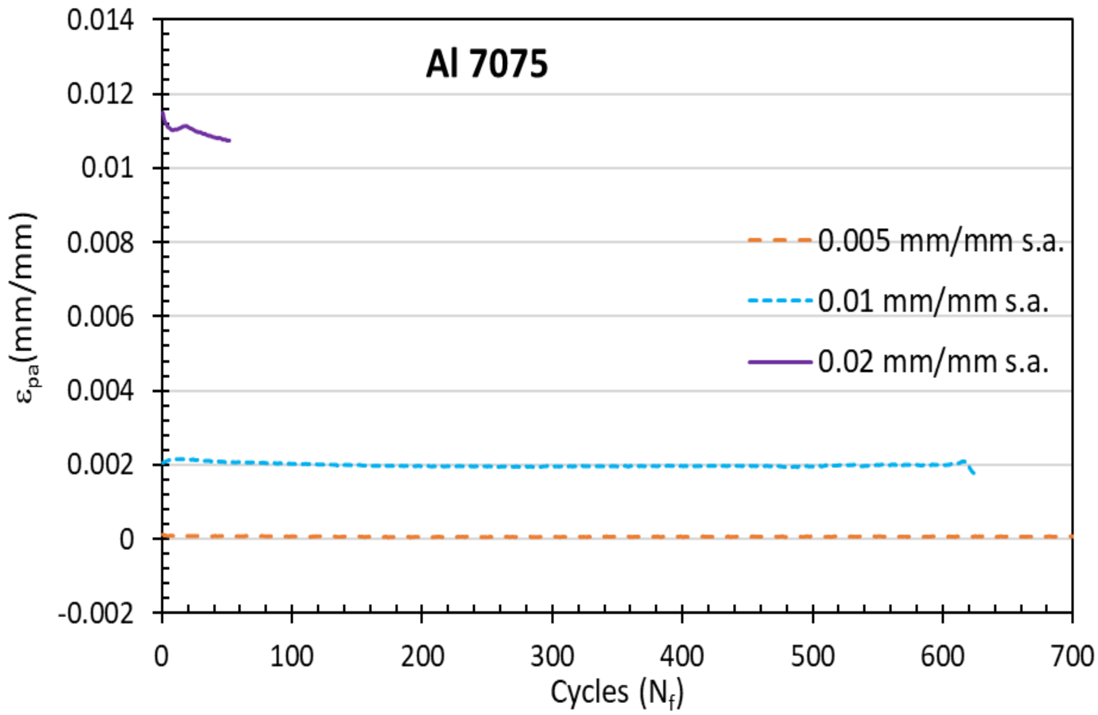

Figure 4.36 Plastic strain amplitude (ε_{pa}) as a function of a number of cycles (N_f) applied at 0.005 mm/mm, 0.01 mm/mm, and 0.02 mm/mm strain amplitude for Al 7075 alloy.

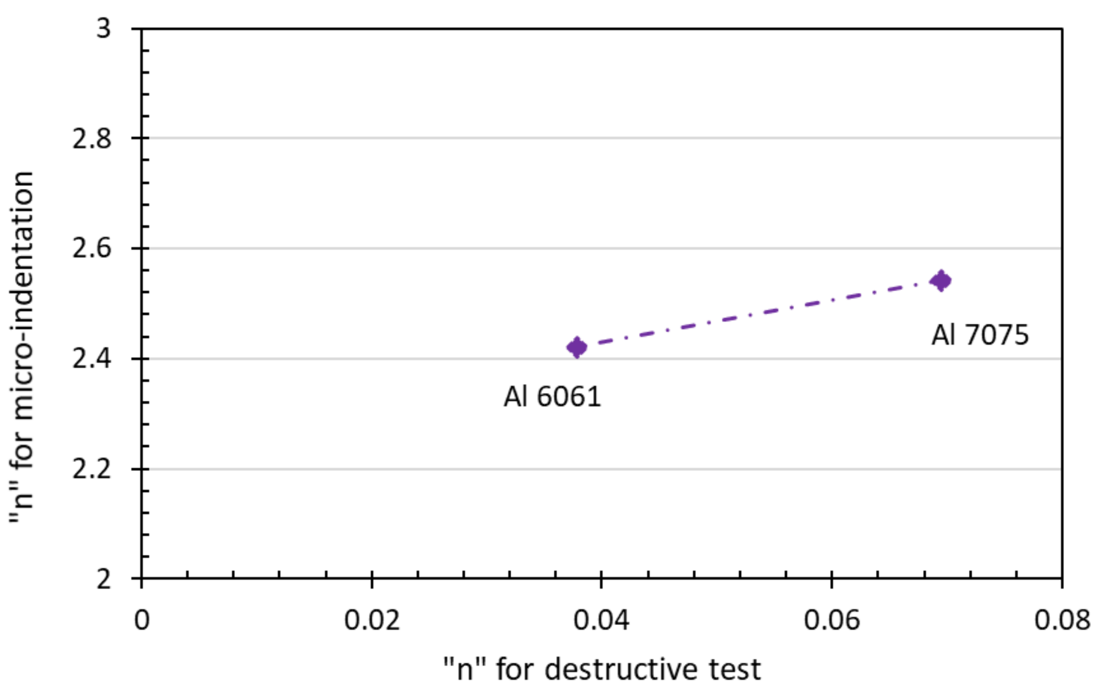

Figure 4.37 Strain hardening exponent "n" attained from cyclic micro-indentations plotted against a strain hardening exponent received from fatigue (destructive) tests for Al 6061 and Al 7075 alloys.

The above figure 4.37 demonstrated the strain hardening exponents resulted from cyclic micro-indentations and fatigue (destructive) tests, as described in sections 4.2.2.3 and 4.3.2.3 for both aluminum alloys Al 6061 and Al 7075. After plotting figure 4.37, it has been noticed that strain hardening exponents "n" obtained from fatigue (destructive) tests are directly proportional to the strain hardening exponent "n" resulted from cyclic micro-indentations. Based on the above figure, the strain hardening exponent "n" for fatigue (destructive) tests could be calculated as a result of an increase in strain hardening exponent for cyclic micro-indentations.

Following Figs. 4.38 and 4.39 show surface roughness "Ra" and scatter in it plotted as a function of fatigue life (%). As described in previous sections, the surface roughness increases with increasing fatigue life. Figure 4.38 shows a variation in surface roughness over fatigue life at two strain amplitudes. It is evident that for both strain amplitudes, Al 6061 shows a similar trend of increasing surface roughness.

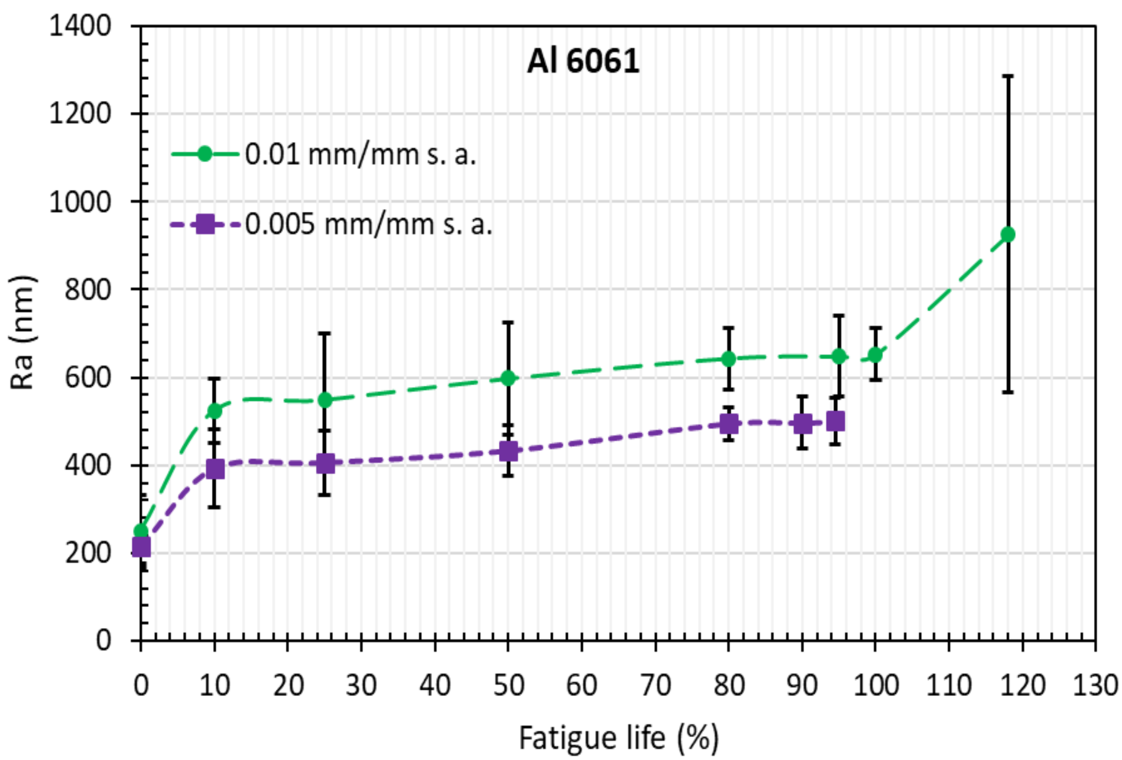

Figure 4.38 Surface roughness (Ra) and scatter in "Ra" versus fatigue life (%) for Al 6061 under fully reversed 0.005 mm/mm and 0.01 mm/mm strain amplitude.

For Al 7075, the results are plotted in figure 4.39. It has been observed that surface roughness for Al 7075 doesn't show a comparable response at two different strain amplitudes. However, the surface roughness response curve obtained at 0.01 mm/mm strain amplitude is somewhat equivalent to the Al 6061.

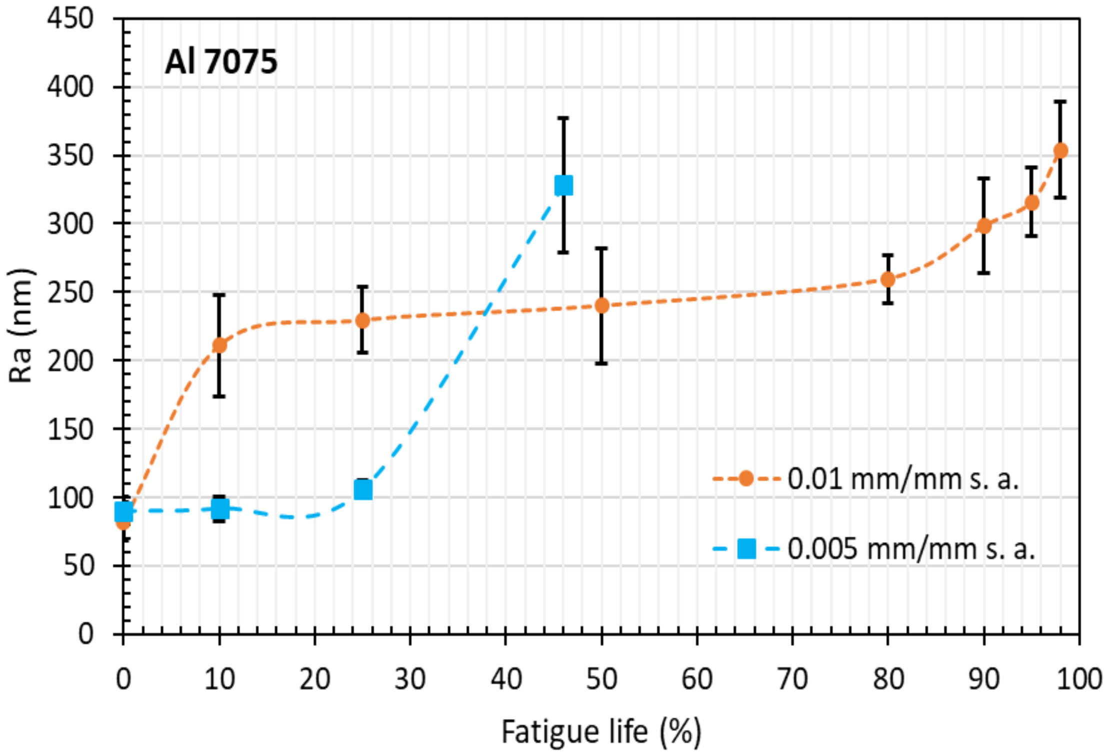

Figure 4.39 Surface roughness (Ra) and scatter in "Ra" versus fatigue life (%) for Al 7075 under fully reversed 0.005 mm/mm and 0.01 mm/mm strain amplitude.

The above data has been normalized to eliminate scatter and observe the effect of normalized roughness on fatigue damage. For doing so, the roughness "R" obtained after each cyclic loading interval was divided by the initial roughness "R_o." That obtained ratio "R/R_o" of roughness is the normalized roughness. The resulted information for Al 6061 and Al 7075 is plotted together, as shown in the following figure 4.40.

It has been concluded that surface roughness for both aluminum alloys is directly correlated to the fatigue damage.

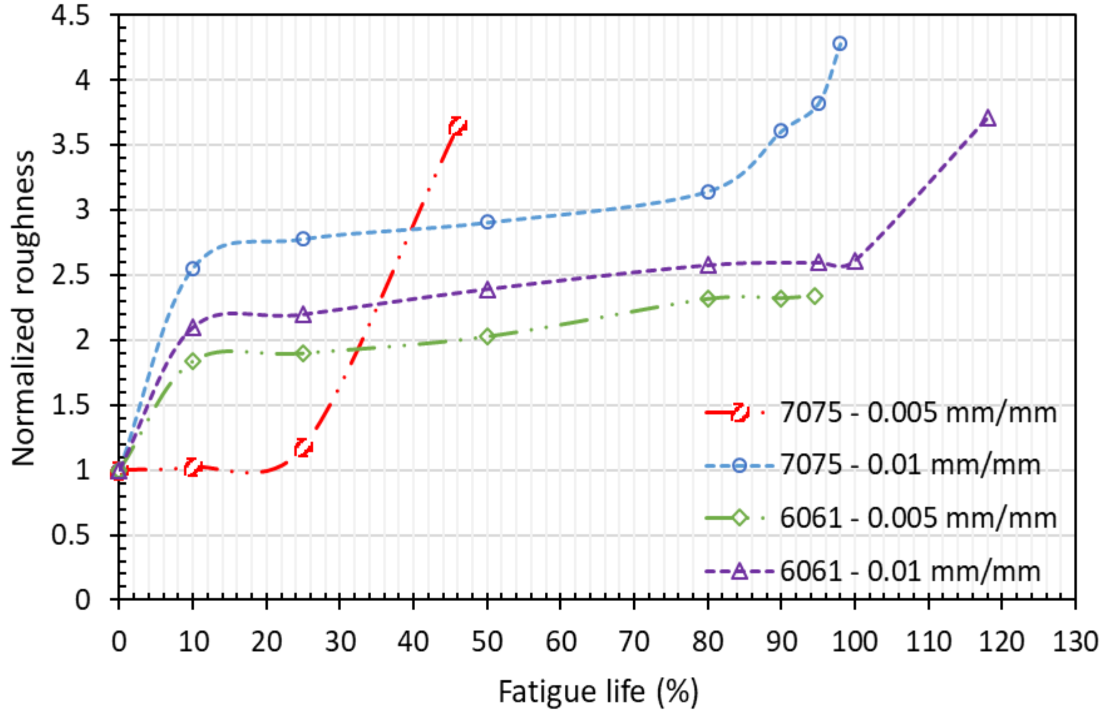

Figure 4.40 Normalized surface roughness (Ra) versus fatigue life (%) for Al 6061 and Al 7075 under fully reversed 0.005 mm/mm and 0.01 mm/mm strain amplitude.

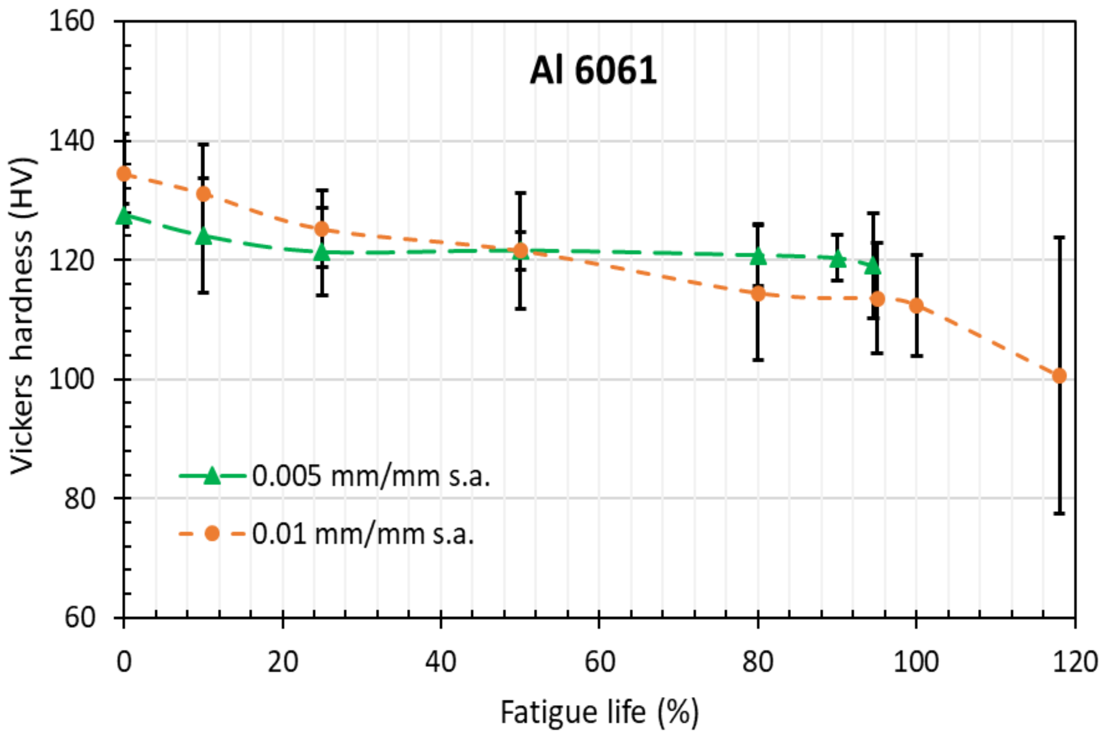

Figure 4.41 Vickers micro-hardness (HV) and scatter in "HV" against fatigue life (%) for Al 6061 under fully reversed 0.005 mm/mm and 0.01 mm/mm strain amplitude.

Similar to surface roughness, the Vickers micro-hardness "HV" is plotted against the fatigue life as shown in Figs. 4.41 and 4.42 for Al 6061 and Al 7075. As demonstrated in the above Figure 4.41, comparatively more falloff in the Vickers micro-hardness has been seen for 0.01 mm/mm strain amplitude than 0.005 mm/mm. Simultaneously, for Al 7075, a minimal reduction in Vickers micro-hardness has been seen for 0.005 mm/mm than 0.01mm/mm strain amplitude. Looking at the micro-hardness values for both materials, it is evident that Al 7075 is a harder material than Al 6061.

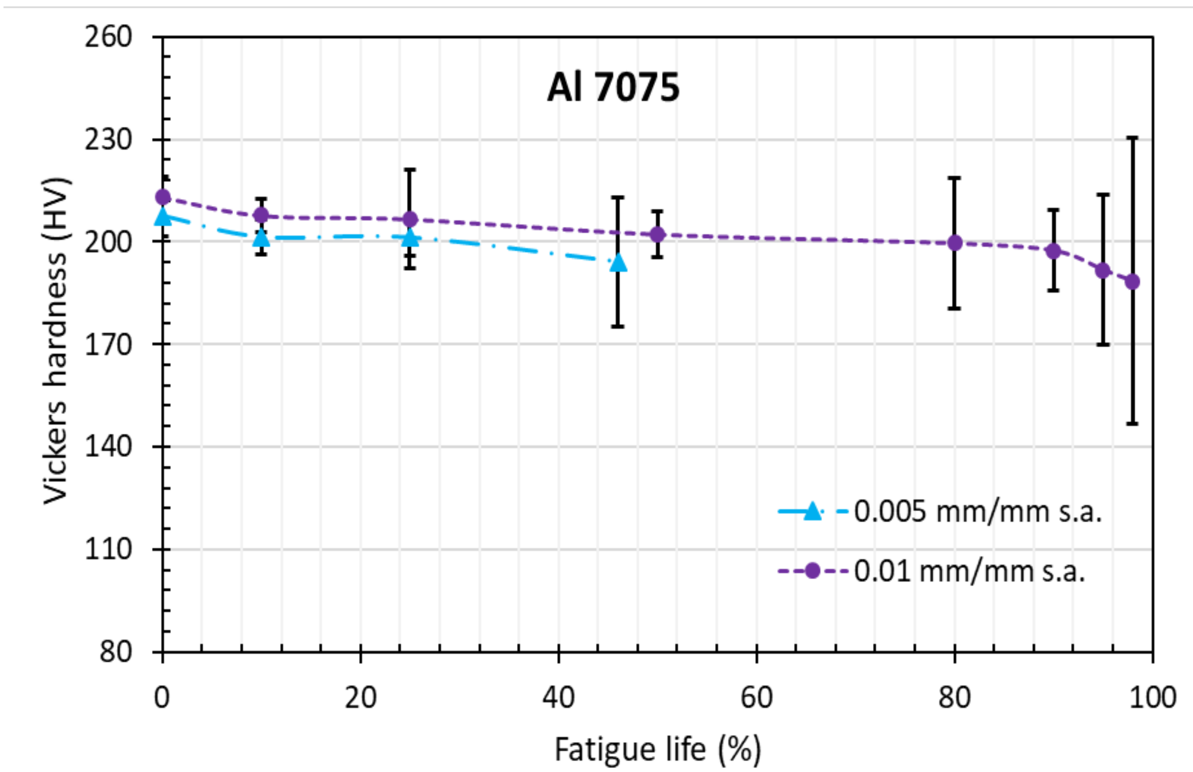

Figure 4.42 Vickers micro-hardness (HV) and scatter in "HV" against fatigue life (%) for Al 7075 under fully reversed 0.005 mm/mm and 0.01 mm/mm strain amplitude.

Analogous to the normalization of surface roughness, a similar process has been applied on the Vickers micro-hardness "HV" for both aluminum alloys. The Vickers micro-hardness "HV" obtained after each fatigue life interval has been divided by the initial Vickers micro-hardness "HV_o" to normalize the micro-hardness. The obtained ratio "HV/HV_o" is the normalized micro-hardness has been plotted against fatigue damage, as shown in Figs. 4.43 and 4.44.

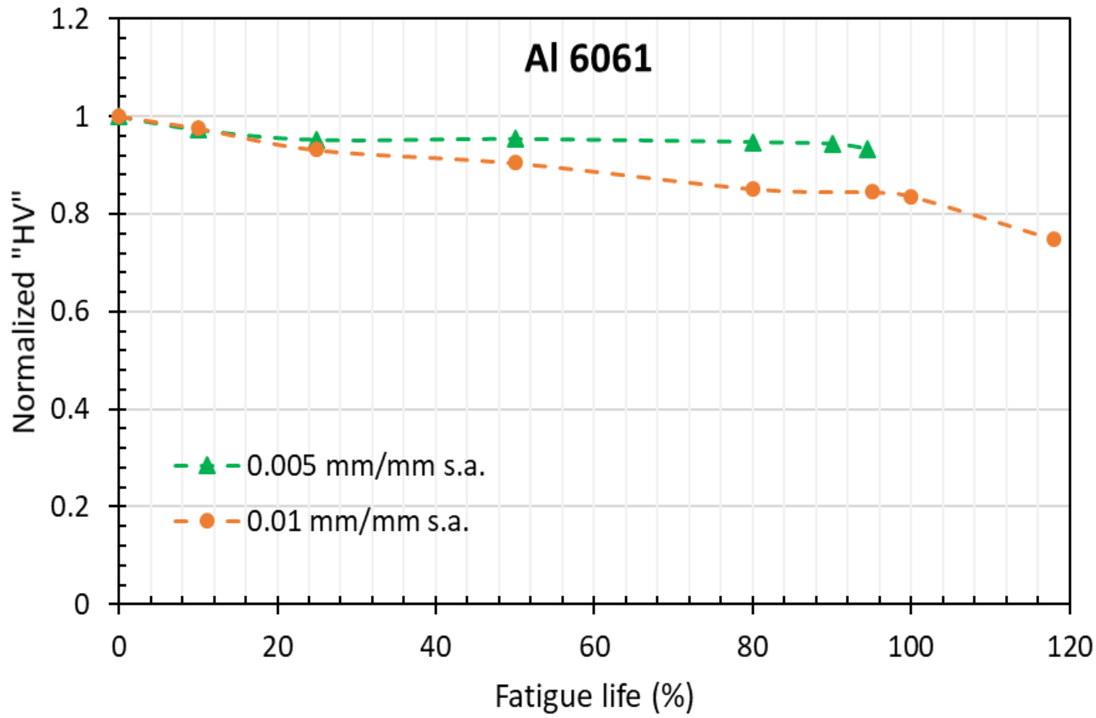

Figure 4.43 Normalized Vickers micro-hardness (HV) against fatigue life (%) for Al 6061 under fully reversed 0.005 mm/mm and 0.01 mm/mm strain amplitude.

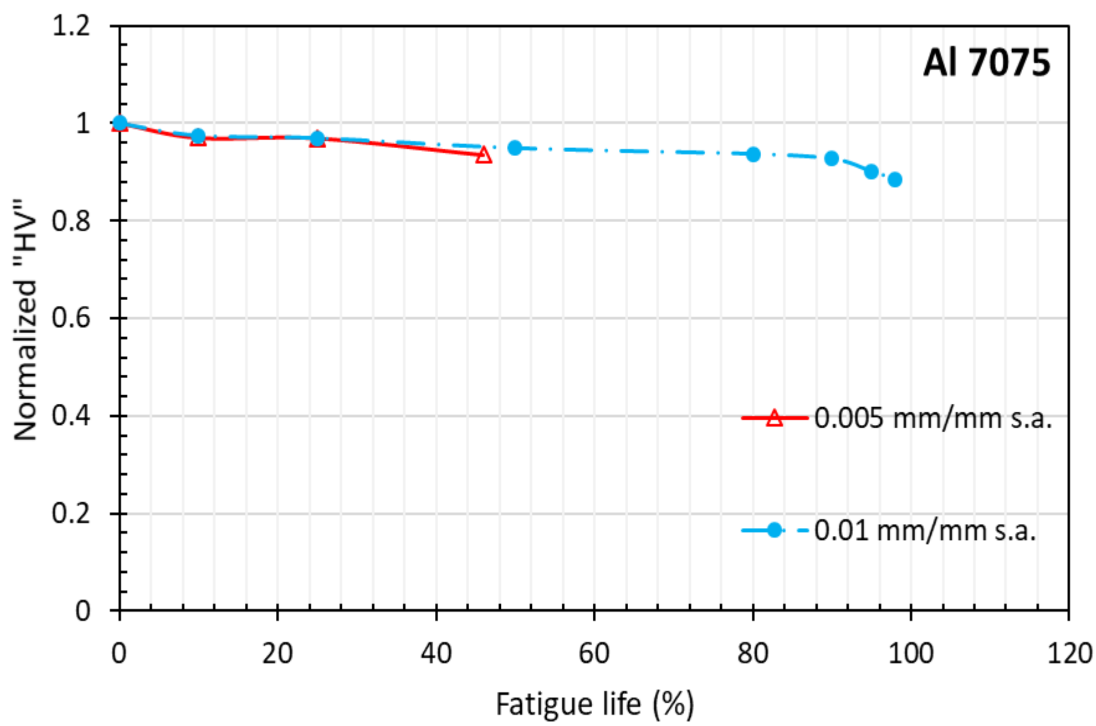

Figure 4.44 Normalized Vickers micro-hardness (HV) against fatigue life (%) for Al 7075 under fully reversed 0.005 mm/mm and 0.01 mm/mm strain amplitude.

The obtained normalized data for Vickers micro-hardness shows that with increasing fatigue damage, the Vickers micro-hardness decreases. A similar response is observed for Al 7075, but the impact is comparatively less than that of Al 6061. The above results come to the conclusion that the Vickers micro-hardness is inversely related to fatigue damage.

Similar to the surface roughness “Ra” and Vickers micro-hardness “HV,” the maximum penetration depth obtained from micro-hardness indentation has been plotted versus the fatigue life (%), as shown in Figs. 4.45 and 4.46. Al 6061 shows a significant increase in maximum penetration depth with increasing fatigue damage for 0.01 mm/mm strain amplitude. However, a minor increment is noticed for 0.005 mm/mm strain amplitude.

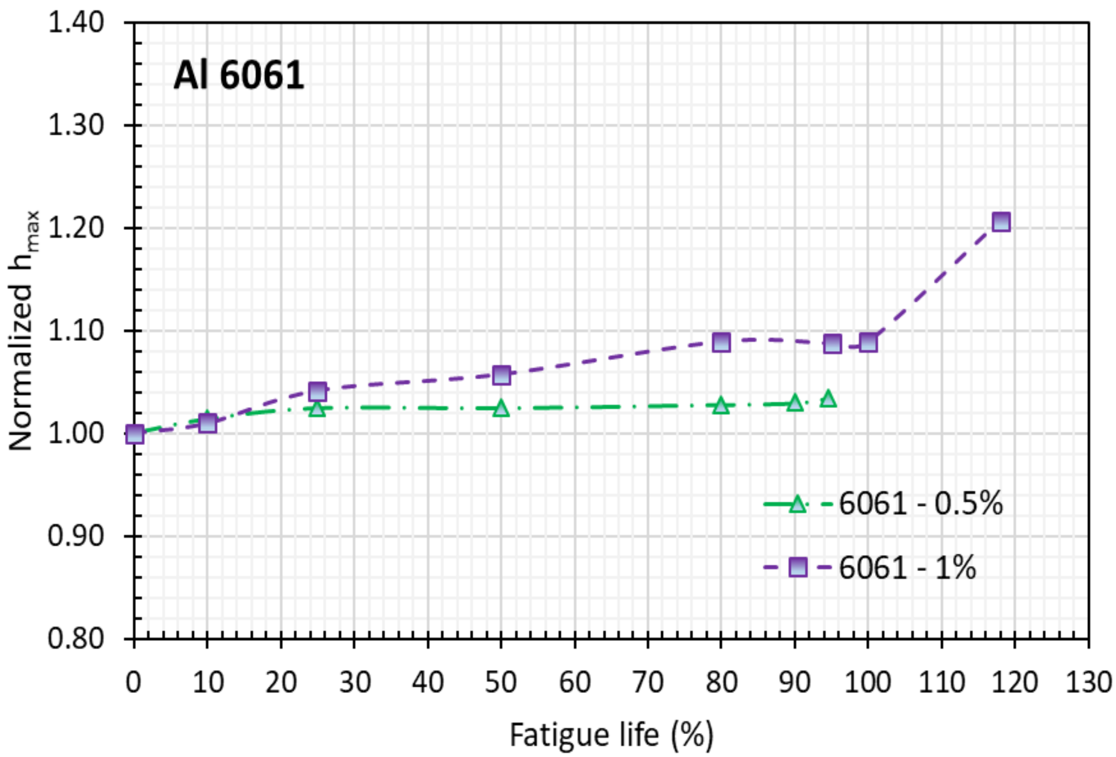

Figure 4.45 Normalized maximum penetration depth (h_{max}) against fatigue life (%) for Al 6061 under fully reversed 0.005 mm/mm and 0.01 mm/mm strain amplitude.

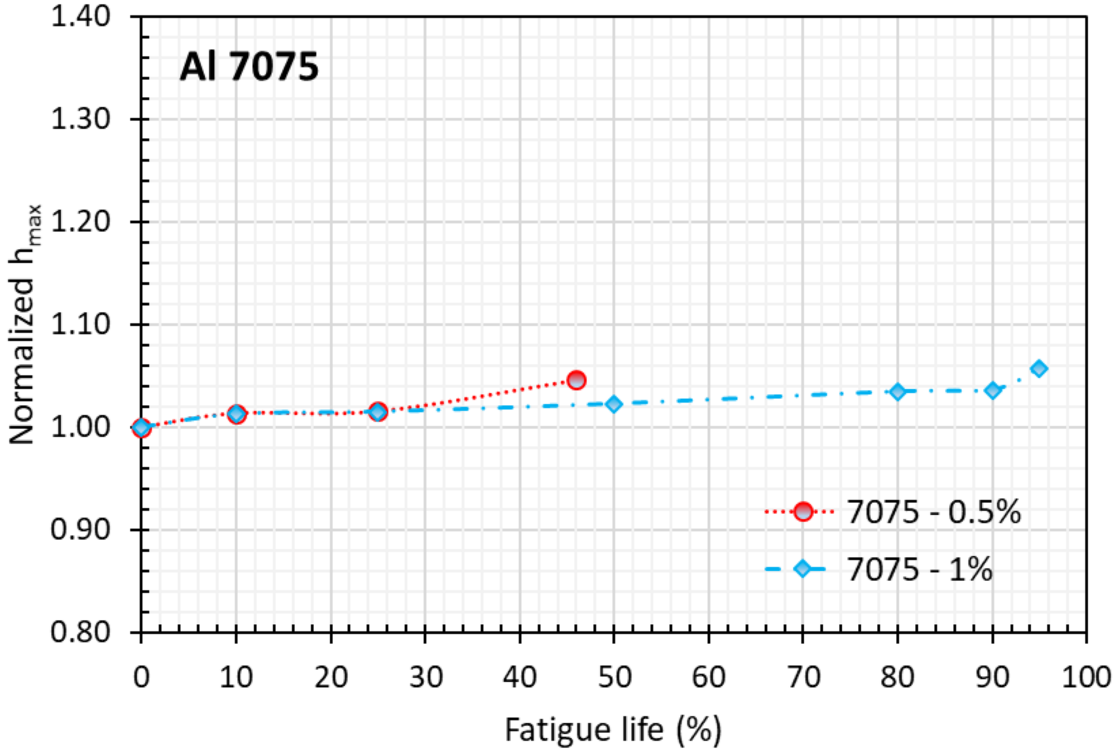

Figure 4.46 Normalized maximum penetration depth (h_{max}) against fatigue life (%) for Al 7075 under fully reversed 0.005 mm/mm and 0.01 mm/mm strain amplitude.

As shown in the above figure 4.46, Al 7075 demonstrates the same response under 0.005 and 0.01 mm/mm strain amplitude. As the fatigue damage is increased, the maximum penetration depth is also seen to be gradually increasing. Based on the Al 6061 and Al 7075 response under two strain amplitudes, it is concluded that maximum penetration depth is directly related to the fatigue damage.

5 CONCLUSION

Aluminum alloys Al 6061 and Al 7075 of T651 temper chosen for this research. Both materials were subjected to various experimental methods such as stress, strain-controlled fatigue tests, micro-hardness indentations, and surface roughness measurements. As mentioned earlier, the outcomes of all the experiments have been employed for the characterization of fatigue damaged. The following conclusions are achieved.

- Instrumented micro-indentations were performed at distinct surface roughness, and it appeared that surface roughness “Ra” and “Rq” had a significant influence on the Vickers micro-hardness. Both aluminum alloys showed a similar response, so it is concluded that Vickers micro-hardness (HV) has an inverse relation to surface roughness.

- Cyclic micro-indentations and fatigue tests were carried out. The obtained strain hardening exponent “n” from above micro-indentations and fatigue (destructive) tests have been correlated. It is determined that there is a direct relationship between strain hardening exponents obtained from fatigue tests and micro-indentations.

- Fatigue damage tests were conducted at two different strain amplitudes. Based on the obtained results, a significant dependence of fatigue damage on the surface parameters (surface roughness, Vickers micro-hardness, and maximum penetration depth) has been observed. It is concluded that surface roughness and maximum penetration depth are directly correlated to the fatigue damage, whereas Vickers micro-hardness is inversely related.

- Normalized slopes for Hysteresis “E/E_o ”and micro-indentations “C/C_o” were also analyzed, but it is noticed that no clear correlation has been observed in the above parameters with increasing fatigue damage.

6 FUTURE WORK

- In this research, intermittent fatigue damage tests at 0.005 and 0.01 mm/mm strain amplitudes under predefined cyclic intervals were performed. Testing it under different strain amplitudes would be recommended to identify how it would alter the surface roughness and Vickers micro-hardness.

- The strain-controlled intermittent fatigue damage tests have been conducted on aluminum alloys. The outcomes under stress-controlled intermittent fatigue damage tests would be crucial to monitor.

- Perform strain controlled and displacement controlled for traditional and micro-indentation test, respectively to observe the fatigue damage behavior. Similar tests under stress controlled and load controlled will help for better understanding.

- The current study investigates the work hardening behavior of a material based on the instrumented cyclic micro-indentations for Al 6061 and Al 7075 aluminum alloys. Finally, having different aluminum alloys tested under the same experimental setup would be essential to identify the material's strain hardening behavior.

7 REFERENCES

[1] FORREST, P. G., 1962, "CHAPTER I - INTRODUCTION," *Fatigue of Metals*, P.G. FORREST, ed., Pergamon, pp. 1–11.

[2] Suraratchai, M., Limido, J., Mabru, C., and Chieragatti, R., 2008, "Modelling the Influence of Machined Surface Roughness on the Fatigue Life of Aluminium Alloy," Int. J. Fatigue, **30**(12), pp. 2119–2126.

[3] Dowling, N. E., 2012, *Mechanical Behavior of Materials: Engineering Methods for Deformation, Fracture, and Fatigue*, Pearson.

[4] Suresh, S., 1998, *Fatigue of Materials*, Cambridge university press.

[5] Anderson, T. L., 2017, *Fracture Mechanics Fundamentals and Applications*, CRC Press, Boca Raton.

[6] Mereuta, V. L., Alexandru, P., and Palaghian, L., 2011, "Microhardness a Possible Characteristic of Fatigue Damage of Metallic Surfaces," Ann. DAAAM Proc. Int. DAAAM Symp., **22**(1), pp. 905–906.

[7] ASTM E8, 2010, "ASTM E8/E8M Standard Test Methods for Tension Testing of Metallic Materials 1," Annu. B. ASTM Stand. 4, (C), pp. 1–27.

[8] Bhat, S., and Patibandl, R., 2011, "Metal Fatigue and Basic Theoretical Models: A Review," Alloy Steel - Prop. Use.

[9] ASTM E466, 2002, "Standard Practice for Conducting Force Controlled Constant Amplitude Axial Fatigue Tests of Metallic Materials," Test, **03**, pp. 4–8.

[10] ASTM E606, 2019, "ASTM E606/E606M-19 Standard Test Method for Strain-Controlled Fatigue Testing.," ASTM Int., **i**.

[11] Moridi, A., 2017, *Powder Consolidation Using Cold Spray*, Springer International

Publishing.

[12] K., K., M. M., N., M. M., R., M. R. M., R., N. M. Zuki, N., and R., D., 2008, “Optimization of Surface Roughness in End Milling on Mould Aluminium Alloys (AA6061-T6) Using Response Surface Method and Radian Basis Function Network,” Jourdan J. Mech. Ind. Eng., **2**(4), pp. 209–214.

[13] E.S. Gadelmawla, M.M. Koura, T.M.A. Maksoud, I.M. Elewa, H. H. S., 2002, “Roughness Parameters,” CCAMLR Sci., **6**, pp. 117–123.

[14] ASTM E384 - 17, 2017, “Standard Test Method for Microindentation Hardness of Materials,” ASTM Int., pp. 1–40.

[15] Oliver, W., & Pharr, G., 1992, “An Improved Technique for Determining Hardness and Elastic Modulus Using Load and Displacement Sensing Indentation Experiments,” J. Mater. Res., **7**(6), pp. 1564–1583.

[16] Giannakopoulos, A. E., and Suresh, S., 1999, “Determination of Elastoplastic Properties by Instrumented Sharp Indentation,” Scr. Mater., **40**(10), pp. 1191–1198.

[17] Venkatesh, T. A., Van Vliet, K. J., Giannakopoulos, A. E., and Suresh, S., 2000, “Determination of Elasto-Plastic Properties by Instrumented Sharp Indentation: Guidelines for Property Extraction,” Scr. Mater., **42**(9), pp. 833–839.

[18] Dao, M., Chollacoop, N., Van Vliet, K. J., Venkatesh, T. A., and Suresh, S., 2001, “Computational Modeling of the Forward and Reverse Problems in Instrumented Sharp Indentation,” Acta Mater., **49**(19), pp. 3899–3918.

[19] Ås, S. K., Skallerud, B., and Tveiten, B. W., 2008, “Surface Roughness Characterization for Fatigue Life Predictions Using Finite Element Analysis,” Int. J. Fatigue, **30**(12), pp. 2200–2209.

[20] Smaga, M., and Eifler, D., 2010, “Effect of Residual Stress and Surface Roughness on the

Fatigue Behaviour of Aluminium Matrix Composites," J. Phys. Conf. Ser., **240**, pp. 3–7.

[21] Xiao, W. L., Chen, H. B., and Yin, Y., 2012, "Effects of Surface Roughness on the Fatigue Life of Alloy Steel," Key Eng. Mater., **525**–**526**(October 2015), pp. 417–420.

[22] Fine, M. E., 1983, *Fatigue Crack Initiation on Slip Bands.*, Pergamon Press Ltd.

[23] Ye, D., Xu, H., Feng, X., Xu, Y., and Xiao, L., 2016, "Depth-Sensing Indentation-Based Studies of Surface Mechanical Behavior and Fatigue Damage Evolution of an Austenitic Stainless Steel Subjected to Cyclic Straining," Mater. Sci. Eng. A, **650**, pp. 38–51.

[24] Lemaitre, J., and Desmorat, R., 2005, *Engineering Damage Mechanics : Ductile, Creep, Fatigue and Brittle Failures*, Springer, Berlin.

[25] Pantelakis, S. G., Petroyiannis, P. V., Bouzakis, K. D., and Mirisidis, I., 2007, "Surface Hardness Increase of 2024 Aluminum Alloy Subjected to Cyclic Loading," Theor. Appl. Fract. Mech., **48**(1), pp. 68–81.

[26] Ye, D., and Wang, Z., 2001, "Approach to Investigate Pre-Nucleation Fatigue Damage of Cyclically Loaded Metals Using Vickers Microhardness Tests," Int. J. Fatigue, **23**(1), pp. 85–91.

[27] ASTM International, 2017, "ASTM E3.34776 Standard Guide for Preparation of Metallographic Specimens," ASTM Stand., **11**(Reapproved 2017), pp. 1–17.

[28] ASTM International, 2019, "ASTM E9 - 19 Standard Test Methods of Compression Testing of Metallic Materials at Room Temperature," ASTM B. Stand., pp. 1–10.